DEVELOPMENT OF FUNCTIONALISED MULTIWALLED CARBON NANOTUBE/POLYANILINE COMPOSITES FOR ELECTRICAL APPLICATIONS

Thesis submitted to

Cochin University of Science and Technology

in partial fulfilment of the requirements

for the award of the degree of

Doctor of Philosophy

Sobha A.P.

Department of Polymer Science and Rubber Technology

Cochin University of Science and Technology

Kochi- 682 022, Kerala, India

August 2015

Development of functionalised multiwalled carbon nanotube/polyaniline composites for electrical applications

Ph. D Thesis

Author

Sobha A.P.
Department of Polymer Science and Rubber Technology
Cochin University of Science and Technology
Cochin- 682 022, Kerala, India
E-mail: apsobha05@gmail.com

Supervisor

Prof. (Dr.) Sunil K. Narayanankutty
Head
Department of Polymer Science and Rubber Technology
Cochin University of Science and Technology
Cochin- 682 022, Kerala, India
E-mail: sncusat@gmail.com

Department of Polymer Science and Rubber Technology
Cochin University of Science and Technology
Cochin- 682 022, Kerala, India

August 2015

Department of Polymer Science and Rubber Technology
Cochin University of Science and Technology
Cochin- 682 022, Kerala, India

Dr. Sunil K. Narayanankutty
Professor & Head

26/08/2015

Certificate

This is to certify that this thesis entitled **"Development of functionalised multiwalled carbon nanotube/polyaniline composites for electrical applications"** is a report of the original work carried out by **Mrs. Sobha A.P.** under my supervision and guidance in the Department of Polymer Science and Rubber Technology, Cochin University of Science and Technology, Cochin-22. No part of the work reported in this thesis has been presented for any other degree from any other institution. All the relevant corrections and modifications suggested by the audience during the pre-synopsis seminar and recommended by the Doctoral committee have been incorporated in the thesis.

Cochin-22

Prof. Sunil K. Narayanankutty
(Supervising Guide)

Declaration

I hereby declare that the thesis entitled "**Development of functionalised multiwalled carbon nanotube/polyaniline composites for electrical applications**" is the original work carried out by me under the supervision of **Prof. Sunil K. Narayanankutty** Department of Polymer Science and Rubber Technology, Cochin University of Science and Technology, Cochin-22 and has never been included in any other thesis submitted previously for the award of any degree.

Cochin - 22   **Sobha A.P.**
26/08/2015

Acknowledgements

I would like to express the deepest appreciation and gratitude to my supervisor, Prof. Sunil K. Narayanankutty, who was inspiring me in many aspects, which are not limited to research and studies. Sir, you are one of those rare persons sensitive to the world around with eyes, ears and mind wide open, observing & absorbing with detachment and equanimity. I am very much grateful to you, for everything that I learned from you, for your understanding and trust in me, for the guidance and wisdom you have given me and for the priceless philosophy that will be carried throughout my life.

I extend my thanks to all the faculty members of PSRT. I gratefully acknowledge Prof. Philip Kurian who inducted me into this department. I had the opportunity to be the student of Prof. K. E. George, Prof. Rani Joseph, Dr. Eby Thomas Thachil and Prof. Thomas Kurian during my course work. I profoundly thank them for sharing their extensive knowledge, guidance and valuable insight in the field of polymer science. I am particularly grateful to Prof. Thomas Kurian for being my research committee member. Many thanks to Prof. Jayalatha Gopalakrishnan for her encouragement and support during my research period, and to Dr. Jyothish Kumar for his suggestions and comments. Thanks to the other teachers Abitha, Sona and Sindhu for their friendship and support. Special thanks to non-teaching staff of this department for their service and technical assistance.

I am grateful to Dr. Jacob Philip and Soumya of Instrumentation department for carrying out the thermal conductivity measurement. I would like to thank Dr. Jacob Philip for his valuable advice. Heartfelt thanks to Dr. Anandan and Sreekala of Electronics department for carrying out EMI shielding efficiency measurements in their lab. I will always cherish the support and effort Sreekala has taken for me. I thank Divya of Chemistry department for doing CV studies for me.

A very special word of thanks to Dr. Sudha T.D and her research group of NIIST, Thiruvanandapuram for helping me to carry out the DC conductivity measurements. I also wish to thank Dr. Suresh. Perumal of IISc Bangalore not only for carrying out the Seebeck coefficient measurement, but also for his vibrant personality and inspiring outlook.

It has been a great pleasure for me to carry out this PhD study along with the cheerful and vibrant research scholars of PS&RT dept. I am deeply indebted to Dr. Pramila Devi, Jebin teacher, Jolly Sir and Dr. Bibin for their valuable suggestions, help and constant encouragement throughout my work. I wish to express my sincere feelings to my lab mates Ajilesh, Resmi, Renju, Bindhu, Dr. Vidya, Dr. Preetha, Molice teacher, Dennymol Teacher, Julie, Ayswarya, Asha, Teena, Sona, Sreejesh, Neena Jibi and Neena Satheesh for their help at various stages of my work. I acknowledge my thanks and appreciation to Abhilash,, Rohith, Manoj Sir, Dr. Nisha, Jayesh, Sreedevi, Sunitha, Dr. Zeena, Dr. Vidya Francis, Dr. Saisy, Dr. Anna, Dhanya, Anju, Bhagyesh, Jisha, Neethu, Shadiya, Remya, Nishad, Soumya, Divya, Asha Paul for their cooperation and good friendship during my research period.

Sincere thanks to the principal Dr Sudha Balagopal, management, staff and students of Vidya Academy of Science and Technology, my second home, for their support, assistance and constant motivation. I remember my beloved friend Ashitha who was and still, is a source of inspiration.

Finally I acknowledge the unbreakable bonds of family. I thank my beloved daughter, husband, parents, mother-in-law and all my family members for their understanding, patience and support. I acknowledge their unconditional love and the willingness they expressed to stand by me during the course of my work.

Sobha A.P.

||||| Preface |||||

Combining intrinsically conducting polymers with carbon nanotubes (CNT) helps in creating composites with superior electrical and thermal characteristics. These composites are capable of replacing metals and semiconductors as they possess unique combination of electrical conductivity, flexibility, stretchability, softness and bio-compatibility. Their potential for use in various organic devices such as super capacitors, printable conductors, optoelectronic devices, sensors, actuators, electrochemical devices, electromagnetic interference shielding, field effect transistors, LEDs, thermoelectrics etc. makes them excellent substitutes for present day semiconductors.

However, many of these potential applications have not been fully exploited because of various open–ended challenges. Composites meant for use in organic devices require highly stable conductivity for the longevity of the devices. CNT when incorporated at specific proportions, and with special methods contributes quite positively to this end.

The increasing demand for energy and depleting fossil fuel reserves has broadened the scope for research into alternative energy sources. A unique and efficient method for harnessing energy is thermoelectric energy conversion method. Here, heat is converted directly into electricity using a class of materials known as thermoelectric materials. Though polymers have low electrical conductivity and thermo power, their low thermal conductivity favours use as a thermoelectric material. The thermally disconnected, but electrically connected carrier pathways in CNT/Polymer composites can

satisfy the so-called "phonon-glass/electron-crystal" property required for thermoelectric materials.

Strain sensing is commonly used for monitoring in engineering, medicine, space or ocean research. Polymeric composites are ideal candidates for the manufacture of strain sensors. Conducting elastomeric composites containing CNT are widely used for this application. These CNT/Polymer composites offer resistance change over a large strain range due to the low Young's modulus and higher elasticity. They are also capable of covering surfaces with arbitrary curvatures.

Due to the high operating frequency and bandwidth of electronic equipments electromagnetic interference (EMI) has attained the tag of an 'environmental pollutant', affecting other electronic devices as well as living organisms. Among the EMI shielding materials, polymer composites based on carbon nanotubes show great promise. High strength and stiffness, extremely high aspect ratio, and good electrical conductivity of CNT make it a filler of choice for shielding applications. A method for better dispersion, orientation and connectivity of the CNT in polymer matrix is required to enhance conductivity and EMI shielding.

This thesis presents a detailed study on the synthesis of functionalised multiwalled carbon nanotube/polyaniline composites and their application in electronic devices. The major areas focused include DC conductivity retention at high temperature, thermoelectric, strain sensing and electromagnetic interference shielding properties, thermogravimetric, dynamic mechanical and tensile analysis in addition to structural and morphological studies.

The   work is presented in seven chapters. A short summary for each chapter is as follows

CHAPTER 1 gives a general introduction to CNTs, conducting polymers, CNT based polymer composites, their synthesis procedures, conduction mechanism, properties and applications.

CHAPTER2 deals with the materials used and the experimental techniques for characterization.

CHAPTER3 describes the synthesis of PANI and PANI/FMWCNT composites through a series of interfacial polymerisation and the study of DC conductivity and thermal stability of DC conductivity of doped PANI and composites. The nanocomposite containing 12.9% CNT as well as PANI was doped with various acids. The samples were characterized by SEM, TEM, TGA and FTIR. High temperature DC conductivity stability studies through cyclic and isothermal ageing is also presented. The role of dopants and FMWCNTs in stabilising the DC conductivity of composites at elevated temperature is also discussed.

In CHAPTER 4 the synthesis and characterisation of PANI/FMWCNT composites by traditional in-situ (single phase) polymerization and dynamic interfacial polymerisation methods are discussed. The composites were characterized by SEM, TEM, XRD, TGA, FTIR, Raman and UV-Vis spectroscopy. The effect polymerisation process on the thermoelectric properties and DC conductivity retention at high temperature is studied.

CHAPTER 5 deals with the synthesis of FMWCNT-PANI based TPU composites through solution casting method and its application to strain sensing. The composites were prepared by solution casting method using

in-situ and ex-situ polymerised PANI-FMWCNT conductive filler. The effect of PANI coating on the morphology, electrical resistivity and resistivity – strain behaviour of these composites are investigated.

CHAPTER 6 FMWCNT/PANI/TPU composites were prepared by in-situ polymerization of aniline in TPU solution in the presence of FMWCNTs, assisted by sonication. The synthesis and characterisation of morphological, thermal and mechanical properties of the composites by FESEM, TGA, DMA and tensile analysis. The electrical and EMI shielding properties of the prepared composites are presented   as a function of FMWCNT content. The homogeneous dispersion of NTs is confirmed by morphology studies.

CHAPTER 7 summarizes major conclusions of the research work.

Contents

Chapter **3**

PANI AND FMWCNT-PANI COMPOSITES THROUGH INTERFACIAL POLYMERISATION - STUDY OF DC CONDUCTIVITY AND CONDUCTIVITY RETENTION...**65 - 103**

Chapter 6
ELECTRICAL, THERMAL, MECHANICAL AND ELECTROMAGNETIC SHIELDING PROPERTIES OF PANI/FMWCNT/TPU COMPOSITES

Chapter 7
CONCLUSIONS

Chapter 1

INTRODUCTION

This chapter presents a brief introduction to carbon nanotubes, conducting polymers, synthesis of CNT based TPU composites, their conducting mechanisms, properties and potential applications. A literature survey on the thermal stability of DC conductivity, thermoelectric properties, strain sensing and EMI shielding properties of CNT based polymer composites are presented. The scope and objectives of the work is also discussed.

1.1 Nano Science

The development of novel materials and methods heralds a new era of innovations in science and technology. Structures created in nanoscale possess fascinating properties with vast potential for use in a wide spectrum of applications. Richard Feynman, the great physicist who in 1959, envisioned potential of manipulation and control of individual atoms and molecules is considered the father of nanotechnology. Another scientist Norio Taniguchi coined the term Nanotechnology a decade later. The development of the Scanning Tunneling Microscope in 1981 was a major landmark in the development of this science. The scientific community has witnessed significant progress ever since.

Nanoscience and Nanotechnology deals with the study of particle sized structures in the scale 1 to 100 nanometers, which find application in almost all branches of science. At this size range, the properties of the particles are governed by the 'quantum' effect. A relevant example is the nanoscale gold particle, which exhibits a fascinating display of red or purple color, instead of the natural yellow. This effect is attributed to the restricted movement of gold's electrons at nanoscale. As the dimension of a material system reduces to nanometer scale, unique physical and chemical characteristics arise. Nano-materials have been mass fabricated by novel synthetic approaches, and have attracted a great deal of interest from scientists and engineers. Carbon, in its diverse forms of compounds and allotropes, also forms one of the most extensively researched nano materials.

1.2 Carbon nanotubes

The Buckminster fullerene C_{60}, discovered in 1985, with 60 equivalent carbon atoms, is an unusual molecule with the highest symmetry (1). In 1991, S. Iijima discovered a tubular form of fullerene, capped at each end and connected by a straight segment of tube (2). These are called carbon nanotubes because the structure is only about a few nanometers wide and are considered to be a rolled-up graphene sheet that forms long concentric cylinders. The length of the nanotubes is significantly greater than the width, creating a large aspect ratio. Bonding in CNTs is essentially sp^2; the circular curvature causes σ bonds to be slightly out of plane, the π orbital is more delocalized outside the tube (2).

There are two main types of CNTs: Single walled carbon nanotubes (SWCNTs) which consist of a single, seamless, rolled up cylinder of a

graphene sheet. These are defined by their diameter and their chirality (Fig. 1.1). The diameter of SWCNTs varies from 0.5 to 5 nm. Multiwalled carbon nanotubes (MWCNTs) are a group of concentric SWNTs (Fig.1.1) often capped at both ends, with diameters in the range from several nanometers up to 200 nm. The intertube spacing in MWCNT is roughly equal to the Vander Waals graphite interplane distance, 0.34 nm (3,4).
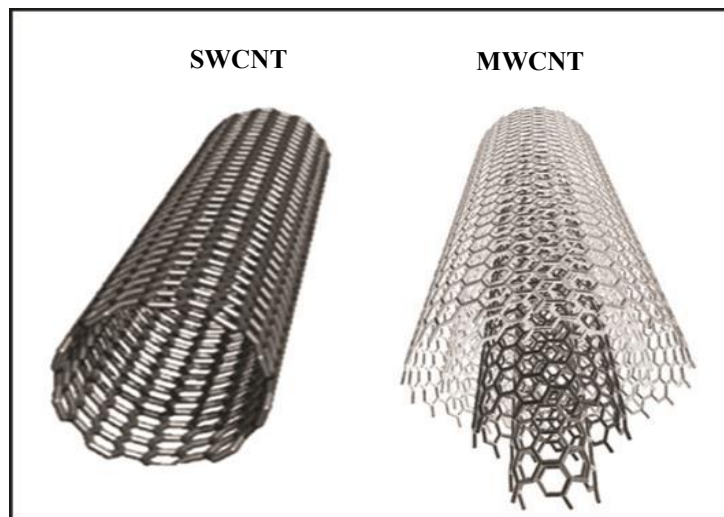
Fig. 1.1: SWCNTs and MWCNTs formed by rolling up a graphene sheet (5)

1.2.1 Structure

The structure of carbon nanotubes is described in terms of the tube chirality, which is defined by the chiral vector Ch and the chiral angle Ө. The chiral vector indicates the manner in which graphene is rolled-up to form a nanotube. The tube chirality is described by the chiral vector as

$$Ch \ = \ na_1 + \ ma_2 \ .... (1.1)$$

where the integers (n, m) indicate the number of steps along the zigzag carbon bonds of the hexagonal lattice and na_1 and ma_2 are unit vectors (Fig.1.2) (5,6). Accordingly, three types of orientation of the carbon atoms around the nanotube circumference are specified. If n = m, the nanotubes are called ''armchair'' and if m = 0, the nanotubes are called ''zigzag''. Otherwise, they are called ''chiral'' (Fig. 1.2). When n-m is a multiple of 3, the tube is chiral and metallic; otherwise, the tube is a semiconductor (6). The chirality of the carbon nanotubes has a huge impact on their properties, especially the electronic ones.

Each MWCNT contains a multi-layer of graphene, and each layer can have different chiralities, so the prediction of its physical properties is more complicated than that of SWCNT.
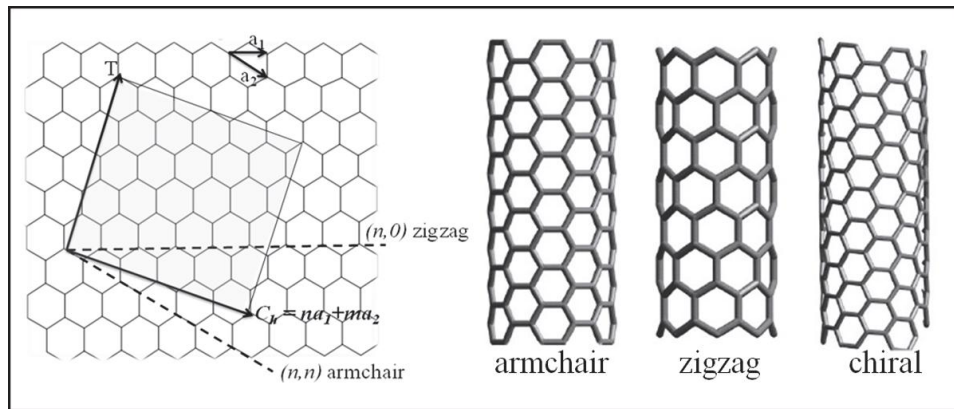
Fig. 1.2: A sheet of graphene rolled to show formation of zigzag (n, 0), armchair (m, m), and chiral (n, m) CNTs (5)

The electron transport property of the MWCNTs is more complicated than SWCNTs. Each of its carbon shells can be metallic or semi conductive, depending on the chirality of the shell. At room temperature, the outer two

shells will interact with each other and contribute to the conductance (7). Experimentally, both metallic and semi conductive behaviour has been observed for the MWNTs. Tubes with more complex conduction behaviour have also been observed (8).

1.2.2 Synthesis

Carbon nanotubes are required in large quantities in laboratories and industry. CNTs can be produced by a variety of processes which can broadly be divided into two categories (1) high temperature evaporation using arc-discharge (8-12) or laser ablation (13,14,) and (2) various chemical vapour deposition (CVD) or catalytic growth processes (15-17). In electric arc method, direct current arc plasma between two graphitic electrodes in an inert atmosphere is generated. This creates a high temperature discharge between the two electrodes. The anode gets consumed and MWCNT deposits are formed on the cathode. Arc-discharge produces MWNTs that are almost perfectly straight and contain very few defects. Addition of a suitable catalyst such as Ni-Co, Co-Y or Ni-Y leads to the formation of SWCNT bundles on the walls of the reaction chamber (18). The yield and properties of the nanotubes depend on factors like the metal concentration, inert gas pressure, type of gas, the current and system geometry. In laser ablation process, a pulsed or continuous laser is used to vaporise a graphite target in an oven at $1200^{o}C$. The oven is filled with an inert gas like He or Ar. Though this method can produce MWCNTs, it is most often used for the production of high quality SWCNTs with minimum defects at yields higher than 70%. The graphite target contains a 1–2% metal catalyst (19).

For commercial purpose, CNT is synthesized by the CVD technique. CVD method is suitable for CNTs in composites, as large quantities at low cost and requiring no further purification can be obtained by this method. There are various CVD processes, but basically they all involve a two-step process which thermally decompose hydrocarbon gases and use metal catalyst particles (Fe,Ni,Co) to grow the nanotubes (20-22). MWNTs are mainly obtained by this method, with high purity but with limited control over structure and diameter. Generally, the experiment is carried out in a flow furnace at atmospheric pressure. The catalyst is placed in a ceramic boat which is then put into a quartz tube. Ivanov et al. (23) utilized a reaction mixture consisting of acetylene and argon which is passed over the catalyst bed kept at temperatures ranging from 500 to 1100°C. Long nanotubes with diameters ranging from 0.6 - 4 nm for SWNTs and 10 - 200 nm for MWNTs can be produced.

1.2.3 Properties of CNTs

The large aspect ratio, nanometer size, the helical structure, sp^2 carbon–carbon bonds and the topology of carbon nanotubes give them excellent mechanical, thermal and electrical properties. These properties have made them a potential candidate for high-tech applications such as in field effect transistor, electron field emitters, probe tips for scanning tunneling microscopy, hydrogen storage, nano tweezers, fuel cells, sensors, EMI shielding, nano-transistors (24-32).

The sp^2bonding between carbon atoms confers outstanding mechanical properties on CNTs. The experimental and theoretical investigations show extraordinary mechanical properties of individual MWCNTs and

SWCNTs with Young's modulus being over 1TPa and a tensile strength of 10 - 200 GPa (33-35). CNTs have been described as being several hundred times stronger than steel and only one-sixth as heavy.

The superior electrical properties of CNTs are due to their unique electronic structure and one dimensional characteristic (36). Structural defects as well as bends or twists are again thought to have a strong effect on the transport properties (37). Theoretical studies of the electronic properties of SWCNTs suggested that nanotube shells can be either metallic or semiconducting depending on their helicity (3). Since MWCNTs have multiple-shell structure, confinement effects disappear, and the transport properties approach that of turbostratic graphite (38). Tans et al. (39) carried out the first experimental transport measurement of individual SWCNTs and showed that there are metallic and semiconducting SWCNTs, verifying the theoretical predictions. The room temperature conductivity was about 10^5 to 10^6 S/m for the metallic nanotubes and about 10 S/m for semiconducting tubes. Depending on the helicities of the outermost shells and the presence of defects, conductivity of individual MWCNTs have been reported to range between 20 and 2×10^7 S/m (40). The thermal conductivity in the axial direction of individual, perfect CNTs is reported to be as high as 3000 W/m/K (41), but have very small values in the radial direction.

The characteristics mentioned above make CNTs a promising filler for the fabrication of new, advanced composite systems. Notable similarities between the conductivity behaviour of nanotube networks and conducting polymers have been pointed out by Kaiser et al. (42). In this regard, composites of π conjugated polymer and CNTs are of importance as conjugated groups of

polymers would interact strongly with the planar graphitic structure of carbon nanotubes (43-45). The excellent properties of these two materials combined, has the potential for the development of still newer materials and devices.

1.2.4 Functionalisation of CNTs

Theoretically, the integration of conducting polymers and CNT produce promising materials. But the superiority of the product is determined by the uniform dispersion of CNTs in the polymer matrix. This step is usually difficult to achieve given the poor dispersibility and insolubility of CNTs (46). Consequently, the resulting composites are of inferior quality and do not exhibit desired properties. To aid the formation of composites with improved quality, different approaches to disperse the CNTs have been reported, which includes chemical functionalisation of the nanotubes and the noncovalent adhesion of surfactant molecules (47,48). Chemical modification of CNTs ensures good dispersion of nanotubes in a medium, and enhances the interaction between the two (47). But chemical functionalisation involves harsh chemical treatments in strong acids such as sulfuric acid and nitric acid which induces defects and shortens the tubes resulting in degradation of their electronic and conducting properties (49). However, for CNTs physically dispersed in conducting polymer matrices, the interaction may not be strong enough for the ultimate transfer of CNT properties. The covalent links between CNTs and polymer matrix can be utilized provided the functionalisation of CNTs is carried out under mild reaction conditions. Baek et al. (50) reported functionalisation of MWGNT with 4-amino benzoic acid via ''direct'' Friedel- Crafts acylation in a mild polyphosphoric acid (PPA)/phosphorous pentoxide (P_2O_5) medium. The reaction condition

in this approach resulted in less destructive chemical modification and the functionalised MWCNT significantly enhanced the electrical conductivity of the resultant composite (51). This kind of covalent grafting of the nanotubes improved nanotube dispersion and creates microscopic interlinking sites.

1.3 Intrinsically Conducting Polymers

Alan J. Heeger, Alan G. MacDiarmid and H. Shirakava discovered in 1977, that a type of conjugated polymer called 'Polyacetylene' could become electrically conductive after undergoing a structural modification process called doping (52). The impact of this discovery was so profound that it won them the Nobel Prize in 2000. The alternating single and double bonds in the polymer chain enabled the electrons to de-localize throughout the whole system and thus many atoms may share them (53,54). This discovery revealed previously unexploited properties in polymers resulting in a new research field namely intrinsically conducting polymers (ICPs). These ICPs combine the typical properties of organic polymers such as low density, environmental stability, resistance to corrosion and low cost of synthesis with the conductivity of metals. They are called "intrinsically conducting polymers" to distinguish them from others which acquire conductivity when loaded with conducting particles such carbon black, metal flakes or graphite.

Today we have a variety of polymers which exhibit electrical conductivity and are often called "organic semiconductors" or "synthetic metals". The structures of a few of these ICPs such as Polyacetylene, Polythiophene, Polypyrrole, Polyparaphenylene, Poly(phenylene vinylene), poly(3,4-ethylenedioxythiophene) and Polyaniline are given in figure1.3.
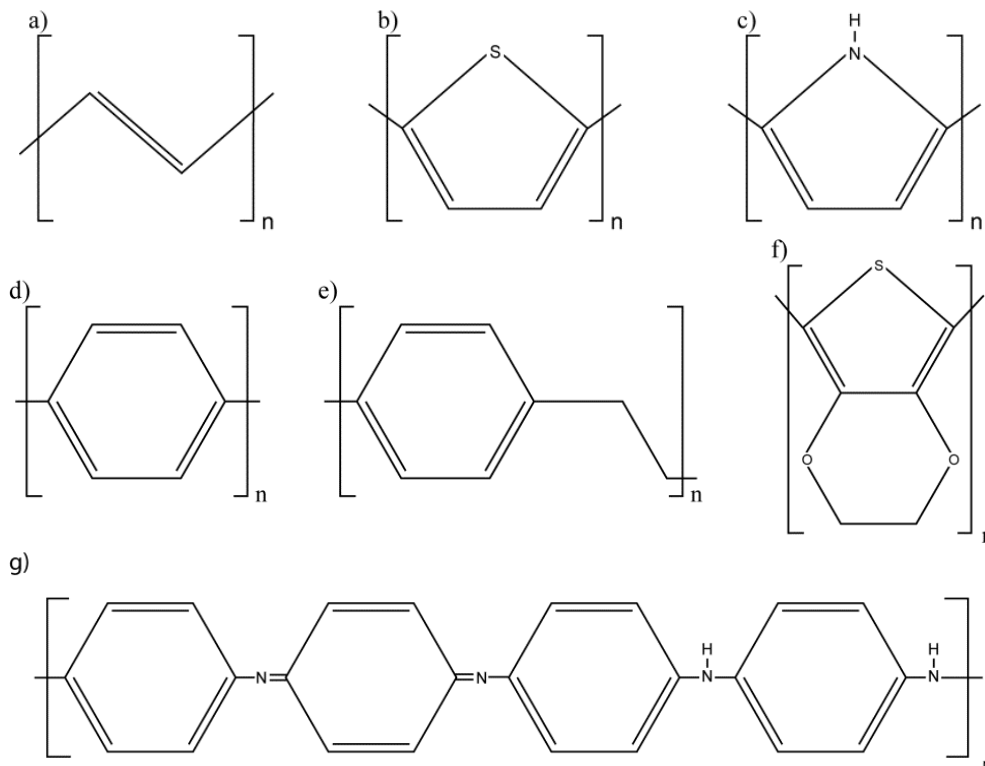
Fig. 1.3: **Example of some conducting polymers**
(a) trans-polyacetylene, (b) polythiophene, (c) Polypyrrole,
(d) poly(phenylene), (e) poly(para-phenylenevinylene),
(f) poly(3,4-ethylenedioxythiophene) and (g) polyaniline

These ICPs are expected to find application in a variety of areas such as lighting and displays, sensors, thermoelectrics, solar cells, EMI shielding, antistatic coatings, separation membranes, lightweight batteries (55-63) etc. Due to their advantages such as easy tailoring of conductivity along with low cost, light weight, easy processability, high flexibility and large surface area, they have started to replace inorganic semiconductors and revolutionise the electronics industry. The extended π-electron systems in ICPs are highly susceptible to chemical or electrochemical oxidation or reduction. Hence the electrical properties of such polymers can be altered by

carefully controlling the process of oxidation and reduction (64). Since these reactions are often reversible, it is possible to systematically control the afore-mentioned property with precision, changing from a highly conducting state, through semiconducting, to an insulating state (64, 65).

1.3.1 Doping

In most of the cases, these ICPs are poor semiconductors in their neutral state and they become conducting only after introduction of electron acceptors/donors by a process known as 'doping'. Doping increases the conductivity by adding mobile charges and delocalizing the electrons along the polymer backbone (54, 66). Dopants interact with the polymer chain by oxidizing or reducing them and do not participate in the charge transport mechanism directly. The doping of conducting polymers involves (1) charge transfer by oxidation (p-type doping) or by reduction (n-type doping), (2) the associated insertion of a counter ion for the overall neutrality, and (3) the simultaneous control of chemical potential (67, 68). When doping is done through oxidation or reduction, the polymer becomes p-doped or n-doped. By oxidation, an electron is removed and the polymer becomes positively charged, which is stabilized locally by an anion. Those charges then migrate in the polymer film creating electrical current. This type of doping is preferred to reductive doping, because the n-doped polymer becomes very unstable when exposed to ambient atmosphere. It will oxidize spontaneously and revert to the neutral state (69). Conjugated polymers canalso be doped by protonic acid doping. This is called non redox doping sincethe number of electrons associated with the conducting polymer chain does not change during doping process. But the energy

levels are rearranged. Polyaniline (PANI) is an example of the doping of an ICP to highly conducting regime by this process (70).

Charge carriers in ICPs can be formed during doping by redox reaction or protonation. The local distortion of the conducting polymer structure, followed by removal of an electron generates a radical cation. Such a radical cation which is partially delocalized over some polymer segments is called a polaron (65). It is named so as it stabilizes itself by polarizing the medium around it. When a second electron is removed from the system, it may come from either a different segment of the polymer chain creating another polaron, or from the first polaron to generate a dication which is referred to as a bipolaron. For trans-Polyacetylene, two equivalent resonance forms exist, (i.e., degenerate ground state) that differ from each other by the position of carbon–carbon single and double bonds. Consequently, when a bipolaron structure is generated, they can readily separate and is known as a soliton (65, 71). Solitons are not formed in conjugated polymers with non-degenerate ground states, such as in polypyrrole, polythiophene and polyaniline (72). Figure 1.4 gives an example of polaron and bipolaron structure for PANI. With the increase in doping level, the population of polarons, bipolarons, and/or solitons increases. At high doping levels, (foreg. 50% in PANI) the individual bipolaron states coalesce to form bipolaron bands. Application of an external electric field makes both polaron and bipolaron mobile via the rearrangement of conjugation and thus gives rise to high conductivity in ICPs. At still higher doping level, two bipolaron bands would gradually broaden producing metal like conductivity (72).
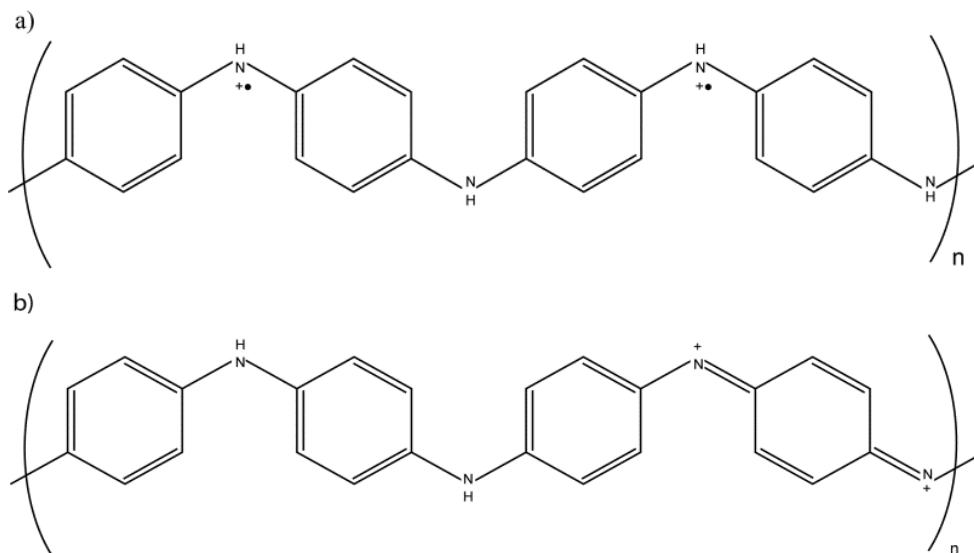
Fig. 1.4: PANI repeating units for (a) polaron form and (b) bipolaron form.

1.3.2 Conduction mechanism in ICPs

The nature of the charge transport mechanism in ICPs is still a matter of debate. Nevertheless, the transport mechanism of the charge-carriers along the polymer backbone chain is described by the Band model as in the case of metals and semiconductors. As discussed, the doping induced changes in electronic structure namely polarons, bipolarons and solitons are responsible for conduction in a single chain molecule of ICPs. But Band theory does not explain accurately the electronic conduction in polymers. Here the atoms are covalently bonded to one another forming polymeric chains that experience weak intermolecular interactions. Thus, macroscopic electronic conduction will require electron movement not only along the chains but also from one chain to another (73). Moreover, most of the ICPs are partially crystalline and partially disordered. Hence polymer matrix consisting of crystalline regions is considered as metallic grains embedded

in a poorly conducting amorphous region (74). The π bonding orbitals and quantum mechanical wave function overlap are responsible for the charge transport in ICPs. But due to inadequacy of π-bonding overlapping between the molecules of disordered organic semiconductors, the concept of quantum mechanical tunneling is appropriate to explain the charge transport in these polymers (75). The conduction between different polymer chains (charge carriers) is generally referred to as "hopping transport". The name is attributed to its quantum mechanical tunneling nature and reliance on the probability function (76). In hopping conduction, the localized states play a major role rather than delocalized bands. The conduction in conducting polymers can be described as the hopping of charge carriers, such as polaron, bipolaron and soliton. Assuming that the electron hopping was dependent on the initial and final energy states between which hopping occurred, a Variable Range Hopping (VRH) model was proposed by Mott and coworkers (77, 78). VRH model predicts that the conductivity can be expressed by

$$\sigma = \sigma_0 \exp(-(\frac{T_0}{T})^{\frac{1}{n+1}})$$

where $\quad T_0 = \frac{24}{\pi r_0{}^3 kN(E_f)} \quad \sigma_0 = \frac{9}{4}\sqrt{\frac{3}{2}}\,\pi e^2 \gamma_0 \sqrt{\frac{r_0\ N(E_f)}{kT}}$

n is the dimensionality of the material, r_0 is the localization length, k is the Boltzmann constant, γ_0 is the phonon vibration frequency, e is the electron charge, $N(E_f)$ is the density of states at the Fermi level, and T is the temperature. This model has been widely used to study conductivity/ temperature correlations in conducting polymers.

Thus, electrical conduction in ICPs is due to the collective effects of intra-chain hopping, inter-chain hopping, and tunneling of charge carriers.

1.3.3 Polyaniline

Among all conducting polymers, Polyaniline (PANI) is unique due to its ease of synthesis, non-redox doping, high environmental stability and wide application. PANI was known since 1862, but it rose to prominence recently owing to its high electrical conductivity on treatment with protonic acids. As of now, it is the most investigated conducting polymer (79).

The general formula for the polyaniline is
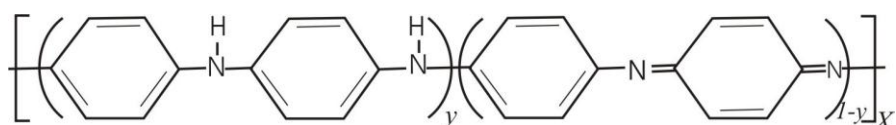
The structures of each repeating unit of PANI tetramer contain benzenoid diamine and or quinoid diimine segments which are present based on the extent of reduction or oxidation. The diversity in physiochemical properties of PANI is traced to the –NH– group. The difference in the composition of amine and imine segments of PANI generates several oxidation states of this material ranging from completely reduced leucoemeraldine to completely oxidized pernigraniline states (79,80). The different forms of PANI can be readily converted to one another by simple redox methods. Out of several possible oxidation states, the 50 % oxidized emeraldine salt (ES) state shows electrical conductivity.

Depending on the neutral intrinsic redox states, PANI is classified as (81).

1) Pernigraniline (y = 0), which is the fully oxidized state with blue/violet color.

2) Nigraniline (y = 0.75), which is the 75% intrinsically oxidized with blue/violet color.

3) Leucoemeraldine (y = 1), which is the fully reduced state having white/clear & colorless appearance.

4) Emeraldine (y = 0.5), which is the 50% intrinsically oxidized.

Emeraldine exist in two forms which are emeraldine base (EB) and emeraldine salt (ES). Among these, the EB is the basic form of PANI which consists of four-ring tetramer structure having two segments of amine and two of imine, and is non-conductive. The dopants can be doped into PANI or de-doped from it reversibly due to their non-redox and physical interaction. The conductive emeraldine salt is produced by the electrostatic attraction between the anions of incorporated dopants and the nitrogen on the backbone of polyaniline (Fig.1.5) (82). Hence the most common route for the synthesis of PANI involves the use of acids in the presence of oxidizing agent such as ammonium persulfate (APS) in which the polymerisation and doping occurs concurrently and may be carried out either electrochemically or chemically (83).

1.3.4 Protonic acid doping in Polyaniline

EB form of PANI can be doped with strong protonic acid to give the highly conducting ES form without changing the total number of electrons associated with it (Fig.1.5) (84).
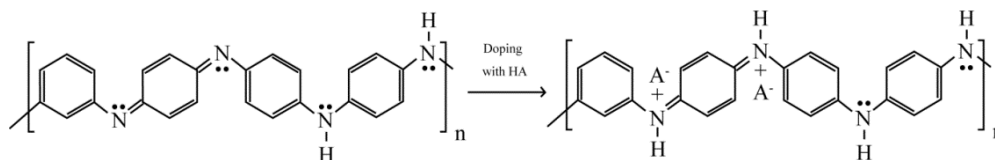
Fig. 1.5: Emeraldine base (insulating form)   Emeraldine salt (conducting form)

Protonation of PANI is accompanied by changes in electronic structure, crystallinity, solubility and the most important one is the increase of electrical conductivity over several orders of magnitude (85,86). Inorganic mineral acids such as HCl, H_2SO_4, etc. are the most frequently used dopants but the doped PANI in most of the cases, is completely insoluble. An important aspect of the protonic acid doping is that upon doping, only the proton is chemically bonded to polymer chain, the anion stays connected to positively charged PANI chain through electrostatic interaction (85). This property of acid doping results in several types of functionalised dopants which impart additional properties to the electrical characteristics of PANI. The dopant anions such as chloride, sulphate, toluene sulphonate, naphthalene sulphonate etc. greatly influence the electrical properties of PANI.

1.4   MWCNT-Polymer composites

To enhance both the electrical performance of conducting polymers and CNTs, one method is to develop carbon nanotube/ICP composites. The combination of CNT with conducting polymer especially PANI, offers new electronic properties based on the morphological tuning and   the electronic interaction between the two (44). CNTs have been reported to improve the electrical properties of insulating polymer matrices, besides enhancing their thermal and mechanical properties. The high surface energies on CNTs due to their nanometer size and high aspect ratio tend to their bundling in

polymer matrix (3). To achieve homogeneous dispersion, de-bundling is essential. Uniformly distributed three dimensional network is required for achieving high electrical conductivity and improved mechanical properties for composites. Introduction of PANI coated CNT into polymer matrix can be an alternative for this problem.

1.4.1 MWCNT-Polyaniline composites

As a conducting polymer PANI has many advantages and its DC conductivity has been recorded at more than 1000S/cm (86). In spite of these desirable properties, certain deficiencies in its inherent characteristics are reported. It has poor thermal stability, lacks consistency in conductivity and has low mechanical strength which will all hinder the longevity of electronic devices (87, 88). As discussed in section 1.2.3, an easy and effective solution lies in the addition of CNTs to PANI, which results in synergism in the electrical property.

The properties of CNT/PANI composites depend on the uniform dispersion of carbon nanotube in the polymer matrix. For the synthesis of CNT-PANI composites, the important approaches are (1) in-situ polymerisation, involving synthesis of PANI in the presence of CNTs (89, 90) and (2) chemical interaction or grafting of polymer chains onto the surface of CNTs by covalent bonding (91). Studies have shown that in-situ polymerisation is the most favored method for synthesizing homogeneous and high performing CNT-PANI composites. In this method, nanocomposite is synthesized by dispersing the nanotubes in the monomer or monomer solution and the resulting suspension is polymerised by standard polymerisation methods. Enhanced electrical properties were reported for the composites

synthesised by in-situ chemical oxidative polymerisation of aniline in the presence of CNT (92-94). According to the authors, effective site-selective interactions between the quinoid ring of PANI and MWNTs facilitated charge-transfer processes between the two components and improved conductivity was observed. In such composites, CNTs could improve the polymer properties by (i) inducing additional structural ordering of the polymer (ii) improve the compactness and conjugation or chain length (iii) higher delocalization of charges and charge carrier mobility (iii) thermal stability (94). The results of in-situ methods (95, 96) indicated that the polymerisation of aniline initiated on the CNT walls, resulting in polymer coated CNTs. Aπ-π interaction between the CNTs and the PANI is proposed by them. Gao et al. (97) synthesised nanocomposites of benzene sulfonic acid functionalised multi-walled carbon nanotubes doped polyaniline via a low-temperature in-situ polymerisation method. The benzene sulfonic acid functionality helped to disperse CNTs homogeneously in the reaction medium and the monomers were adsorbed on the surface of CNTs. This was achieved due to the hydrogen bonding between the functionalised groups and the amino groups of monomer. Many methods prevail, of which the preparation method via interfacial polymerisation demands more attention.

1.4.1.1 Interfacial polymerisation

It is well-known that polyaniline synthesised through different polymerisation process shows varied morphology, crystallinity and electrical conductivity. For the synthesis of PANI/CNT nanocomposites with good conducting properties, a method leading to formation of a thin, well-aligned and highly ordered polymer chain on nanotubes is desirable. Interfacial

polymerisation of aniline in presence of carbon nanotubes at an aqueous-organic interface is reported to be the most efficient method for meeting the above requirement (96-99). Salvatierra et al. (96) report of CNT/PANI nanocomposites obtained through interfacial polymerisation. The results indicated that the polymerisation of aniline started at the carbon nanotube walls, which resulted in a final material in which the CNTs capped by a fibrous polymer shell. With 25% CNTs, DC conductivity of 9.5 Scm^{-1} was achieved. On the basis of several characterization techniques, they provided a model for the carbon nanotube/polyaniline interactions. Jeon et al. (98) polymerised aniline through an in-situstatic interfacial polymerisation to yield the mixture of PANI and PANI-FMCWNT composites. From the cyclic voltammetry and conductivity measurements, they reported that PANI-FMWCNT displayed significantly improved conductivity and capacitance over PANI homopolymer. When the same group (99) attempted a simple suspension polymerisation, better yield resulted but conductivity declined compared with that from static interfacial polymerisation.

These CNT based polymer composites are useful for developing new applications in electronic and semi-conductor devices, as the substitute of semiconducting polymer or inorganic semiconductor. PANI-MWNT composites, having synergic effect on conducting property are used in many applications like organic light-emitting diodes, energy storage devices, thermoelectrics, sensitive materials for photovoltaic devices, EMI shielding, sensors, etc.

1.4.1.2 Thermal stability of conductivity

Thermal stability of conductivity of conducting nanocomposites is important. This is because they are exposed to high temperatures during

their fabrication process and once incorporated into functional devices they are required to withstand extremes of climatic conditions such as high temperature and strong sunlight. So, to enhance the thermal stability of conductivity and thereby improve the life span of devices, a detailed analysis of thermal ageing of conductivity is required.

Previous reports on improved thermal stability of polyaniline composites are abundant. But studies on the effect of high temperature on stability of electronic transportation of polyaniline and its composites are few. Wang and Rubner (100) synthesised polyaniline doped with hydrochloric acid, sulphuric acid, methane sulfonic acid and p-toluene sulphonic and their conductivity stability was examined at different elevated temperatures under different environments. According to them, the conductivities of all doped polymers decayed at varying temperatures, with loss in conductivity most pronounced at or higher than 150°C. Prokes et al. (101) studied the effect of addition of inorganic salts to PANI sulphate and found that it showed improved stability of the electrical properties at high temperatures. This research group has done several studies on the conductivity ageing of polyaniline at elevated temperatures and suggested the reason for conductivity degradation to deprotonation, oxidation and cross linking reactions among PANI molecules (102,103). Rannou et al. (104) suggested that the decrease in the conductivity of doped PANI appears as a result of three major degradation processes namely dedoping, oxidation/hydrolysis/ scission of the chains and cross linking. In the model put forward they proposed that the effect of ageing is to increase the width of insulating barriers between highly conducting islands, the latter being progressively nibbled by a diffusive oxidation process.

Regarding CNT-based PANI composites, Ansari et al. (105) synthesised DBSA doped PANI/MWCNT nanocomposite and studied the stability of the nanocomposites in terms of DC electrical conductivity retention. According to them, MWCNT/PANI nanocomposites showed better structural and thermal stability of DC conductivity than pure PANI. They suggested that these composites could replace PANI in various electrical and electronic applications. In another study, Cabezas et al. (106) investigated the effect of carbon nanotubes on thermal ageing and electrical conductivity of composite films containing MWCNT/ PANI nanofibres. They reported that when subjected to thermal treatment, the presence of nanotubes retarded the loss of dopants from polyaniline and enhanced the thermal stability in electrical conductivity of the composite thin films. Also there was an increase in temperature for conductivity degradation and a significant reduction in the rate of degradation of conductivity of the composite thin films.

These studies on conductivity degradation of PANI and its composites on thermal treatment, show that retention of DC conductivity at elevated temperature opens a field for further research.

1.4.1.3 Thermoelectric properties

Thermoelectric energy conversion has received great attention as heat is directly converted to electricity in these systems using a class of materials called thermoelectric materials (Fig.1.6). This type of energy conversion can be widely used as a special power source and as a novel energy harvesting system as in waste heat recovery and high efficiency solar energy conversion (107). The fundamental problem in creating efficient thermoelectric (TE) materials is that they must be very good at conducting electricity while keeping

thermal conductivity to the minimum. In most materials, increase in electrical conductivity is generally accompanied by an increase in thermal conductivity too. Hence, the main focus of the research on TE materials is to improve electrical conductivity while keeping thermal conductivity low. A measure of thermoelectric efficiency (Z) is often described as $Z = S^2\sigma/k$, where S, σ, and k, respectively, are Seebeck coefficient, electrical conductivity, and thermal conductivity (108). The Seebeck coefficient is defined as the voltage generated per degree of temperature difference between two points ($S = -\Delta V/\Delta T$). In general, high Seebeck coefficient and electrical conductivity and low thermal conductivity result in high performance of thermoelectric materials. But in typical thermoelectric materials, strong correlations between these parameters make Z improvement extremely difficult.
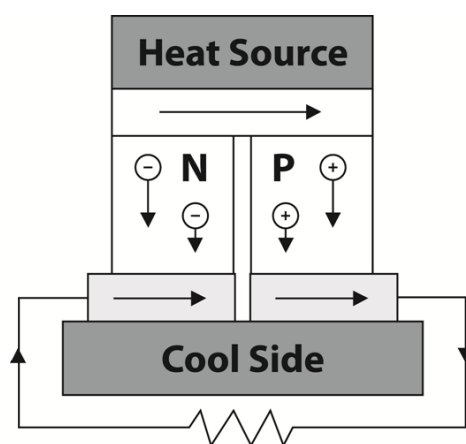

Fig. 1.6: Principle configuration of single TE couple for power generation

Usually research in thermoelectric materials is concentrated on inorganic semiconductors such as PbTe, Bi_2Te_3 etc. But their poor processability, high cost, toxicity and high density act as barriers in their commercial use (109). In this situation we need materials that are light weight, economical, easily

processable and having good thermoelectric property. Recently, ICPs have gained a special status owing to their wide range of applications. Though ICPs have low electrical conductivity and Seebeck coefficient as compared to the state-of-the-art inorganic thermoelectric materials, their low thermal conductivity can be considered an advantage for thermoelectric applications (110-113). Polyaniline (PANI) has gained special importance among conducting polymers due to its good processability, environmental stability, economic feasibility and tunable electrical properties. Furthermore its properties can be improved by selecting the method of polymerisation, and by the dopants and fillers used. CNTs with their excellent intrinsic electrical properties and structural characteristics have been used in the fabrication of many advanced functional materials. There are reports of enhanced thermoelectric properties of CNT filled polymer composites which maintain low thermal conductivity (114-116). This extraordinary behaviour is ascribed to thermally disconnected, but electrically connected energy carrier pathways. Meng et al. (114) synthesized PANI/MWCNT nanocomposites by a two-step process using thick CNT networks as a nanocomposite template. They obtained PANI/MWCNT composites with remarkably enhanced Seebeck coefficient and Power factor with relatively low thermal conductivities. They attributed this to the size-dependent energy-filtering effect caused by the nanostructured PANI coating layer enwrapping the CNTs. Similarly Yao et al. (115) reported that incorporation of SWCNTs into polyaniline resulted in dramatic improvement in both electrical conductivity and Seebeck coefficient. At the same time thermal conductivity of the composites, even with high SWNT content showed low values thereby satisfying the so-called "phonon-glass/electron-crystal" property required for thermoelectric materials. These

studies revealed that the preparation of PANI/MWCNT composites can be an effective way of producing relatively low density, economical and efficient TE materials. But, these research works, lack the information regarding the effect of polymerisation process on the morphology, crystallinity and thermoelectric properties of PANI/MWCNT composites. It is well-known that polyaniline synthesised through different polymerisation process shows different morphology, crystallinity and electrical conductivities. For the synthesis of PANI/CNT nanocomposites with good conducting properties, a method leading to formation of a thin, well-aligned and highly ordered polymer chain on nanotubes is desirable. This conformation of the molecular chains is expected to increase carrier mobility in composites leading to a simultaneous improvement in DC conductivity and Seebeck coefficient.

1.4.2 MWCNT/Elastomer composites

Carbon nanotubes have been reported to improve the electrical properties of insulating polymer matrices besides enhancing their thermal and mechanical properties. Elastomeric matrix composites are reported to exhibit multi functionality and are suitable for the development of conductive polymer composites for flexible strain sensing and EMI shielding applications (117,118). The majority of elastomers are thermosets, which are chemically cross linked during the process of vulcanization. In thermoplastic elastomers (TPE), instead of chemical crosslinks, the hard segments have a glass transition temperature or melting temperature below the working temperature of the polymer, and act as physical crosslinks. Thermoplastic polyurethane (TPU) which possesses rubber-like elasticity can be considered as an interesting candidate for developing CNT-filled composites for a number

of applications because of its excellent mechanical properties, resistance to chemicals and unique combination of elastomeric properties and processability which does not require vulcanization (119).

1.4.2.1 CNT/Thermoplastic polyurethane composites

Thermoplastic polyurethane is an elastomeric block copolymer consisting of a soft phase containing either polyester or polyether, reinforced by hard micro domains of an aromatic diisocyanate extended with a short-chain diol. The mechanical, physical and chemical properties of TPU can be tailored by changing the molecular chain structure and the content of soft segment and hard segment (120). TPU makes an interesting candidate for developing ICP and or CNT-filled composites for a number of applications in electrostatic imaging, sensing, electrostatic dissipation, EMI shielding etc. (121). Several studies have reported the preparation of PANI/TPU and CNT/TPU composites using various processes like solution and melt processing (122). It is reported that strong interfacial adhesion between CNTs especially, with the functionalised MWNTs and TPU matrix contribute to the improvement of the mechanical properties of TPU/MWNT composites without sacrificing the elongation at break (123).

1.4.2.2 Synthesis of conductive TPU composites through in-situ polymerisation

The poor dispersion of CNTs in elastomers hinders the utilization of high conductivity and high aspect ratio of CNTs in composites. Though functionalisation can improve the dispersion, it has a deteriorating effect on conductivity. Functionalisation under mild reaction condition can reduce this effect, but the less number of functional groups is not sufficient, for overcoming the van der Waal's force operating among the CNTs.

In this context, various strategies are taken up researchers in order to prevent the agglomeration and achieve a homogeneous dispersion of CNTs. Hwang et al. (124) modified the MWCNTs by a polymer wrapping method using poly (3-hexylthiophene) [P3HT] to achieve a homogeneous dispersion of MWCNTs in PDMS. They report that the percolation threshold of the composites was significantly lowered by the presence of P3HT. The electrical conductivity decreased with increasing P3HT concentration on the MWCNT surface, as it disturbed electron tunneling between MWCNTs and hence lowered the electrical conduction among MWCNTs. It is clear that novel methods to the in-situ polymerisation of polyaniline in TPU attempted by following researchers is significant.

However, the approaches that involve weak interactions such as polymer wrapping around the surface of CNT may not be the best option for the ultimate transfer of CNT properties to the insulating matrix. Instead, in-situ polymerised CNT-PANI filler could serve better for the maximum enhanced properties.

Denice et al. (125) obtained conducting, free standing films of PANI. DBSA/TPU by in-situ polymerisation of aniline in TPU. The in-situ blend preparation method was able to produce PANI.DBSA/TPU blends with enhanced compatibility, resulting in a fine dispersion and fine conducting pathways. The results revealed that the extent of the conducting polymer dispersion in the isolating polymer matrix exerts a strong influence on the electrical properties. Lakshmi et al. (126) synthesised PANI/TPU composites through in-situ polymerisation of aniline in TPU. They found the composite useful for microwave absorption and can be a potential candidate for EMI shielding applications. Also the mechanical properties of the composite film

were found to be satisfactory for normal service conditions. The interfacial adhesion between PANI and TPU improved the dispersion as well as the transport and mechanical properties. Similarly in-situ polymerisation of aniline in TPU matrix containing CNTs can be an efficient method for uniform dispersion of NTs in the matrix.

1.4.4.3 Percolation threshold

For a conductive polymer composite composed of an insulating polymer and conductive filler, electrical conduction is mainly described by three phenomena namely, percolation, hopping conduction, and fluctuation induced tunneling between the conductors. According to percolation theory (127), the continuous network of conducting filler is the only pathway for electron transporting. The transition of the composite from an insulator to a conductor, as explained by percolation theory, is depicted in the figure 1.7.
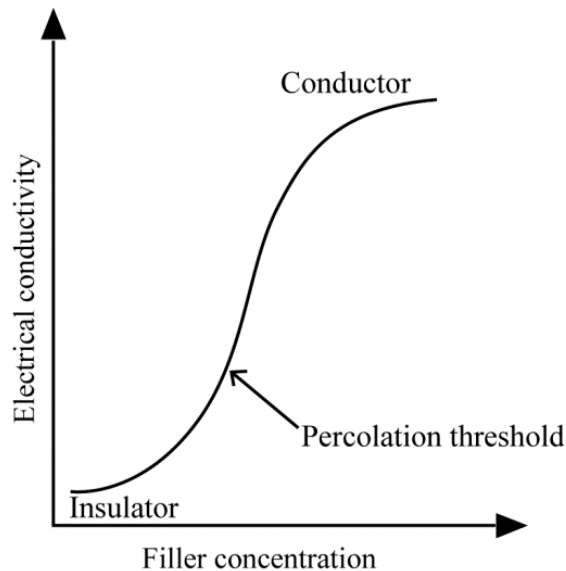

Fig. 1.7: Formation of conductive networks with filler loading

At low filler concentration the composite remains insulating as the filler particles cannot form an interconnecting network. As the filler content increases the filler particles start to form percolative network, effecting a transition from insulator to conductor. The minimum volume fraction of fillers required so as to form a continuing conductive network within the composite is called the electrical percolation threshold (127,128). Near the percolation threshold, conductivity of composites experiences a sudden rise of several orders of magnitude. According to percolation theory,

$$\sigma = \sigma_0 \, (v\text{-}v_c)^t \, \dots\dots\dots\dots\dots\dots\dots\dots\dots\dots\dots\dots\dots\dots\dots\dots\dots\dots (1.2)$$

for $v > v_c$

where σ is the electrical conductivity of the composite, σ_0 is a constant for a particular filler–polymer combination, v is the volume fraction of filler, v_c is the percolation threshold, the exponent 't' is related to sample dimensionality, i.e., t = 1, 1.33, or 2.0 for one, two, or three dimensions, respectively (127,129). The equation is valid at concentrations above the percolation threshold. Percolation threshold of conductive composites depends on conductivity, geometry and aspect ratio of the filler. CNT, high aspect ratio nanofiller is reported to form a network at a lower filler loading, decreasing the percolation threshold (130). For an insulating matrix, uniform distribution of well-dispersed, individual NTs can significantly decrease the percolation threshold. In order to achieve better dispersion, the affinity of NTs to the polymer matrix has to be improved and interfacial tension between NTs and fillers has to be reduced. Other techniques such as functionalisation of NTs, non-covalentcoating of NTs etc. has been attempted and yielded results, but with many short comings.

1.5 Applications

1.5.1 Strain Sensing

Structural health monitoring of any structure is essential be it in the field of engineering, medicine, space or ocean research. A strain sensor measures the deformation of a structure or component by experiencing the same deformation as that of the component. Usually, deformation of a strain sensor material results in change of any of its measurable properties. In an electro-mechanical strain sensor, which is a conductor or semi-conductor, the strain applied results in change of electrical properties. Sensing mechanism of the electromechanical sensors is related to change in electrical conductivity under the effect of pressure, displacement and strain and can be explained by the percolation theory (131,132).

One of the basic assumptions in percolation theory is that the filler is an infinite conductor, while the matrix is an infinite resistor, and there is no contact resistance between the fillers (127,133). But it is highly possible that barriers are present between conductive fillers and the electrons need to tunnel through these barriers by quantum mechanical tunnelling which creates tunnelling resistance. The characteristic behaviour of this tunnelling resistance is its temperature dependence. Various models such as Fluctuation Induced Tunnelling (FIT) and Variable Range Hopping (VRH) model have been developed to describe the tunnelling resistance in disordered solid. The VRH model is often used to describe the conduction mechanism of CNT composites or mats (134). Also there are reports of the charge transportation mechanism in polymer/MWNT composite regulated by the FIT model (135).

Regarding the deformation of conductive network in the composite which leads to a change in the resistivity or resistance, researchers have adopted different approaches when models were built for the strain dependent resistivity behaviour. The fundamental factors considered by them are (1) the variation of the number of conductive path; as some of the conductive pathways will be broken down with deformation that will definitely lead to an increase of the resistivity, (2) the variation of the inter-particle distance; as the electrons need to tunnel through a barrier between two conductive fillers when travelling through the conductive network of the composite. When the composite is deformed, this inter-particle distance may be increased, which leads to an increase of the resistivity (136). Knite et al. (137) proposed a model for the strain-dependent resistivity results of polyisoprene/CB composites based on these aspects. Zhang et al. (138) identified charge transport mechanism of amino-functionalised MWNT/ polyurethane-urea elastomeric composite sensor material as a fluctuation induced tunneling. According to them, the prediction for the gap width modulation by this model is well supported by the resistivity-strain dependence for the 5%–80% range of strain. For strains in the range 0%–5%, the resistivity-strain dependence is dominated by the deformation of the conductive network.

1.5.1.1 CNT/Elastomer composites in Strain sensing

Conventional strain sensors such as metal-foil strain gauges, though convenient to use, suffer a number of disadvantages such as poor flexibility, low gauge factor, low dynamic range, long term stability etc. In this context, CNT/elastomer composites with their high elasticity and ability to cover

surfaces of different shapes, large strain sensing range, and wide working range can be utilized in vast and varied environments. In an attempt to modify the strain sensitivity of CNT based elastomeric composites, Costa et al. (139) investigated the piezoresisitive properties of tri-block copolymer styrene–butadiene–styrene/CNT composites, which showed gauge factors up to 120. They reported that linearity obtained between strain and electrical resistance makes these composites interesting for large strain piezoresisitive sensors applications. Similarly, Kang et al. (140) examined the strain response of the MWCNT/ethylene–propylene–diene rubber composite and found that it was possible to measure tensile and compressive strains by using a 20 weight% MWCNT/ethylene–propylene–diene rubber composite. Recent works on TPU composites showed that they can sustain very large deformations and possess excellent thermophysical properties. MWCNT/TPU composites with their strong interfacial adhesion, stress transfer and excellent strain sensitivity have a greater potential to exhibit better piezoresistivity properties. Slobodian (141) et al. developed a highly deformable composite composed of a network of entangled carbon nanotubes embedded in polyurethane. The gauge factor of the composite increased linearly with strain from values around 4 at the start of deformation to nearly 69 at 400 % strain. This property as a strain sensor has been demonstrated in orthopedics and rehabilitation. Bautista-Quijano et al. (142) reported the enhanced piezoresistivity of MWCNT/segmented polyurethane (SPU) composites having sensing applications in prosthetics, biomedical devices, and smart textiles. For the composites at 8 weight % MWCNT, the piezoresisitive signal allowed to measure strains up to 400 % before electrical depercolation did occur. Zhang et al. (143) reported the resistivity response

under cyclic loading of TPU/MWNT elastomeric nanocomposite films fabricated by a solution process with good nanotube dispersion and low percolation threshold (0.35 weight %). At 5% strain, the strain-dependent resistance showed good recoverability and reproducibility, but when larger strains were applied, only a small part of the resistance was recoverable. Bilotti et al. (144) fabricated a highly conductive TPU/CNT fibre by a continuous extrusion process. The TPU/CNT fibres were sensitive to both static and cyclic deformation, which give them potential uses in smart textiles. Lin et al. (145) demonstrated that mixed carbon fillers and functionalised carbon nanotubes were vital for preparing TPU based strain sensors with tunable sensitivity. This study provided a unique method for the preparation of high-performance conducting polymer composite (CPC) strain sensors with a large range of resistivity-strain sensitivity.

1.5.2 Electromagnetic Interference Shielding

Due to the high operating frequency and bandwidth of electronic equipments, electromagnetic interference (EMI) has attained the tag of an 'Environmental pollutant'. EMI has negative effects on other electronic devices and also on all forms of live organisms. Electromagnetic radiation affects electrical circuits and prevents them from functioning efficiently at the receiving end. Electromagnetic Interference (EMI) is the process by which electromagnetic disturbance is transferred from one electronic equipment to another through radiation, conducted paths (or both) (146). So, commercial electronic products should meet prescribed standards of electromagnetic compatibility, i.e., the property of a device by virtue of which its emissions do not deter the device itself or others, from achieving

performing efficiency. EMI shielding denotes the reflection and/or absorption of electromagnetic radiation by a material which resists the penetration of the EM waves through the shield (147). The ability of shielding material to attenuate EM waves is called shielding effectiveness (SE).

The EMI SE of a material is expressed in terms of ratio of incoming (incident) and outgoing (transmitted) power. The EMI attenuation offered by a shield may depend on the three mechanisms: reflection and absorption of the wave as it passes through the shield's thickness and multiple reflections of the waves at various interfaces (Fig.1.8).
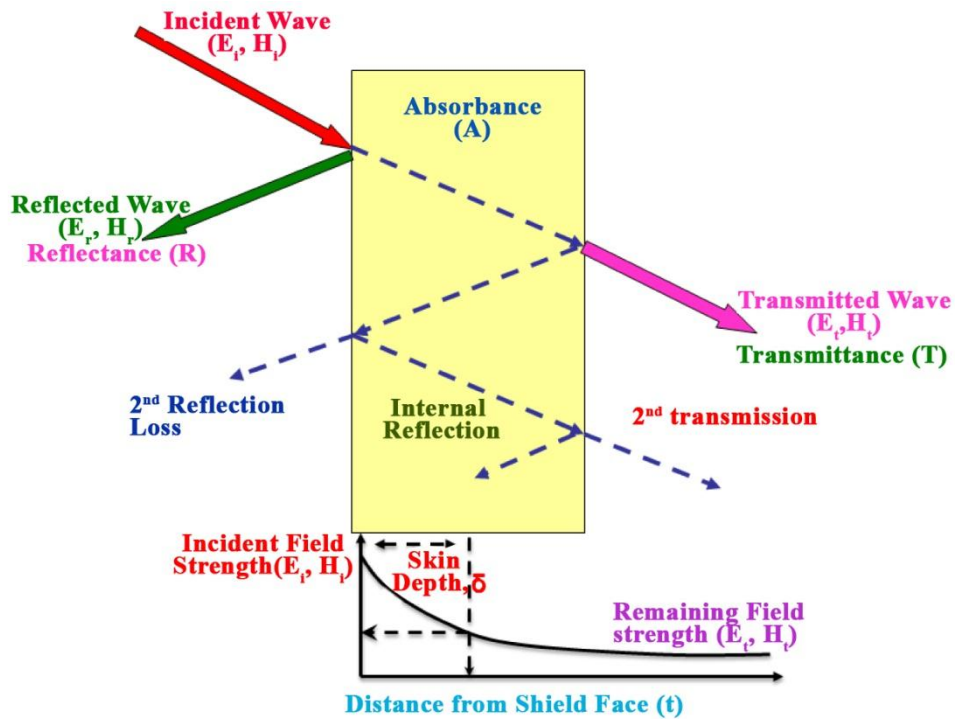

Fig.1.8: The three different mechanisms of EMI shielding

Therefore, SE of EMI shielding materials is determined by three losses viz. reflection loss (SE_R), absorption loss (SE_A) and multiple reflection losses (SE_M) and can be expressed as (148)

$$SE_{TOTAL} = SE_A + SE_R + SE_M = 10 \log_{10} P_I/P_T = 20 \log10 E_I / E_T \ldots\ldots\ldots(1.3)$$

Where P_I is the incident energy field, P_T is the transmitted energy field, and E is the root mean squares of the electric field strengths of the electromagnetic wave. When SE total > 10 dB, SE_M can be neglected (148) and it is usually assumed that

$$SE_{TOTAL} = SE_A + SE_R$$

1.5.2.1 CNT/Polymer composites in EMI Shielding

Metals have excellent capability in attenuating EM waves and initially, metallic components were used for shielding purpose. But certain properties of these metal housing shields such as high density, susceptibility to corrosion, complexity and expensive processing limited their use (149). Metals also reflect radiation and cannot be used in applications where absorption is desired such as in stealth technology. Among the various materials experimented, polymer composites based on CNTs showed great promise. CNTs use both mechanisms of reflection and absorption to attenuate the incident wave. High strength and stiffness, extremely high aspect ratio and good electrical conductivity of CNT make it a filler of choice for shielding applications (31). Despite these advantages, a homogeneous dispersion of CNTs in a polymer matrix is difficult to attain. This results in low electrical conductivity of these nanocomposites. Many

groups have attempted strategies to improve the dispersion of CNTs and thereby improve electrical conductivity. Yang et al. (150) introduced MWCNTs into polystyrene and studied the EMI shielding behavior of the composites. They achieved a SE of 20 dB at 7 wt% MWCNT loading. Saini et al. (151) showed that incorporation of PANI/MWCNT in Polystyrene matrix improved the SE to the range of 23 to 46 dB depending on the chemical composition of PANI/MWCNT filler and shield thickness. Recently the same group (152) had introduced a facile, scalable and commercially viable melt blending approach involving use of twin-screw extruder with melt recirculation provision, for uniform dispersion of up to 4.6 vol% multiwall carbon nanotubes (MWCNTs) within polypropylene random copolymer (PPCP). The improved dispersion led to a very low percolation threshold (0.19 vol %) with a EMI SE value of 47 dB (>99.99% attenuation). Besides this, high tensile strength of 42 MPa and good thermal stability demonstrated its potential for making light weight, mechanically strong and thermally stable EMI shields. According to these reports, parameters such as aspect ratio, conductivity, orientation, dispersion and concentration of NTs influence percolation threshold, conductivity and EMI SE of the polymer composites. The Processing method also has a crucial influence on these parameters. Huang et al. (153) prepared functionalised-MWCNTs/poly (methyl methacrylate) (PMMA) composites by in-situ and ex-situ routes and found that in-situ formed composites give superior SE (17 dB at 12 GHz) at comparative loading than ex-situ formed composites. From the aforementioned discussion, it is evident that in-situ polymerisation is an easy method for obtaining low percolation threshold, high conductivity and high EMI SE.

Scope and objectives of the work

The unique properties of CNTs and intrinsically conducting polymers facilitate their use in organic electronics. But issues such as maintaining a strong interaction between CNTs and ICPs in the composites and retaining the thermal stability of the conductivity remain as major challenges. This thesis aims to tackle these issues. To achieve good compatibility between CNT and PANI, CNTs can be made more polar by attaching appropriate functional groups under mild conditions. Interfacial polymerisation of aniline in presence of CNT can improve interaction between CNTs and PANI. Ideal conductive filler should possess low percolation threshold, high conductivity as well as consistency in conductivity and good mechanical properties for the polymer matrix. Use of these composites in organic devices demands stable and high electrical conductivity.

The objectives of the thesis are to synthesise core-shell nanoparticles of CNT and PANI with high conductivity as well as with good thermal stability of conductivity. These PANI coated CNTs can be used as efficient fillers in polymer matrix making it a candidate material for real applications such as in thermoelectric, strain sensing and EMI shielding.

The objectives of this work are-

- To develop PANI-FMWCNT core-shell nanostructures through interfacial polymerisation process to achieve high and stable electrical conductivity.

- To understand the effect of temperature on conductivity of PANI and PANI-FMWCNT composites doped with different dopants

- To develop PANI-FMWCNT composites with good Seebeck coefficient, high electrical conductivity and low thermal conductivity.

- To develop PANI-FMWCNT/TPU strain sensors with improved sensitivity, gauge factor and reversibility.

- To evaluate the experimental values of strain sensitivity with theoretical values.

- To develop PANI-FMWCNT/TPU composites with high electromagnetic shielding effectiveness along with low percolation threshold, good thermal stability and mechanical properties.

References

[1]   H.W. Kroto, J.R. Heath, S.C. O'Brien, R.F. Curl, R.E. Smalley, *Nature*, 318, 1985, p.6042

[2]   S. Iijima, *Nature*, 56, 1991, p.354.

[3]   R. Saito, G. Dresselhaus, M.S. Dresselhaus, Physical Properties of Carbon Nanotubes, Imperial College Press, London, 1999.

[4]   R.H. Baughman, A.A. Zakhidov, W.A. De Heer, *Science*, 297, 2002, p.787.

[5]   E.T. Thostenson, Z.F. Ren, T.W. Chou, *Compos Sci Technol*, 61, 2001, p.1899.

[6]   M.S. Dresselhaus, G. Dresselhaus, R. Saito, *Carbon*, 33, 1995, p.883.

[7]   P. Avouris, *Chem. Phys*., 281, 2002, p.429.

[8]   T.W. Ebbesen, P.M. Ajayan, *Nature*, 358, 1992, p. 220.

[9]   D.S. Bethune, C.H. Kiang, M.S.de Vries, G. Gorman, R. Savoy, J. Vazquez, R. Beyers; *Nature*, 363, 1993, p.605.

[10]   C. Journet, W.K. Master, P. Bernier, A. Loiseau, M. Lamy de la Chapelle, S. Lefrant, P. Deniard, R. Lee, J.E. Fischer, *Nature*, 388, 1997, p.756.

[11]   D.T. Colbert, J. Zhang, S.M. McClure, P. Nikolaev, Z. Chen, J.H. Hafner, D.W. Owens, P.G. Kotula, C.B. Carter, J.H. Weaver, A.G. Rinzler, R.E. Smalley, *Science*, 266, 1994, p.1218.

[12]   M. Cadek, R. Murphy, B. McCarthy, A. Drury, B. Lahr, R.C. Barklie, M. Panhuis, J.N. Coleman, W.J. Blau, *Carbon*, 40, 2002, p. 923.

[13]   A. Thess, R. Lee, P. Nikolaev, H. Dai, P. Petit, J. Robert, C. Xu, Y.H. Lee, S.G. Kim, A.G. Rinzler, D.T .Colbert, G.E. Scuseria, D. Tomanek, J.E. Fischer, R.E. Smalley; *Science*, 273, 1996, p. 483.

[14]   A.G. Rinzler, J. Liu, H. Dai, P. Nikolaev, C.B. Huffman, F.J. Rodriguez-Macias, P.J. Boul, A.H. Lu, D. Heymann, D.T. Colbert, R.S. Lee, J.E. Fischer, A.M. Rao, P.C. Eklund, R.E. Smalley, *Appl. Phy. A,* 67, 1998, p. 29.

[15]   H.M. Cheng, F. Li, G. Su, H.Y. Pan, L.L. He, X. Sun, M.S. Dresselhaus, *Appl. Phys, Lett.*, 72, 1998, p. 3282.

[16]   C.N.R. Rao, A. Govindaraj, R. Sen, B.C. Satishkumar, *Mater. Res. Innovat.*, 2, 1998, p.128.

[17]   R. Andrews, D. Jacques, A.M. Rao, F. Derbyshire, D. Qian, X. Fan, E.C. Dickey, J. Chen, *Chem. Phys, Lett.*, 303, 1999, p. 467.

[18]   D.S. Bethune, C.H. Kiang, M.S.de Vries, G. Gorman, R. Savoy, J. Vazquez, R. Beyers; Nature, 363, 1993, p. 605.

[19]   T. Guo, P. Nikolaev, A. Thess, D.T. Colbert, R.E. Smalley; *Chem. Phys, Lett.*, 243, 1995, p. 49.

[20]   S .Sinnott, R. Andrews, *crit. rev. solid state mater. Sci.*, 26, 2001, p. 145.

[21]   M. Endo, K. Takeuchi, S. Igarashi, K. Kobori, M. Shiraishi, H.W. Kroto, *J. Phys. Chem. Solids*, 54, 1993, p.1841.

[22] A.M. Benito, Y. Maniette, E. Munoz, M.T. Martinez, *Carbon*, 36, 1998, p.681.

[23] V. Ivanov, J.B. Nagy, P. Lambin, A. Lucas, X.B. Zhang, X.F. Zhang, D. Bernaerts, G. Tendeloo, S. Amelinckx, J. Landuyt, *Chem. Phys. Lett*., 223, 1994, p. 329.

[24] Tans, S.J., A.R.M. Verschueren, and C. Dekker, *Nature*, 393, 1998, p.49.

[25] Rinzler, A.G., J.H. Hafner, P. Nikolaev, L. Lou, S.G. Kim, D. Tomanek, D. Colbert, R.E. Smalley, *Science*, 269, 1995,p.1550.

[26] Dai, H., J.H. Hafner, A.G. Rinzler, D.T. Colbert, and R.E. Smalley, *Nature*, 384, 1996, p.147.

[27] S.M. Lee, Y.H. Lee, *Appl. Phys. Lett*., 76, 2000, p.2877.

[28] P. Kim, C. M. Lieber, *Science*, 286, 1999, p. 2148.

[29] C. Yu, K. Choi, L. Yin, J.C. Grunlan, *ACS nano*, 5, 2011, p. 7885.

[30] P. Dharap, Z. Li, S. Nagarajaiah, E.V. Barrera, *Nanotechnology*, 15, 2004, p.379

[31] M.H. Al-Saleh, U. Sundararaj, *Carbon*, 47, 2009, p.1738.

[32] T. Nishino, T. Ito, Y. Umezawa Y, *Anal. Chem*., 74, 2002, p.4275.

[33] J.P. Salvetat, J.M. Bonard, N.H. Thomson, A.J. Kulik, L. Forro, W. Benoit, L. Zuppiroli; Appl. Phys. A-Mater., 69, 1999, p. 255.

[34] E.W. Wong, P.E. Sheehan, C.M. Lieber, *Science*, 277, 1997, p. 1971.

[35] K.T. Lau, D. Hui, *Compos. Part B-Eng*., 33, 2002, p. 263.

[36] G. Dresselhaus, M.S. Dresselhaus, J. Jorio, *Ann. Rev. Mater. Res.*, 34, 2004, p. 247.

[37] C.L. Kane, E.J. Mele, *Phys. Rev. Lett.*, 78, 1997, p. 1932.

[38]   L.X. Benedict, V.H. Crespi, S.G. Louie, M.L. Cohen, *Phys. Rev. B*, 52, 1995, p.14935.

[39]   S.J. Tans, M.H. Devoret, H. Dai, A. Thess, R.E. Smalley, L.J. Geerligs, C. Dekker; *Nature*, 386, 1997, p. 474.

[40]   T.W. Ebbesen, H.J. Lezec, H. Hiura, J.W. Bennett, H.F. Ghaemie, T. Thio, *Nature*, 382, 1996, p. 54.

[41]   P. Kim, L. Shi, A. Majumdar, and P.L. McEuen, *Phys. Rev. Lett.*, 87, 2001, p. 215502.

[42]   A.B. Kaiser, G.S. Duesberg, S. Roth, *Phys. Rev. B*, 57, 1998, p. 1418.

[43]   M. Cochet, W.K. Maser, A.M. Benito, M.A. Callejas, M.T. Martinez, J.M. Benoit, J. Schreiber, O. Chauvet, *Chem. Commun.*, 40, 2001, p. 1450.

[44]   Li WK, J. Chen, J.J. Zhao, J.R. Zhang, J.J. Zhu, *Mater. Lett.*, 59, 2005, p. 800.

[45]   X.L. Liu, J. Ly, S. Han, D.H. hang, A. Requicha, M.E. Thompson, C.W. Zhou; *Adv. Mater.*, 17, 2005, p. 2727.

[46]   B. Zhao, H. Hu, R.C. Haddon, *Adv. Funct. Mater.*, 14, 2004, p. 71.

[47]   S, Ramesh, L.M. Ericson, V.A. Davis, R.K. Saini, C. Kittrell, M. Pasquali, W.E. Billups, W.W. Adams, R.H. Hauge, R.E. Smalley, *J. Phys. Chem. B*, 108,2004, 8794.

[48]   L. Vaisman, G. Marom, H.D. Wagner, *Adv. Funct. Mater*., 16, 2006, p.357.

[49]   Y. Zhang, Z. Shi, Z. Gu, S. Iijima, *Carbon*, 38, 2000, p. 2055.

[50]   J.B. Baek, C.B. Lyons, L.S. Tan, *J.Mate.Chem.*, 14, 2004, p. 2052.

[51]   I.Y. Jeon, H.J. Lee, Y.S. Choi, L.S. Tan, J.B. Baek, *Macromolecules*, 41, 2008, p.7423.

[52]   C. K. Chiang, C.R. Fincher Jr, Y.W. Park, A.J. Heeger, H. Shirakawa, E.J. Louis, S.C. Gau, and A.G. MacDiarmid; *Phys. Rev. Lett.,* vol. 39, 1977, p. 1098.

[53]   W. Brutting; 'Physics of organic semiconductors', KGaA, Weinheim, Wiley-VCH Verlag GmbH & Co, 2005.

[54]   T.A. Skotheim; Handbook of conducting polymers. CRC Press, 1998.

[55]   A.C. Arias, J.D. MacKenzie, I. McCulloch, J. Rivnay, A. Salleo, *Chem. Rev.*, 110, 2010, p. 3.

[56]   L. Li, Y. Shi, L. Pan, Y. Shia and G. Yu, *J. Mater. Chem. B*, 3, 2015.

[57]   J. Janata and M. Josowicz, *Nat. mater.*, 2, 2003, p. 19.

[58]   H. Yan, N. Sada, and N. Toshima, *J. Therm. Anal. Calorim.* 69, 2002. P. 881.

[59]   C.J. Brabec, N.S. Sariciftci and J.C. Hummelen, *Adv. Funct. Mater.*, 11, 2001, p. 15.

[60]   Y. Wang and X. Jing, *Polymer. Adv. Tech.*, 16, 2005, p. 344.

[61]   D.C. Trivedi, S.K. Dhawan, *J. Mater. Chem.*, 2, 1992, P. 1091.

[62]   S.C. Huang, I.J. Ball, R.B. Kaner, *Macromolecules*, 31, 1998, P. 5456.

[63]   H. Tsutsumi, S. Yamashita, T. Oishi, *J. Appl. Electrochem.*, 27, 1997, p. 477.

[64]   G.G. Wallace, G.M. Spinks, P.R. Teasdale, Conductive Electroactive Polymers, Technomic Publication, Pennsylvania, 1997.

[65]   J.L. Brédas, GB Street, *Acc. Chem. Res.*, 18, 1985, p. 309.

[66]   A.G. MacDiarmid and A.J. Heeger, *Synth. Met.*, 1, 1979/80, P. 101.

[67]   W.P. Su, J.R. Schrieffer, A. Heeger, *J. Phys. Rev. Lett.*, 42, 1979, P. 1698.

[68]   T.C. Clarke, R.H. Geiss, J.F. Kwak, G.B. Street, *J. Chem. Soc., Chem. Commun.,* 12, 1978, 489

[69]   J. Przyluski, S. Roth, *Mater. Sci. Forum*, 42, 1989, P. 17.

[70]   A.J. Heeger, S. Kivelson, J.R. Schrieffer, W.P. Su, *Rev. Mod. Phys.*, 60, 1988, P.781.

[71]   S. A. Brazovskii, N. N. Kirova, *Mol. Cryst. Liq. Cryst.*, 216, 1992, p.151.

[72]   P. Chandrasekhar, Conducting polymers, fundamentals and applications: a practical approach, Kluwer Academic Publishers, 1999.

[73]   J.M.G. Cowie, Chemistry and Physics of Modern Materials, IInd Ed. Blackie, USA, Chapman and Hall, New York, 1973.

[74]   V.N. Prigodin, AJ Epstein - *Physica B*, 338, 2003, p. 310.

[75]   A. Nabok, Organic and inorganic nanostructures, Artech House, 2005.

[76]   J. Hirsch, *J. Phys. C Solid State*, 12, 1979, p. 321.

[77]   Electronic Porcesses in Non-Crystalline Materials, 2nd ed; N.F. Mott, E.A. Davis, Eds.; Oxford: Claredon, 1979.

[78]   A.J. Epstein, H. Rommelmann, R. Bigelow, H.W. Gibson, D.M. Hoffmann, D.B. Tanner, *Phys. Rev. Lett.*, 50, 1983, p.1866.

[79]   S. Bhadra, D. Khastgir, N.K. Singha and J.H. Lee, *Prog. Polym. Sci.*, 34, 2009, p. 783.

[80]   A.G. MacDiarmid, J.C. Chiang, A.F. Richter, and A.J. Epstein, *Synth. Met.*, 18, 1987, p. 285.

[81]   E.M. Genies, A. Boyle, M. Lapkowski, and C. Tsintavis, *Synth. Met.*, 36, 1990, p. 139.

[82]   E. Kang, K. Neoh and K. Tan, *Prog. Polym. Sci.*, 23, 1998, p. 277.

[83]   F. Lux, *polymer*, 35, 1994, p. 2915.

[84]   J. Chiang, A. Mac Diarmid, *Synth. Met.*, 13, 1986, p.193.

[85]   A. Pron, P. Rannou, *Prog. Polym. Sci.*, 27, 2002, p.135.

[86]   S. Srivastavaa, S.S. Sharmaa, S. Agrawala, S. Kumara, M. Singha, Y.K. Vijaya, *Synth.Met.*, 160, 2010, p. 529.

[87]   N. Chandrakanthi, M.A. Careem, *Polym. Bull.*, 44, 2000, p.101.

[88]   A.L. Cabezas, Y. Feng, L. Zheng, Z. Zhang, *Carbon*, 5 9, 2 0 13, p. 2 7 0.

[89]   X. Zhang, J. Zhang, Z. Liu, *Appl. Phys. A*, 80, 2005, p. 1813.

[90]   L. Li, Z.Y. Qin, X. Liang, Q.Q. Fan, Y.Q. Lu, W.H. Wu, M.F. Zhu, *J. Phys. Chem. C*, 113, 2009, p. 5502.

[91]   B. Zhao, H.Hu, R.C. Haddon, *Adv. Funct. Mater.*, 14, 2004, p. 71.

[92]   M. Cochet, W.K. Maser, A.M. Benito, M.A. Callejas, M.T. Martínez, J.M. Benoit, J. Schreiber, and O. Chauvet, *Chem. Commun.*, 16, 2001, p. 1450.

[93]   J. Xu, P. Yao, L. Liu, Z. Jiang, F. He, M. Li, J. Zou, *J. Appl. Polym. Sci.*, 118, 2010, p. 2582.

[94]   W. Feng, X.D. Bai, Q. Lian, J. Liang, X.G. Wang, K. Yoshino, *Carbon*, 41, 2003, p.1551.

[95]   B. Philip, J. Xie, J.K. Abraham and V.K. Varadan, *Polym. Bull.*, 53, 2005, p. 127.

[96]   R.V. Salvatierra, M.M. Oliveira, and A.J.G. Zarbin, *Chem. Mater.* 22, 2010, p.5222.

[97]   B. Gao, Q. Fu, L. Su, C. Yuan, X. Zhang, *Electrochim. Acta*, 55, 2010, p. 2311.

[98]   I.Y. Jeon, L.S. Tan and J.B. Baek, *J. Polym. Sci.*, vol.48, 2010, p. 1962.

[99]   H.J. Choi, I.Y. Jeon, S.W. Kang, J.B. Baek, *Electrochim. Acta*, 56, 2011, p. 10023.

[100] Y. Wang and M.F. Rubner, *Synth. Met.*, 47, 1992, p.255.

[101] J. Prokes, I. KrÏivka, E. Tobolkova, J. Stejskal, *Polym. Degrad. Stab.*, 68, 2000, P.261.

[102] J. Prokes, J. Stejskal, *Polym. Degrad. Stab*, 86, 2004, p.187.

[103] J. Prokes, M. Trchova, D. Hlavata, J. Stejskal, *Polym. Degrad. Stab.*, 78, 2002, p.393.

[104] P. Rannou, M. Nechtschein, J.P. Travers, D. Bernera, A. Walter and D. Djurado, *Synth. Met.*, 101, 1999, p.734.

[105] M.O. Ansari, F. Mohammad, *Compos. Part B-Eng.*, 43, 2012, p.3541.

[106] A.L. Cabezas, Y. Feng, L.R. Zheng and Z.B. Zhang, *Carbon*, 59, 2013, p.270.

[107] G.Chen, M.S.Dresselhaus, G.Dresselhaus, J.P.Fleurial and T.Caillat, *Int. Mater. Rev*., 48, 2003, p. 45.

[108] D.M. Rowe, CRC Handbook of Thermoelectrics; CRC Press: Boca Raton, 1995.

[109] C. Yu, Y.S. Kim, D. Kim, J.C. Grunlan, Nano Lett., 8, 2008, p.4428.

[110] K.C. See, J.P. Feser, C.E. Chen, A. Majumdar, J.J. Urban and R.A. Segalman, *Nano Lett.*, 10, 2010, p. 4664.

[111] Q. Yao, L. Chen, X. Xu and C. Wang, *Chem. Lett.*, 34, 2005, p. 522.

[112] D. Kim, Y. Kim, K. Choi, J.C. Grunlan and C. Yu, in *ACS Nano*, 4, 2010, p.513.

[113] H. Yan, N. Ohta, N. Toshima, *Macromol. Mater. Eng.*, 286, 2001, p.139.

[114] C. Meng, C. Liu, S. Fan, *Adv. Mater.*, 22, 2010, p. 535.

[115] Q. Yao, L. Chen, W. Zhang, S. Liufu, X. Chen, *ACS Nano*, 4, 2010, p. 2445.

[116] R.C.Y. King, F. Roussel, J.F. Brun, C.Gors, *Synth. Met.*, 162, 2012, p. 1348.

[117] J.H. Kong, N.S. Jang, S.H. Kim, J.M. Kim, *Carbon*, 77, 2014, p.199.

[118] T.K. Gupta, B.P. Singh, S. Teotia,V. Katyal, S.R. Dhakate & R.B. Mathur, *J. Polym .Res.,* 20, 2013, p.169.

[119] Z. Liu, G. Bai, Y. Huang, Y. Ma, F. Du, F. Li et al., *Carbon*, 45, 2007, p. 821.

[120] L.T.J. Korley, S.M. Liff, N. Kumar, G.H. McKinley and P.T. Hammond, *Macromolecules*, 39, 2006, p.7030.

[121] H. Deng, L. Lin, M. Ji, S. Zhang, M. Yang, Q. Fu, *Prog. Polym. Sci.*, 39, 2014, p. 627.

[122] A.K. Barick, D.K. Tripathy, *Mater. Sci. Eng.*, 176, 2011, p. 1435.

[123] A.M.F. Lima, V.G. Castro, R.S. Borges, G.G. Silva, *Polímeros*, 22, 2012, p.117.

[124] J. Hwang, J. Jang, K. Hong, K.N. Kim, J.H. Han, K. Shin, C.E. Park, *Carbon*, 49, 2011, p.106

[125] D.S. Vicentini, G.M.O. Barra, J.R. Bertolino, A.T.N. Pires, European Polymer Journal, 43, 2007, p. 4565.

[126] K. Lakshmi, H. John, K.T. Mathew, R. Joseph, K.E. George, *Acta Mater.*, 57, 2009, p.371.

[127] D. Stauffer and A. Aharony, Introduction to Percolation Theory, Second ed. London, Taylor & Francis; 1992, p. 17.

[128] B.E. Kilbride, J.N. Coleman, J. Fraysse, P. Fournet, M. Cadek, A. Drury, S. Hutzler, S. Roth, W.J. Blau, *J. Appl. Phys*., 92, 2002, P. 4024.

[129] M. Weber and M.R. Kamal, *Polym. Compos.,* 18, 1997, p.711.

[130] W. Bauhofer, J. Kovacs, Compos. Sci. Technol., 69, 2009, p.1486.

[131] J.S. Wilson, Sensor technology handbook, Newnes, 2005.

[132] H. Bottger and V.V. Bryksin: 'Hopping conduction in solids', VCH, Deerfield Beach, FL, 1985.

[133] E.K. Sichel, Carbon black-polymer composites Plastics engineering 1982, Dekker, New York.

[134] Y.H. Lee, D.H. Kim, H. Kim, B.K. Ju, *J. Appl. Phys.*, 88, 2000. P. 4181.

[135] P. Sheng, E.K. Sichel, J.I. Gittleman, *Phys. Rev. Lett*., 40,1978. P.1197.

[136] R. Zhang, Conductive TPU/CNT composites for strain sensing, PhD thesis, Queen Mary, University of London, London, 2009.

[137] M. Knite, V. Teteris, A. Kiploka and J. Kaupuzs, Sensor Actuat. A-Phys., 110, 2004, p. 142.

[138] R. Zhang, M. Baxendale, T. Peijs, Phys. Rev. B, 76, 2007, 195433.

[139] P. Costa, A. Ferreira, V. Sencadas, J.C. Viana and S. Lanceros-Méndez, *Sensor Actuat. A-Phys.*, 201, 2013, p. 458.

[140] I. Kang, M.A. Khaleque, Y. Yoo, P.J. Yoon, S.Y. Kim, K.T. Lim, *Compos. Part A:Appl. Sci.* 42, 2011, p. 623.

[141] P. Slobodian, P. Riha, P. Saha, *Carbon*, 50, 2012, p. 3446.

[142] J.R.B. Quijano, F. Aviles, J.V.C. Rodriguez, *J. Appl. Polym. Sci.*, 130, 2013, p. 375.

[143] R. Zhang, H. Deng, R. Valenca, J. Jin, Q. Fu, E. Bilotti and T. Peijs, *Compos Sci Technol*.74, 2013, p. 1.

[144] E. Bilotti, R. Zhang, H. Deng, M. Baxendale, T. Peijs, *J. Mater Chem*., 20, 2010, p. 9449.

[145] L. Lin, S. Liu, Q. Zhang, X. Li, M. Ji, H. Deng, Q. Fu, *ACS Appl. Mater. Inter*., 5, 2013, p. 5815.

[146] M.I. Montrose, EMC and the Printed Circuit Board, New York, John Wiley & Sons, 1999.

[147] D.D.L. Chung, *Carbon*. 39, 2001, p. 279.

[148] N.F. Colaneri, L.W. Shacklette, *IEEE Trans Instrum. Meas*., 41, 1992, p.291.

[149] J.C. Huang, *Adv. Polym. Technol*. 14, 1995, p. 137.

[150] Y. Yang, M.C. Gupta, K.L. Dudley, R.W. Lawrence RW, *Nano Lett*.,5, 2005, p.2131.

[151] P. Saini, V. Choudhary, B.P. Singh, R.B. Mathur, S.K. Dhawan, *Synth. Met*.,161,2011,p.1522

[152] P. Verma, P. Saini, R.S. Malik, V. Choudhary, *Carbon*, 89,2015, p.308

[153] Y.L. Huang, S.M. Yuen, C.M. Ma, C.Y. Chuang, K.C. Yu, C.C.Teng, *Compos. Sci. Technol*., 69, 2009, p.1991.

.....౪ఇఴ.....

Chapter **2**

MATERIALS AND CHARACTERIZATION TECHNIQUES

This chapter describes the materials and methods used for characterising the composites under investigation.

2.1 Materials

Thermoplastic polyurethane (TPU), (Estane 58315, an 85A aromatic polyether based TPU) was supplied by Lubrizol Advanced Materials, Cleveland, Ohio. The specific gravity is 1.12.

Multi-walled carbon nanotubes (MWCNT) were obtained from Nanoshel LLC, USA. They were of 95% purity with a diameter of 15-30 nm and length 30-50µm.

Aniline was purchased from Merck Specialities Pvt. Ltd. Mumbai and was double distilled before use.

Ammonium persulphate (APS), naphthalene-2-sulfonic acid (NSA), hydrochloric acid (HCl), 4-aminobenzoic acid, polyphosphoric acid (PPA), phosphorous pentoxide (P_2O_5), chloroform ($CHCl_3$) and tetrahydrofuran

(THF) were purchased from S.D. Fine Chem, Mumbai, India, and were used without further purification. All solutions were prepared in distilled water.

2.2 Characterization techniques

A detailed account of the characterization techniques employed in elucidating the various sample properties is being portrayed.

2.2.1 Morphology studies

The morphology and microstructure of the samples have been investigated through the following microscopy techniques.

2.2.1.1 Scanning Electron Microscope (SEM)

Scanning electron microscope (SEM) was used to examine the morphology of the pristine MWCNT, FMWCNT, synthesized PANI, FMWCNT-PANI and FMWCNT-PANI/TPU samples. Research in ICPs and CNT-polymer composites has utilized SEM to investigate the presence of nanostructures on the polymer surface as well as embedded into the polymer matrix. The samples were mounted on SEM stubs using carbon tape and then sputter coated with a thin layer of gold to avoid charging during analysis. In a typical SEM, an electron beam and a beam in a cathode ray tube is simultaneously scanned across the surface of the sample. A signal is then produced by scattered electrons resulting in an image with a three dimensional appearance (1).

The SEM images were obtained using a JEOL model JSM 6390 LV and JEOL JSM-5600 LV scanning electron microscope. An accelerating voltage ranging from 10- 30 kV, was used depending on different imaging

purposes. Images were located at multiple locations to assess the dispersion, homogeneity and agglomeration of CNTs.

2.2.1.2 Field Emission Scanning Electron Microscope (FESEM)

The microstructure of the FMWCNT-PANI/TPU composites was observed using Hitachi SU6600 Variable Pressure Field Emission Scanning electron microscope (FESEM), which gave better images compared to conventional SEM. Here a field emission gun provided very narrow probing beams with high as well as low energies, providing an improved spatial resolution, minimal sample damage and charging. This helped to get very clear, less electrostatically distorted and high resolution images. The microscope was operated at an accelerating voltage of 20 kV. The top surface was directly observed with SEM. As a higher accelerating voltage was used in this case, the CNTs in the composite could be charged by this voltage and emit enriched secondary electrons (2). FESEM image of the composite could give some insight on the dispersion/agglomeration states of the CNTs in the TPU matrix.

2.2.1.3 Transmission Electron Microscope (TEM)

High-resolution images were obtained with transmission electron microscope (TEM). TEM was used to determine the dispersion, alignment and coating thickness of PANI on CNTs. Also the length and diameter of individual filler particles could be obtained. In TEM, the principle involves an electron beam, which is transmitted through a specimen that must be less than 200 nm thick, in a stable high vacuum system (3, 4). The samples could be magnified between 100-100,000 times. TEM provided very useful information for crystalline materials while amorphous materials are more

difficult to analyze using the TEM. TEM was performed in a JEOL 300 KV HRTEM microscope with an accelerating voltage of 200 kV. The samples were prepared by dropping an N-methylpyrrolidinone (NMP) dispersion of sample on standard copper grids covered by a thin film of amorphous carbon.

2.2.2 Spectroscopy

2.2.2.1 Raman Spectroscopy

Raman Spectroscopic measurements of the samples were recorded in the range $200cm^{-1}$ -$1800cm^{-1}$ with a Bruker RFS27 R spectrometer using Nd: YAG laser with a 100mW operating at 1064nm.

Raman spectroscopy is based on Raman Effect which is related to the scattering of light when a monochromatic radiation passes through a transparent substance. It is one of the most powerful tools for analysis and identification of molecular structure, effects of bonding environment etc. on materials ranging from carbon nanotubes to polymers. The G band, located near 1600 cm^{-1}, could be used to determine the orientation of the carbon nanotubes in a composite by measuring the Raman spectra at angles 0-90°. The G band peak also allowed the determination of the carbon nanotube type, metallic or semiconducting, of the carbon nanotube being observed. The peak broadens for semiconducting tubes and narrows for metallic tubes, allowing the tube type to be distinguished (5). The D-band, which is found in the range of 1250 – 1450 cm^{-1}, is due to the defects within the graphitic structure of carbon nanotubes. This band illustrated the differences between a perfect carbon nanotube (low intensity) and an imperfect carbon nanotube (high intensity). Hence this peak also changes with the functionalization of carbon nanotubes. The presence of CNTs in the PANI/MWNT composites,

the interactions between PANI and CNTs could be indicated by Raman spectroscopy(6).

2.2.2.2 Fourier Transform Infrared Spectroscopy(FTIR)

FTIR spectroscopy is employed for the identification of functional groups in FMWCNT, PANI and FMWCNT-PANI and analysis of interaction between CNT and PANI. The infrared (FTIR) spectra of samples were recorded from KBr sample pellets using a Nicolet Magna-5700 spectrometer with a resolution of 4 cm^{-1}.

Fourier Transform Infra-Red (FTIR) spectroscopy is an important tool for structural elucidation and identification of various types of materials. In this method, the infrared radiation is (400-4000cm^{-1}) is passed through the sample where some of it gets absorbed and some transmitted. All molecules have specific frequencies at which they rotate or vibrate corresponding to discrete energy levels. As the different functional groups absorb at their unique characteristic frequencies, the resulting spectrum representing the molecular absorption and transmission, is a molecular fingerprint of the sample (7).

2.2.2.3 Ultra Violet -Visible (UV-Vis) Spectroscopy

UV–Vis spectroscopy was carried out on FMWCNT-PANI composites to study the interfacial interaction between the two. The analysis was performed on a double beam spectrophotometer (UV-3010). The samples were ground into a fine powder and then dispersed in NMP to form a stable dispersion (0.005mgml^{-1}).

The absorption of light in the ultraviolet (l0 - 420 nm) and visible (420-700 nm) regions by a sample is measured in Ultraviolet–visible spectroscopy. The absorption of light in this region depends on the nature of chemical groups present in the structure. When a radiation of energy in the UV-Vis region falls on the sample, there can be various possible transitions which are σ-σ*, n-σ*, π-π* and n-π* depending on the sample under analysis. Among these transitions, n-π* transition requires the least amount of energy and gives rise to an absorption band at longer wavelengths (8). By analyzing the UV-Vis absorption spectra of materials, it is possible to estimate the absorption coefficient α, direct and indirect band-gap energies and the density of states.

2.2.3 X-Ray Powder Diffraction (XRD) Analysis

XRD of FMWCNT, FMWCNT-PANI composites were performed using a Bruker AXS D8 Advance X-ray Powder Diffract meter using CuK_α radiation (λ = 1.54 A°). XRD results were obtained in the range 2Θ = 3° to 60° at a scan rate of 4 °/min. A tube current of 25mA and an accelerating potential of 35kV was applied to the X-ray tube.

XRD is an important tool for analyzing crystal structures and atomic spacing. The structure determination is based on the interference of monochromatic X-rays and the crystalline sample (9). In XRD, X-Rays are impinged and reflected X-Rays are collected at a known angle relative to the sample (10). The scattered beam is used to determine the atomic structure of the lattice. For an incident ray, at an angle θ, according to Bragg's equation, path difference is given by,   nλ = 2d sin θ

Where, n is an integer, d is the distance between atomic layers in the crystal, λ is the wavelength, and θ is the angle of incidence.

If Bragg's equation is satisfied, a peak will be observed. By comparing the obtained peaks in the XRD pattern to database information about crystalline structures, the material could be identified. For polymers, as they contain both crystalline and amorphous regions, the X-ray diffraction patterns may contain a mixture of sharp and diffused patterns. Hence the diffractograms contains sharp peaks, corresponding to the ordered regions and the diffused and broader portions corresponding to the irregular ones. It is well-established that for intrinsically conducting polymers, crystallinity has a significant influence on the conductivity retention. At elevated temperature, conductivity ageing happens to amorphous regions easily when compared to the crystalline regions.

2.2.4 Thermogravimetric (TGA) Analysis

TGA of MWCNT, FMWCNT and FMWCNT-PANI composites was performed on a Q 50, TA Instruments Thermogravimetric Analyser with a programmed heating of 10°C/min starting at room temperature and proceeding up to 800°C in atmospheric air. The thermal stability of FMWCNT-PANI/TPU samples in the present study was determined under nitrogen atmosphere.

Thermo-gravimetric analysis (TGA) is a technique to analyze the thermal stability of materials. The materials are heated to degradation and the weight of the sample as a function of temperature (and/or as a function of time) with a controlled temperature program was recorded (11). Sample

and reference were heated by a single source and the temperatures are measured by thermo couples embedded in the sample and reference, and attached to their pans. A derivative weight loss is plotted against temperature to understand the point where the weight loss is maximum. The purity and composition of a sample can be determined using this technique.

2.2.5 DC Conductivity Measurements

In this work, the DC conductivity measurements were performed using two setups.

1. For PANI and FMWCNT-PANI composites, whose conductivity is more than 10 S/m, the conductivity of pellets were measured using the standard four-probe method using a Keithley 6881 programmable current source and a 2128 A nano-voltmeter supplied by Keithley, as per the standard procedure ASTM F 43-99. The powdered samples were compressed into pellets of 13mm diameter and about 1-2mm thick disk using a hydraulic press operated at a pressure of 200 MPa. The conductivities of the samples were measured at three different positions, and an average of nine readings was used for conductivity calculations. The conductivity (σ) was calculated using Van der Pauw relation

$$\sigma = \frac{\ln 2}{\pi \times d} \times \frac{I}{V}$$

Where d is the thickness of the disc, I is the current and V is the voltage. A constant current was passed with a direct current (DC) voltage source through two outer electrodes and an output voltage was

measured across the inner electrodes with the voltmeter. The pelleted sample was placed in a temperature controlled chamber before the measurement.

To investigate the stability of DC Conductivity of samples at elevated temperature, the pelleted samples were subjected to cyclic thermal ageing and isothermal accelerated ageing. In cyclic thermal ageing, the temperature of the sample pellet was raised from 30°C to 150°C and cooled back to 30°C. DC conductivity was measured at every 10°C intervals. This constituted one cycle. The duration of one cycle is about 4hours. The pellet was cooled for 90 minutes. Four more cycles were performed on the same pellet. In isothermal ageing studies, the pellets were heated to 50, 80, 110, and 140°C in the thermostatted chamber. The DC conductivity measurements were performed at an interval of 15 minutes.

2. For FMWCNT-PANI /TPU samples, whose conductivity is less than 10 S/m, the DC conductivity of the composites was measured by a standard two-probe electrode configuration using a Keithley 2400 nano voltmeter. Conductivity of the unstrained samples was calculated using the formula

$$\sigma = \frac{L}{R \times T \times W}$$

Where σ is the electrical conductivity in S/m, L is the sample's length in m, W is the sample width in m, T is the thickness in m, and R is the measured resistance in Ω.

2.2.6 Thermal Conductivity Measurements

An improved photo pyroelectric technique (12) was used to determine the thermal conductivity of the composites. A 70 mW He-Cd laser with a wavelength of 442 nm, intensity modulated by a mechanical chopper (SRS Model, SR540), was used as the optical heating source. A PVDF film with a thickness of 28 lm with Ni-Cr coating on both sides was used as the pyroelectric detector. The output signal was measured with a lock-in amplifier (SRS Model, SR830). The modulation frequency was kept above 60 Hz to ensure that the detector, sample, and the backing medium were all thermally thick during the measurements. In the experiment we measured the variations of the pyroelectric signal amplitude and phase with modulation frequency. The thermal diffusivity and thermal effusivity of the samples were then derived from these. From the values of thermal diffusivity and thermal effusivity, the thermal conductivity of the samples were calculated.
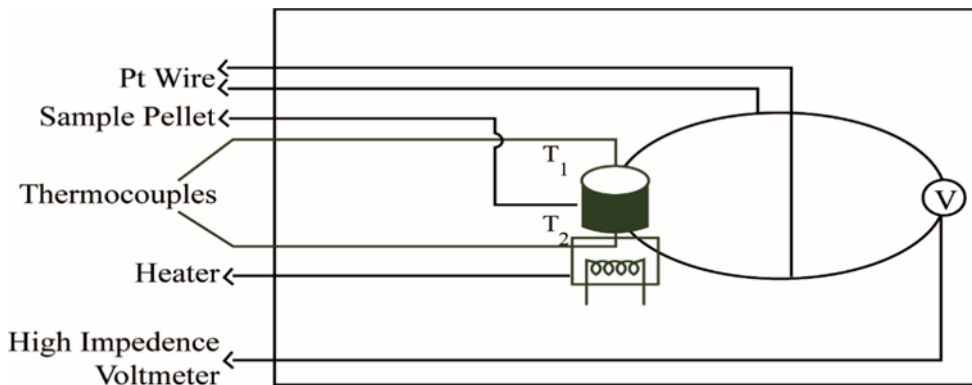
2.2.7 Seebeck coefficient Measurements

Fig. 2.1: Experimental set up for measurement of Seebeck coefficient

Seebeck coefficient (S) values were measured based on the differential method. S values were measured by mounting the sample between two silver blocks. One of the block acts as hot side and the other as cold side. A temperature gradient was maintained across the sample. It was measured using thermocouples. Silver wires were electrically connected to the Ag blocks and the voltage drop was measured with them (Fig. 2.1) (13). Seebeck coefficient was measured by applying a constant temperature difference of 10K between the two phases of the pellet from 295K to 355K. The potential difference (ΔV) was measured and Seebeck coefficient at temperature (T) was obtained as $S = -\Delta V / \Delta T$.

2.2.8 Measurement of strain sensing properties

The strain sensitivity measurements were performed on a Shimadzu Universal Testing Machine (model AG-I) coupled with the Keithley 2400 nanovoltmeter (Fig. 2.2). The composite films were clamped between copper electrodes, creating a gauge length of 50mm. The samples were stretched at the tensile speed of 2mm/min. A constant current was passed along the axial direction of the film and the corresponding resistance (R) was systematically measured for various strains. The resistivity (ρ) was calculated using the formula

$$\rho = \frac{R \times T \times W}{L}$$

In order to study the strain sensing reproducibility of the composite films, twenty elongation/ contraction cycles were conducted. Cyclic deformation consisted of stretching to 20% strain at the tensile speed of 2 mm/min and then releasing to the initial position.
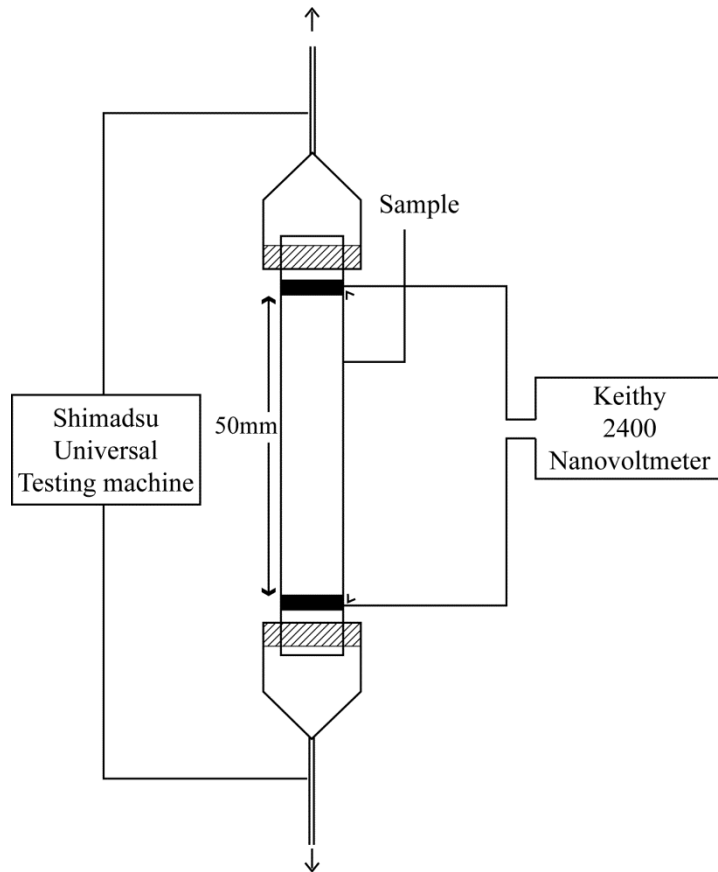
Fig. 2.2: Experimental set-up for measurement of electrical resistance R of the composite sample as function of tensile strain.

2.2.9 Tensile Analysis

Mechanical properties of TPU nanocomposites were studied using a Shimadzu Universal Testing Machine (model AG-I) with a load cell of 10 kN capacity. The specimens used were dump bell shaped. The gauge length between the jaws at the start of each test was adjusted to 40 mm and the measurements were carried out at a crosshead speed of 150 mm/min at room temperature (30°C).

The ability of a material to resist breaking under tensile stress is an important property of elastomers. The force per unit area required to break a material in such a manner is called the tensile strength. The tensile modulus is the ratio of stress to elastic strain in tension. The elongation at break is the percentage increase in length that occurs before it breaks under tension. Ultimate elongation values of several hundred percent are common for elastomers. The combination of high tensile strength and high elongation leads to materials of high applicability.

2.2.10 Dynamic Mechanical Analysis (DMA)

Dynamic mechanical analyser (DMA Q-800, TA Instruments) was used to study viscoelastic properties of TPU/CNT composites. Rectangular shaped specimens of approximately 6mm × 1.5mm × 0.5mm size were used. The samples were tested under tension mode at a frequency of 1 Hz over a temperature range of -60°C to 60°C. The temperature ramp was kept at 5$^{\mathrm{o}}$C/min.

2.2.11 Measurement of EMI shielding efficiency

The EMI shielding efficiency (SE) measurement was performed with a ZVB20 vector network analyzer (VNA) in the frequency range of 8 to 12 GHz (X-band). The rectangular samples of 1mm thickness were inserted into rectangular sample holder which matches the internal dimensions of X-band waveguide. Figure 2.3 shows a schematic diagram of network analyzer used to measure the EMI shielding properties. A network analyzer consists of a signal source, a receiver and a display. The source dispatches a signal at a single frequency to the material under test (MUT). The receiver is adjusted to that frequency to detect the reflected and transmitted waves from

the material. Scatter parameters, also called S-parameters, were used to calculate shielding parameters in a two-port EMI shielding setup. The S-parameters describe the performance of a two-port EMI shielding setup completely (14).
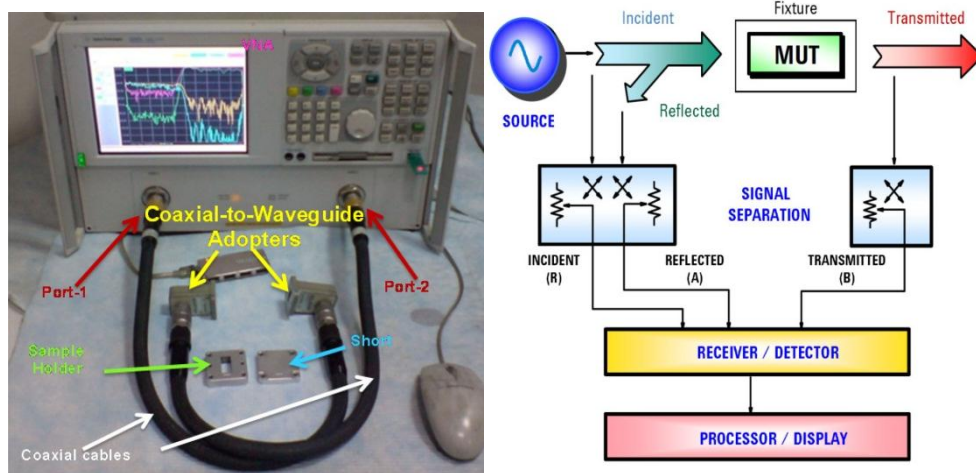

Fig. 2.3: Two port VNA (left) and its internal block diagram (right) (15)

The S-parameters are defined as,

$| S_{11} |$: Reflected voltage magnitude divided by the incident voltage magnitude in port 1

$| S_{12} |$: Transmitted voltage magnitude from port 2 to port 1 divided by incident voltage magnitude in port 2

References

[1]   M.P. Stevens, Polymer Chemistry: an Introduction, 3rd Ed. New York: Oxford. Oxford University Press, New York, 1999.

[2]   J. Loos, A. Alexeev, N. Grossiord, C. E. Koning, O. Regev, *Ultramicroscopy*, 104, 2005, p.160.

[3] D.B. Williams, D.B. and C.B. Carter, Transmission Electron Microscopy: A Text book for Materials Science, Plenum Press, New York, 1996.

[4] M. Shahinpoor , K. J. Kim, *Smart. Mater. Struct.*, 14, 2005,p.197.

[5] C.A. Cooper, R.J. Young, M. Halsall, *Composites Part A*, 32,2001, p.401.

[6] J. R. Wood, Q. Zhao, H. D. Wagner, Composites Part A, 32, 2001, p.391.

[7] Banwell and McCash, Fundamentals of Molecular Spectroscopy, Tata McGraw Hill Publishing Company Ltd., 4th edn., New Delhi,1995.

[8] Perkampus and Heinz-Helmut, UV-VIS Spectroscopy and Its Applications, Springer-Verlag, 1992.

[9] J. Als-Nielsen, D. McMorrow, Elements of Modern X-Ray Physics, Wiley, New York, 2001.

[10] B.D. Cullity and S.R. Stock, Elements of X-ray Diffraction, Prentice Hall, New Jersey, 2001.

[11] B.Wunderlich, Thermal Analysis, Academic Press, 1990.

[12] C.Janardhanan, D.Thomas, G. Subodh, S. Harshan, J.Philip, M.T. Sebastian, *J. Appl. Polym. Sci*., 124, 2012, p.3426.

[13] V. Ponnambalam, S. Lindsay, N.S. Hickman, and T.M. Tritt*, Rev. Sci. Instrum.,* 77, 2006, p.073904.

[14] M. Arjmand, Calgary, AB, Canada, University of Calgary, PhD Thesis, 2014.

[15] P. Saini, M. Arora, cdn.intechopen.com, 2012.

.....ೞೞ.....

Chapter **3**

PANI AND FMWCNT-PANI COMPOSITES THROUGH INTERFACIAL POLYMERISATION - STUDY OF DC CONDUCTIVITY AND CONDUCTIVITY RETENTION*

MWCNTs were functionalised under mild reaction conditions. Nanocomposites of FMWCNT and PANI were synthesised through dynamic interfacial polymerization process, with varied CNT content ranging from 0 to 1g. Presence of CNTs influenced polymerisation of aniline. SEM and TEM results indicated that interfacial polymerisation in presence of CNT induced formation of a tubular composite with thin PANI coating on the surface of CNTs. With 12.9% CNT, polymerisation of aniline was mostly on the surface of CNTs. DC conductivity of this composite showed highest improvement. The composite as well as PANI was protonated with different dopants.

The high temperature DC conductivity stability was investigated through cyclic thermal ageing and isothermal ageing studies. Composites exhibited good retention in conductivity. Both PANI and composites containing NSA and TSA had a higher thermal stability of electrical properties. On thermal cyclic treatment up to 150°C, electrical conductivity for PANI samples rapidly dropped to 42–59% of their initial values, while PANI-FMWCNT samples showed only 80–87% decrease after the fifth cycle. Isothermal ageing studies also supported improved thermal stability of conductivity in composites. FTIR spectra showed effective site-selective interactions between the quinoid ring of PANI and CNTs. TGA analysis confirmed strong interaction between PANI chains and CNTs. The role of CNTs and dopants in stabilising the DC conductivity of composites at elevated temperature is discussed.

3.1 Introduction

Application of PANI and MWCNT based PANI composites in hi-tech areas such as electrochemical displays, sensors, thermoelectrics, catalysis, capacitors, anti-corrosion coatings, electromagnetic shielding, and secondary batteries are dependent on their consistency in conductivity. Earlier studies on thermal ageing of DC conductivity are few on PANI and its composites. The studies revealed that conductivity ageing for PANI occurred at elevated temperatures and attributed the reason to deprotonation, oxidation and cross linking reactions among PANI molecules (1-3). The high temperature conductivity stability of composites is influenced by factors such as the method of polymerisation, dopants used etc., an area which has not been critically viewed so far.

This work aims at the synthesis of a highly ordered PANI chain on MWCNTs which can remain unperturbed upon heating and retain conductivity at high temperature. PANI and MWCNT-based PANI composites were synthesised by dynamic interfacial oxidative polymerisation using ammonium persulphate (APS) as oxidant with various dopants. Dynamic interfacial method was used here because static interfacial method cannot incorporate whole of the nanotubes as some of them will settle down at the bottom of the reaction vessel. For the synthesis of homogeneous composites, the MWCNTs were functionalised with 4-aminobenzoyl functional groups by Friedel craft's reaction under mild reaction conditions as per method proposed by Lee et al. (4). This functionalisation method is unique in diminishing damages to MWCNT while retaining its electrical conductivity. Conductivity of these systems depends upon doping and the dopant used.

The effect of various dopants on DC conductivity of various samples at elevated temperature is investigated. Inorganic acids such as hydrochloric acid (HCl), sulphuric acid (H_2SO_4) and organic sulfonic acids like paratoluenesulphonic acid (TSA), naphthelene-2-sulfonic acid (NSA) were used as dopants. A series of interfacial polymerisations of PANI on FMWCNT was performed in an aqueous-organic interface to understand the effects of FMWCNT/Aniline ratio on morphology and DC conductivity of the composite samples. The high temperature DC conductivity stability was investigated through cyclic accelerated ageing and isothermal ageing studies.

3.2 Experimental Procedure

3.2.1 Functionalisation of MWCNTs

The 4-aminobenzoyl functionalised MWCNTs was synthesised via direct Friedel-Crafts acylation in a mild polyphosphoric acid/phosphorous pentoxide medium as per the method by Lee (4). 20g MWNT, 40g 4-aminobenzoic acid, 600g PPA and 150g P_2O_5 were placed in a resin flask equipped with high-torque mechanical stirrer, nitrogen inlet and outlet. The flask, immersed in oil bath was gently heated to 100°C and the reaction mixture was stirred for 1 h. The reaction mixture was then heated to 130°C and stirred for 72 h under nitrogen atmosphere. The dark homogeneous mixture was poured into water. The precipitate was collected by suction filtration and soxhlet extracted using distilled water for the first 3 days, followed by methanol for another 3 days. The precipitate was finally freeze-dried for 48 h. The resultant 4-aminobenzoyl functionalised multi-walled carbon nanotubes are termed FMWCNT.

3.2.2 Synthesis of PANI and PANI- FMWCNT composites through dynamic interfacial polymerisation method

Synthesis of PANI and PANI-FMWCNT composite samples involves polymerisation of aniline in a water/chloroform interface with ammonium per sulphate (APS) as oxidant. Aniline and CNTs were in the organic phase and APS in the aqueous phase. Six samples of nanocomposites were synthesised by varying the CNT amount and fixing the amount of aniline. Different amounts (0, 0.2 g, 0.4 g, 0.6 g, 0.8 g, 1 g) of FMWCNTs were dispersed in 100 ml of $CHCl_3$ by sonication for 30 minutes and 4.65 g aniline was added and sonication was continued for another 30 minutes. 11.25 g APS was dissolved in 200 ml. of 1 M HCl. Nanocomposite was prepared by the following method. The inorganic solution was added to the organic solution kept in a 500 ml beaker at 0-5°C. The reaction mixture was kept under magnetic stirring. The mixture turned green, indicating the formation of PANI emeraldine salt (ES). The two phase solutions were kept at 0-5°C for 12 hr under stirring. After words, the aqueous phase was transferred to another beaker. Treatment with fresh quantities of chloroform was done five times to remove the organic phase. The samples were filtered, washed repeatedly with distilled water and finally with acetone. It was then dried at 80°C for 24 h. The composites were denoted as PC(0), PC(0.2), PC(0.4), PC(0.6), PC(0.8) and PC(1).

3.2.3 Dedoping

The samples thus prepared were de-doped using large excess of 0.5M NH_4OH to obtain the corresponding emeraldine base (EB). The solution containing PANI/FMWCNT composite was kept overnight under vigorous stirring and then filtered. The residue was washed with 500 ml of 0.5M NH_4OH. The de-doped samples were dried for 48 h under vacuum at 80°C.

3.2.4 Doping with Acid Dopants

The PC (0.6) composite and PC(0) thus obtained in the EB form was protonated with (1) 1.5 M HCl (2) 1.5M H_2SO_4 (3) 1.5 M TSA (4) 1.5 M NSA solution in water. Protonation was achieved by extended mixing of de-doped samples with the acid solution for 24 hrs. The solutions were filtered and a dark green emeraldine salt (ES) was obtained. The samples were denoted PANI-HCl/FMWCNT, PANI-H_2SO_4/FMWCNT, PANI-TSA/FMWCNT and PANI-NSA/FMWCNT. The PC (0) samples were denoted PANI-HCl, PANI-H_2SO_4, PANI-TSA and PANI-NSA.

3.2.5 Characterisation

The morphology of the samples was probed by SEM and TEM. Thermo gravimetric analysis (TGA) were performed on a Q50, TA instruments Thermogravimetric analyser with a programmed heating of 10°C/min starting at room temperature and proceeding up to 800°C in an air atmosphere. The FTIR spectra of samples were recorded from KBr sample pellets using a Nicolet Magna-5700 FTIR spectrometer. The DC conductivity of doped and dedoped samples as well as the cyclic thermal ageing and isothermal ageing studies were measured using a Keithley 6881 programmable current source and a 2128A nano-voltmeter as described in section 2.2.6.

3.3   Results and Analysis

3.3.1 Functionalisation of MWCNT

Functionalisation of MWCNTs with 4-aminobenzoic acid is confirmed using IR, Raman spectroscopy and TGA. The TGA thermograms of MWCNTs and FMWCNT are shown in figure 3.1a. The significant weight loss of

MWCNTs, mainly attributed to the oxidation of nanotubes, starts from 510°C onwards leaving a residue of 1.02%. FMWCNT sample displays weight loss of about 20.1% in the temperature range of 420–530°C owing to oxidation of aminobenzoyl groups grafted on the surface of FMWCNTs. Afterwards, there was a steady weight loss in the region 600 - 650°C for further oxidation of CNTs. This indicates improved thermal stability of FMWCNT which agrees with previous results (5).
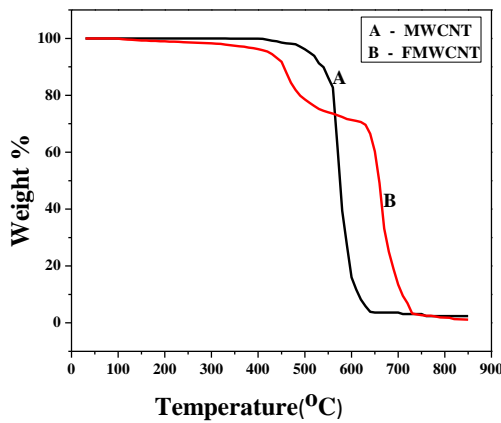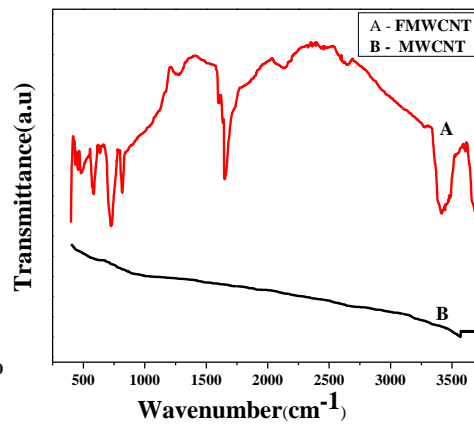
Fig. 3.1a: TGA curves   **Fig. 3.1b: FTIR spectra**
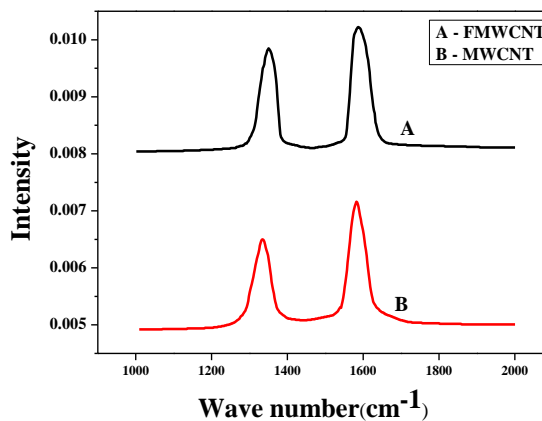
Fig. 3.1c: Raman spectra

Figure 3.1b shows FTIR spectra of MWCNTs and FMWCNTs. The spectrum of neat MWCNTs is featureless. The spectrum of FMWNTs shows new peaks at 1648cm^{-1} (aromatic carbonyl C=O stretching) and 3,413cm^{-1} (amine N–H stretching). These results indicate the functionalisation of MWCNTs with 4-aminobenzoic acid.

The Raman spectra of MWCNTs and FMWCNTs are shown in Figure 3.1c. The CNTs exhibit a strong band at 1580 cm^{-1} (G mode) and at 1350 cm^{-1} (D mode). The G band is assigned to the in-plane vibrations of the graphitic wall and reveals the order and integrity of CNTs. The disorder-induced D band originates from the defects in the graphitic structure (6,7). The intensity ratio between the D band and G band (I_D/I_G) is sensitive to the surface character of MWCNTs, which is the index of graphitization degree of MWCNTs (7). For pristine MWCNTs, the I_D/I_G ratio is found as 0.77(8). The ratio is increased to 0.83 for FMWCNTs. This suggests a reduction in the degree of order and increase in the amorphous carbon on the surface of MWNTs as a result of functionalization. As the increment is small, it is inferred that integrity and order of curved grapheme sheets on the surface of MWNTs has not been greatly altered.

3.3.2 Morphology

The SEM images of pristine MWNT and FMWCNT, shown in figure 3.2A and B respectively indicate that quite some bundling of nanofibers occurs during functionalisation. This results in an increase in nanotube diameter. Bundling is due to the polarity of functionality present on the CNTs (4). The SEM image in figure 3.2(C) for PC(0) sample, shows the presence of PANI nanofibers with a diameter in the range of 48-66 nm.
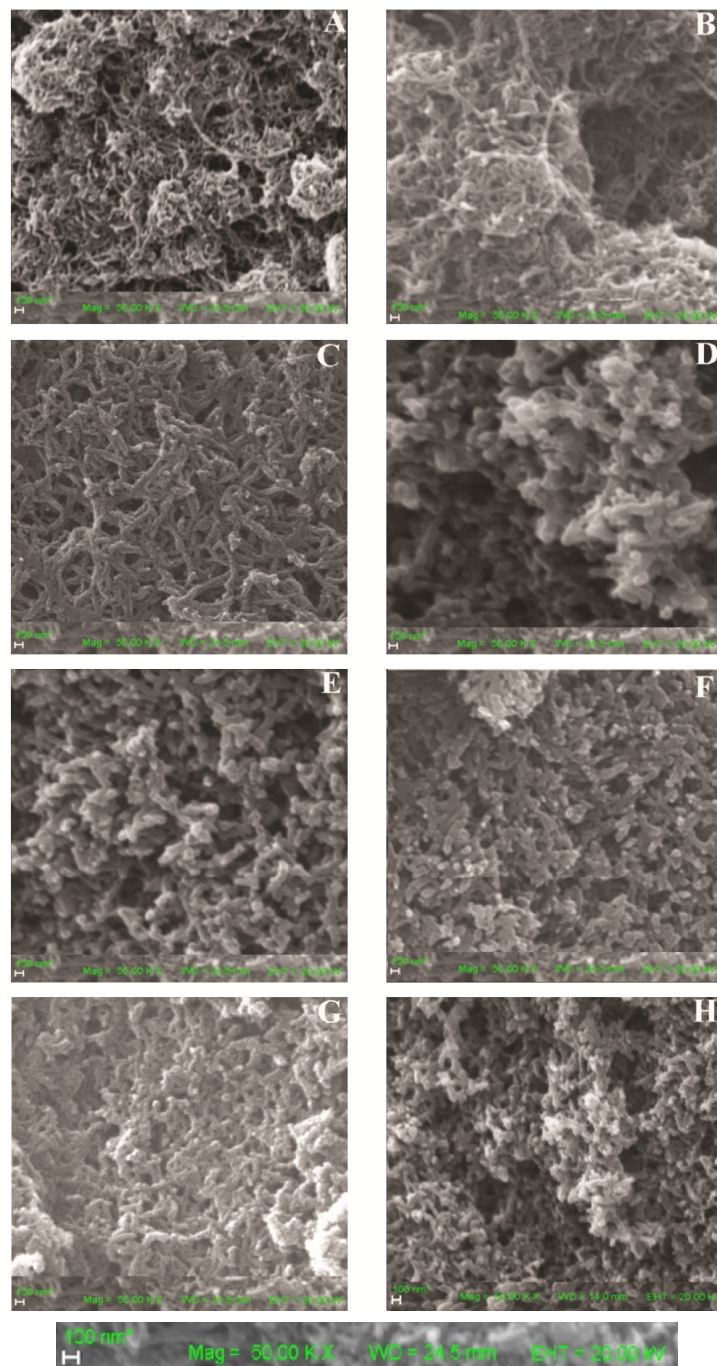
Fig 3.2: SEM image of (A) MWCNT (B) FMWCNT (C) PC(0), (D) PC(0.2) (E) PC(0.4) (F) PC(0.6) (G) PC(0.8) and (H) PC(1).

In interfacial polymerization with stirring, small drops of organic phase containing aniline gets dispersed in aqueous phase. Aniline molecules move to the interface and polymerisation occurs at the interface. The formed polymer then migrates to the aqueous medium (9-11). When the polymer leaves the interface, spontaneous termination of polymerisation process occurs. Thus interfacial polymerisation efficiently avoids secondary growth of polymer and nanofibres of superior quality are obtained. The PANI fibers obtained here are of good quality but for some irregularities in the form of non-uniform thickness and agglomerates.

The SEM images of nanocomposites [Fig. 3.2(D)–(H)] exhibit tubular-type morphology with core–shell structure, the CNTs being the core encapsulated by a PANI shell. Surface of tubular composites is smooth-indicating the formation of polymer chain through homogeneous nucleation. All composites reveal uniform dispersion of the FMWCNTs in the PANI matrix without any aggregation. CNT has a tendency to agglomerate and sonication has helped in deagglomeration as there is no bundling observed in SEM images of the composites. Also no free CNTs can be seen in the SEM images and it can be assumed that the polymerization is beginning at the surface of CNTs resulting in PANI coated nanotubes. For neat MWNTs, a uniform dispersal in the polymer matrix is difficult to achieve because of its long and entangled structure. The 4-aminobenzoyl functionality improves the dispersion of CNTs in aniline. This functionality on the surface of CNTs interacts with the hydrogen and nitrogen atoms in the $-NH_2$ group of aniline through hydrogen bonds (-CO…HN-) (12). This ensures the adsorption of aniline monomer on the surface of CNTs during sonication and can promote extended conjugation of the PANI chains during polymerisation process. A

close examination of the micrographs reveals that the thickness of the coating is decreased as the CNT content increased. For PC composite (0.2), the average diameter of the composite is 130 nm while it is reduced to 82 nm in PC (1). This indicates that by varying the ratio of aniline monomer and CNTs, the thickness of PANI layer on nanotubes can be effectively controlled. In this experiment, the formation of nanocomposites involves strong interaction between aniline and nanotubes. During interfacial polymerisation with APS, two nucleation sites (initiation sites) are available i.e., (1) aminobenzoyl radical grafted on CNTs and (2) aniline radical adsorbed on CNTs. Aniline gets polymerised on the surface of CNT at the interface and PANI coated FMWCNT diffuses gradually into the aqueous phase avoiding secondary growth. This special advantage of interfacial polymerisation contributes to narrow size distribution of PANI coating in core-shell structures. The influence of CNT content is such that, at low CNT level, the PANI chains formed at the aqueous-organic interface gets deposited on the PANI coated nanotubes and thereby increases the thickness of the composites. But with an increase in nanotube content, polymerisation is confined to the CNT surface only. Considering the principles of heterogeneous catalysis, the reaction take place along the surface of CNT due to low activation energy (13).

The thickness and uniformity of PANI coating on CNT is studied on the nanocomposite sample PC (0.6). Figure 3.2F and 3.3 show the SEM and TEM images respectively of this sample. TEM image of this sample is a proof for the existence of a polymer coating on CNT and its thickness. TEM image confirms the highly extended and well aligned polymer chain encapsulation formed on CNTs. The diameter of 65 composite tubes was measured from SEM images and it was confirmed with TEM image (Fig. 3.3).

From the size distribution curve (Fig. 3.4), the average diameter of the tubes are found to be 93 nm (diameter varying from 78 nm to 110 nm). This indicates that the thickness of PANI coating is 50-60 nm in this composite. The influence of PANI coating thickness on the DC conductivity of various samples is discussed in the next section.
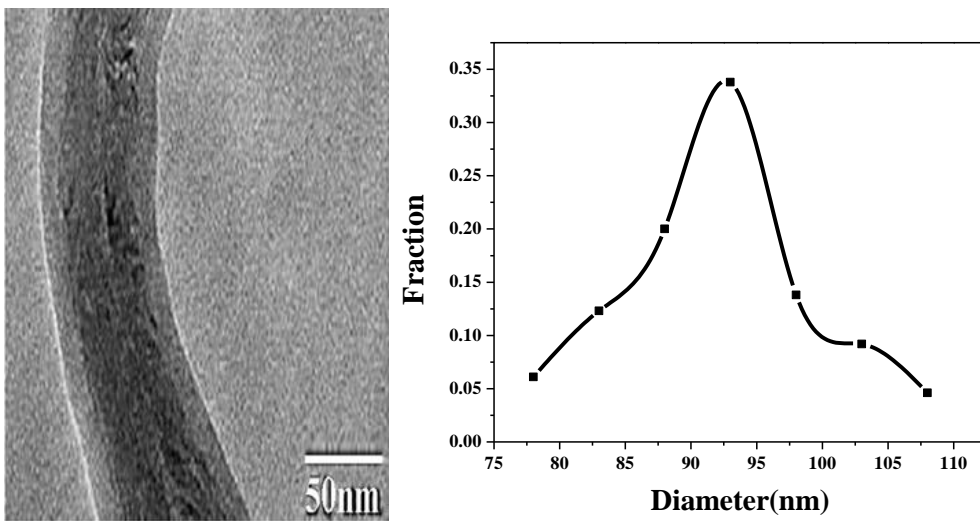

Fig. 3.3: TEM image of PC (0.6)   Fig. 3.4: Size distribution curve of PC (0.6)

3.3.3 DC Conductivity

The room temperature conductivity of all the doped samples given in figure 3.5(a) shows a fall in conductivity in the semiconductor range. The conductivity of pure PANI is 23 S/m and that of the composites is increased by one order in magnitude compared to PANI.

The increase in electrical conductivity of composites compared to pure PANI is due to the charge-transfer effect from the quinoid ring of PANI to CNTs (14). The excellent transport properties and high aspect ratio

of CNTs help them to interconnect efficiently with the conducting channels and conducting grains of the PANI coated over them (15). A striking observation is the remarkable improvement in DC conductivity of the nanocomposite, PC (0.6). The conductivity of PC (0.6) increases to 412 S/m from 233 S/m of PC (0.4).
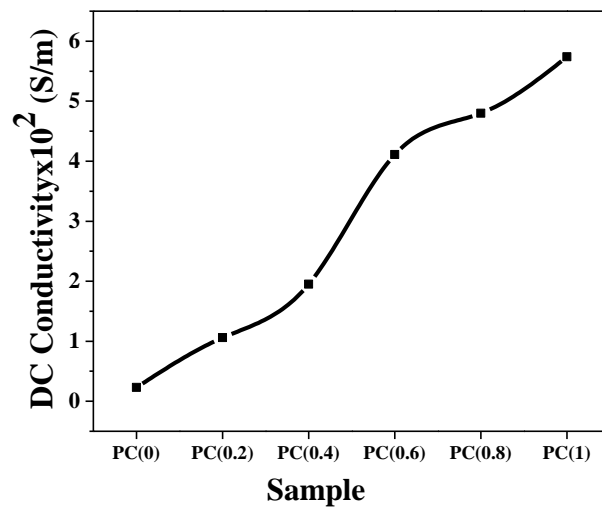

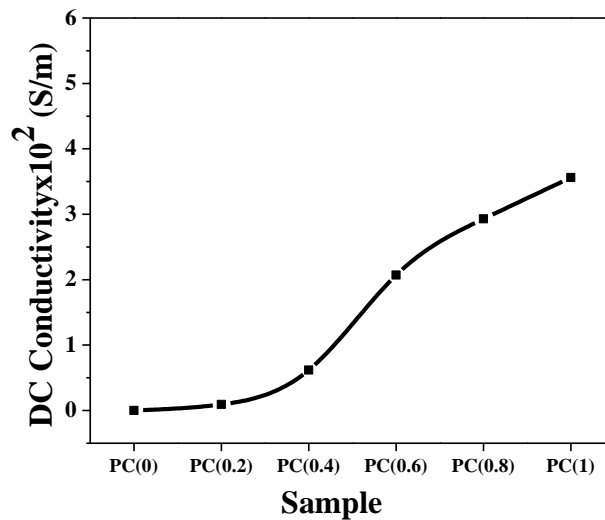**Fig. 3.5(a): DC conductivity of various samples**

Fig. 3.5(b): DC conductivity of dedoped samples

This behaviour can be explained by considering the role of CNTs as efficient "conducting bridge" leading to improved conductivity (16). The morphology studies reveal that due to the efficient templating effect of CNTs in the composite formation of PC (0.6), uniform and thin polymer chains result here. The PANI chains remain strongly bonded to the tubes. With their high aspect ratio, the CNTs interconnect the conducting ES sequence effectively. Improved charge transfer from the quinoid moiety of PANI to CNTs take place contributing to enhanced carrier mobility and increased electrical conductivity. Thus PC (0.6) exhibits remarkably superior conductivity. In samples PC (0.8) and PC (1), there is improvement in conductivity. But the aim of this work is to achieve maximum conductivity with minimum quantity of CNTs. In order to confirm this observation, the samples were dedoped and the conductivity was measured (Fig.3.5b). Sample PC (0.6) showed an improvement of one order revealing the efficient tunnelling of charge carriers through PANI base. A thin coating of PANI base allows efficient tunnelling of charge carriers through PANI base (17). In this experiment this tunnelling effect is achieved with very low CNT content of 12.9% through interfacial polymerisation. Konyushenko et al. (17) have studied the effect of PANI base coating on the conductivity of PANI/MWCNT composites. They concluded that at high MWCNT loading, a non-conducting PANI base is not a true insulator, but it could probably mediate the charge carrier transfer over short distances between the neighbouring CNT, similar to the protonated conducting PANI.
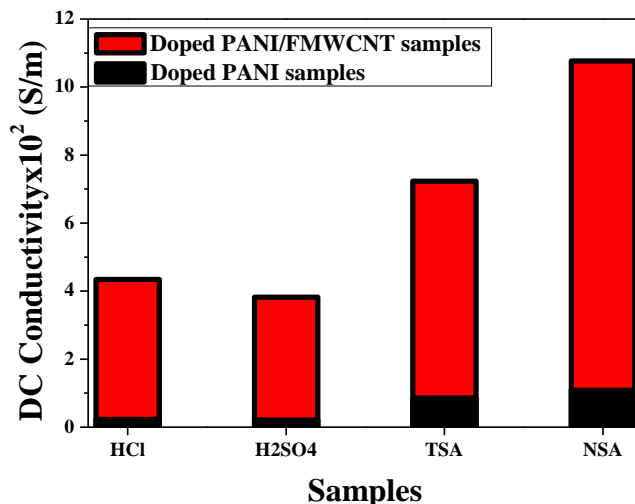
Fig. 3.6: DC conductivity of samples

For doped PANI and composites, organic sulfonic acid doped samples showed better DC conductivity (Fig. 3. 6). Large counter ions of TSA and NSA can keep the chains in a more expanded confirmation thereby leading to increased delocalization of charge carriers (18). This improves DC conductivity of sulfonic acid doped samples.

3.3.4 Fourier Transform Infrared Spectroscopy

Figure 3.7(a) and (b) shows the FTIR spectra for doped PANI and doped PANI-FMWCNT composites respectively. All characteristic spectra of PANI are reflected in PANI-CNT composites. There are no new peaks, only a few obvious changes in the form of shifts in certain peaks are observed. Thus introduction of CNTs doesn't damage the backbone structure of PANI. The peak at 1136 -1143 cm-1 is a characteristic of the so-called electron-like band described by MacDiarmid et al. (19). It is observed that the peaks at 1136–1143 in pure PANI samples are shifted to lower wave numbers

(1124–1128) in composites. The highest down shift is for NSA doped sample. This shift can be due to the higher protonated state and intensive interaction between CNTs and PANI chain (16).
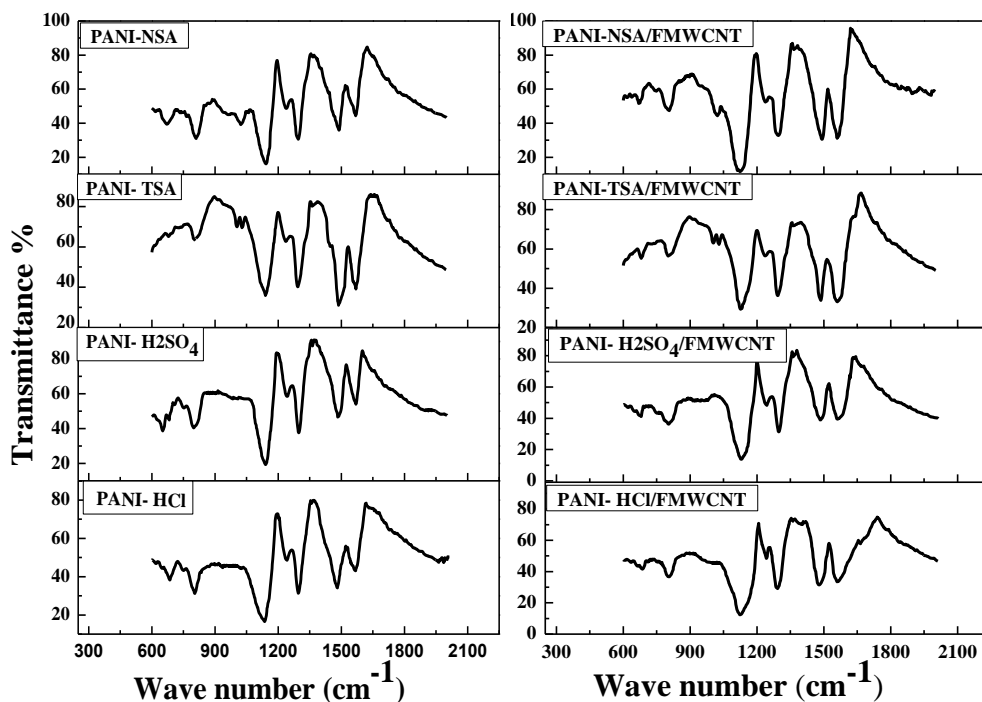

Fig 3.7(a): FTIR spectra of doped PANI

Fig 3.7(b): FTIR spectra of doped PANI-FMWCNT

The intensity of this band (E band) is measured for different samples [Fig. 3.8(a)]. It is observed that for composites, in this particular band, the intensity is increased. This can be ascribed to the charge transfer interactions between the π conjugated surfaces of MWCNT and quinoid moiety of doped PANI (20). Organic sulphonic acid doped samples shows higher increment, as these interactions can be stabilised by the counter ions of TSA and NSA. This agrees with the measured conductivity values.
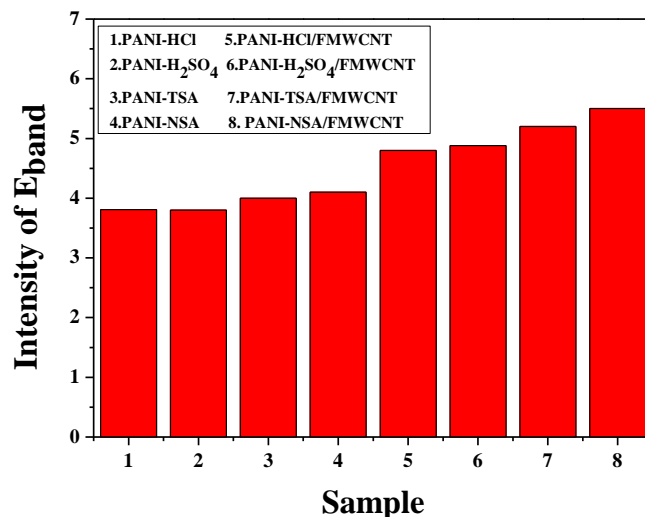
Fig. 3.8(a): Intensity of E$_{band}$
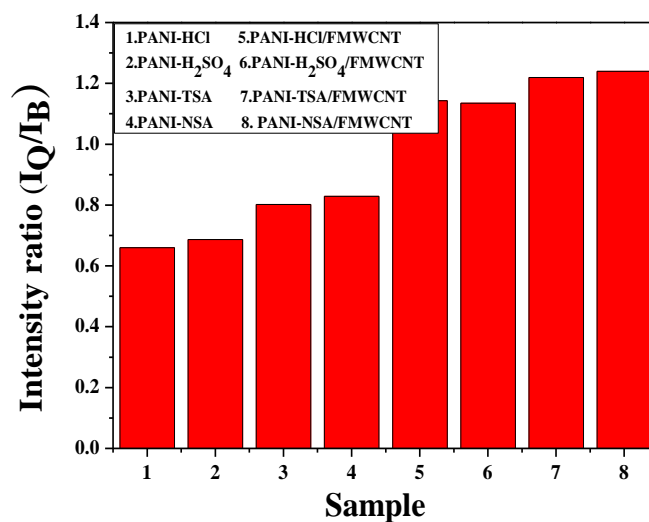
Fig. 3.8(b): Intensity ratio (I$_Q$/I$_B$)

Reversal of relative intensity of the quinoid and benzenoid bands in the composites compared to pure PANI is also observed. The characteristic bands around 1570 and 1485 cm^{-1} correspond to the C=C stretching vibrations of quinoid and benzenoid rings, respectively (21). The spectra of composites

exhibited an increased quinoid (Q) to benzenoid (B) band intensity ratio (I_Q/I_B) compared to pure PANI. A comparison of I_Q/I_B for various samples is given in [Fig. 3.8(b)]. The increased ratio reveals the richness of the composite with quinoid units that can be assigned to strong interaction between π bonded surface of CNTs and conjugated PANI ring through quinoid ring. These site-selective interactions between the quinoid ring of the PANI and CNTs are likely to promote the stabilization of the quinoid ring structure in the composite. This leads to more conductive bipolaronic structure which is confirmed by improved DC conductivity results. Among the samples, better characteristics are exhibited by sulphonic acid dopants, especially NSA. It is reasonable to believe that compared to Cl$^-$ and SO$_4^{2-}$, large counter ions such as toluene sulphonate and naphtalene sulphonate can keep the polymer chains in a more expanded confirmation. This can promote the interaction between the π electrons of dopant anion and the aromatic rings of the PANI resulting in improved conductivity.

3.3.5 Thermogravimetric Analysis

The results of TGA analysis of neat PANI, PANI-FMWCNTs are given in Figure 3.9. PANI exhibits three-step decomposition ie: release of water molecules, dopant, and oxidation of polymer chain. Release of moisture occurs over a range of temperature 50–110°C. Later on release of dopant occurs at around 150–275°C. HCl being more volatile is lost at an early temperature of 115°C. It is evident from Table 3.1 that PANI doped with HCl and H$_2$SO$_4$ has lower thermal stability towards de-protonation. Compared to HCl and H$_2$SO$_4$ dopants, TSA and NSA doped PANI exhibit higher thermal stability. This is confirmed by additional thermal stability

of DC conductivity of these samples at high temperature. The main weight loss which is due to oxidative degradation of PANI occurs over a wide temperature range of 340–600°C.
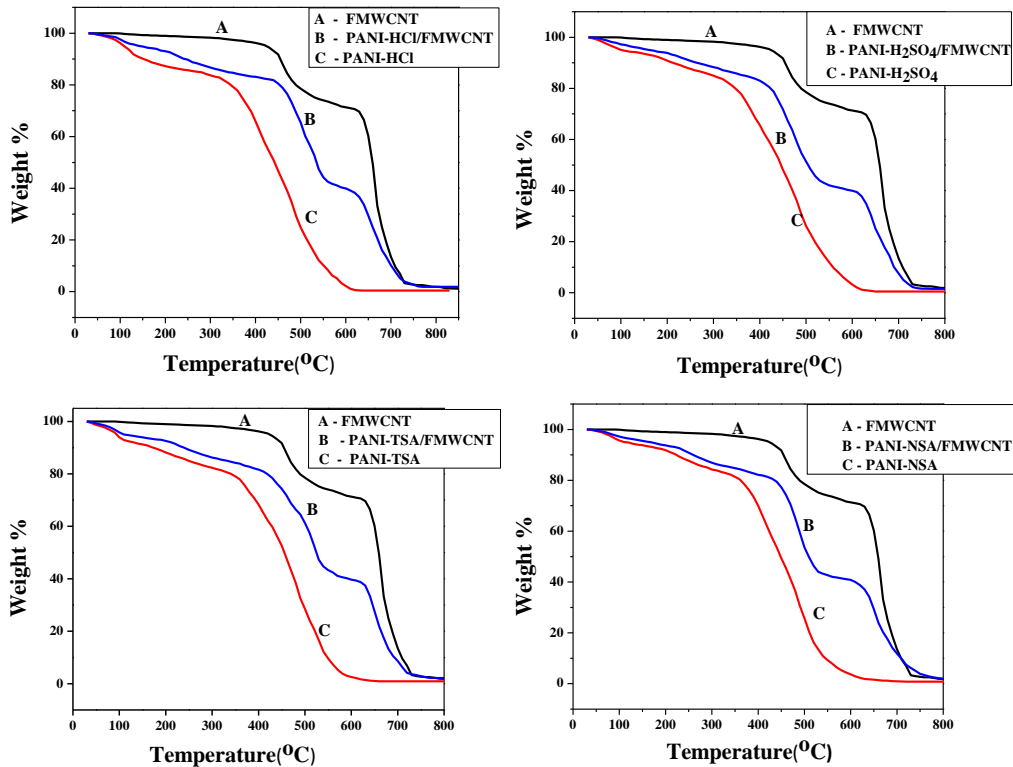
Fig. 3.9: TGA curves of PANI and composite samples

TGA thermograms of PANI-FMWCNTs given in figure 3.9 illustrate the elevated thermal stability of nanocomposites after the introduction of CNTs. In composites the dopant showed better thermal stability and dopant molecules are retained till 200°C. This agrees with high temperature retention of DC conductivity of composites. These dopant molecules are more easily confined and stabilized among compact and well-aligned nanotubes. These stabilising

interactions are responsible for binding dopants to the system due to which their release is delayed. This is reflected in DC conductivity retention of PANI-CNT composites during cyclic ageing and isothermal ageing studies which will be discussed in later sections. Regarding the polymer chain degradation, as demonstrated in Table 3.1, the maximum degradation temperature (T_{max}) for PANI is increased by 30–35°C in the composite compared to neat PANI.

This increase in T_{max} is indicative of high thermal stability of PANI in the composite. This result suggests that there is a good interaction between PANI and nanotubes and that the nanotube surface is uniformly coated by PANI. This strong interaction is possible through charge transfer mechanism from conjugated polymer chain to nanotubes (22). Another interesting observation is the additional weight loss at about 610°C in all composites. This weight loss is not characteristic of either PANI or nanotubes. In morphology studies it is seen that polymerisation of aniline occurs on the aminobenzoyl radical moiety of nanotubes and aniline radical adsorbed on nanotubes. The PANI chains covalently bonded to nanotubes are strongly bound and this polymer-nanotube interface can remain undecomposed till 610°C. These polymer-nanotube interfaces stay intact providing additional thermal stability to the composites. So the covalent grafting and strong interaction between polymer chains and nanotubes result in additional thermal stability of composites.

Table 3.1: Thermal analysis data for PANI and PANI-FMWCNT composites

Sample	$T_{loss\ of\ dopant}$ (°C)	$T_{max.}$ for oxidative degradation 1 (°C)	$T_{max.}$ for oxidative degradation II (°C)
PANI-HCl	115	478	
PANI-HCl/FMWCNT	202	512	690
PANI-H2SO4	150	480	
PANI-H2SO4/FMWCNT	205	511	687
PANI -TSA	175	485	
PANI-TSA/FMWCNT	220	516	693
PANI-NSA	180	485	
PANI-NSA/FMWCNT	227	520	696

3.3.6 Thermal stability of DC Conductivity

The DC conductivity retention of composites was examined through cyclic thermal ageing and isothermal accelerated ageing.

3.3.6.1 Cyclic thermal ageing

The results from cyclic thermal ageing (Fig.3.10) suggest that some observations are common for all samples.

1)   All samples exhibit semiconductor behaviour – electrical conductivity increases with increasing temperature.

2)   For doped PANI samples the conductivity increased to a maximum and then started decreasing. The behaviour of PANI-FMWCNT composites is slightly different, their conductivity reaches a maximum and then the rate of increase reduces.

3)   After the first cycle there is a significant drop in conductivity for all samples. Pure PANI samples were subjected to large decrease, while in the case of composites a lesser decrease resulted.

4)   In the subsequent cycles, though there is a decrease, it is negligible and stabilization of conductivity is achieved.

5)   After completion of one cycle, the samples again show increase in conductivity in subsequent cycles. For neat PANI samples the extent of increase is low while PANI-FMWCNT composites are capable of reaching higher conductivity.

6)   Sulphonic acid doped samples exhibit better conductivity retention compared to inorganic acid doped samples.

The increase in DC conductivity of samples with variation in temperature indicates 'thermal activated' conduction phenomena. But when raised to higher temperatures, the conductivity reaches a maximum and after a certain point there is reduction in conductivity. The cyclic ageing studies for PANI-HCl sample and PANI-H$_2$SO$_4$ (Fig.3.10A and B) show a maximum value for conductivity at around 100°C. For PANI-TSA and PANI-NSA (Fig.3.10C and D) it is at 110°C. Thereafter a decrease in conductivity is seen for all doped PANI samples. In the case of PANI/FMWCNT composites (Fig.3.10E, F and G), the conductivity increases linearly up to 150°C. But there is a reduction in the rate of increase in conductivity after 100°C. During cyclic ageing, doped PANI samples undergo considerable loss in conductivity.

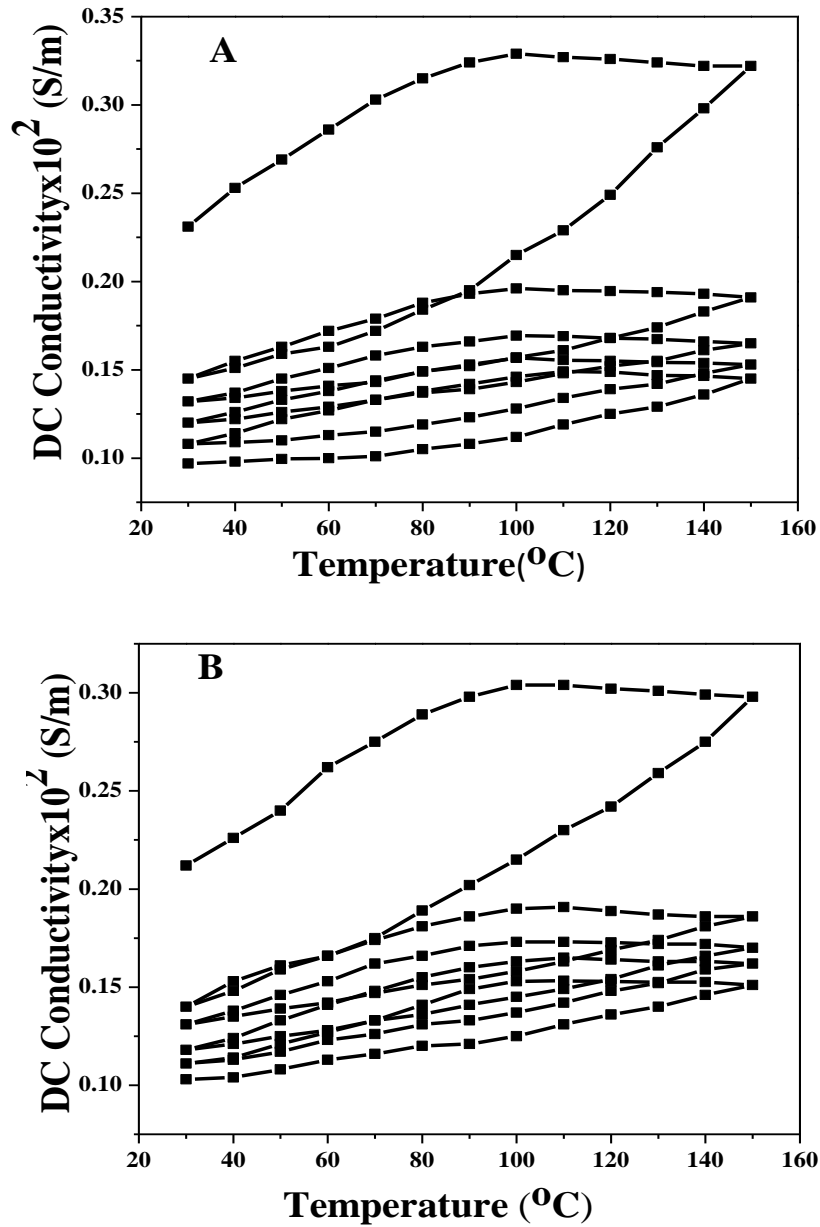**Fig. 3.10: The temperature dependence of DC conductivity under cyclic ageing up to 150°C for (A) PANI-HCl and (B) PANI-H₂SO₄**

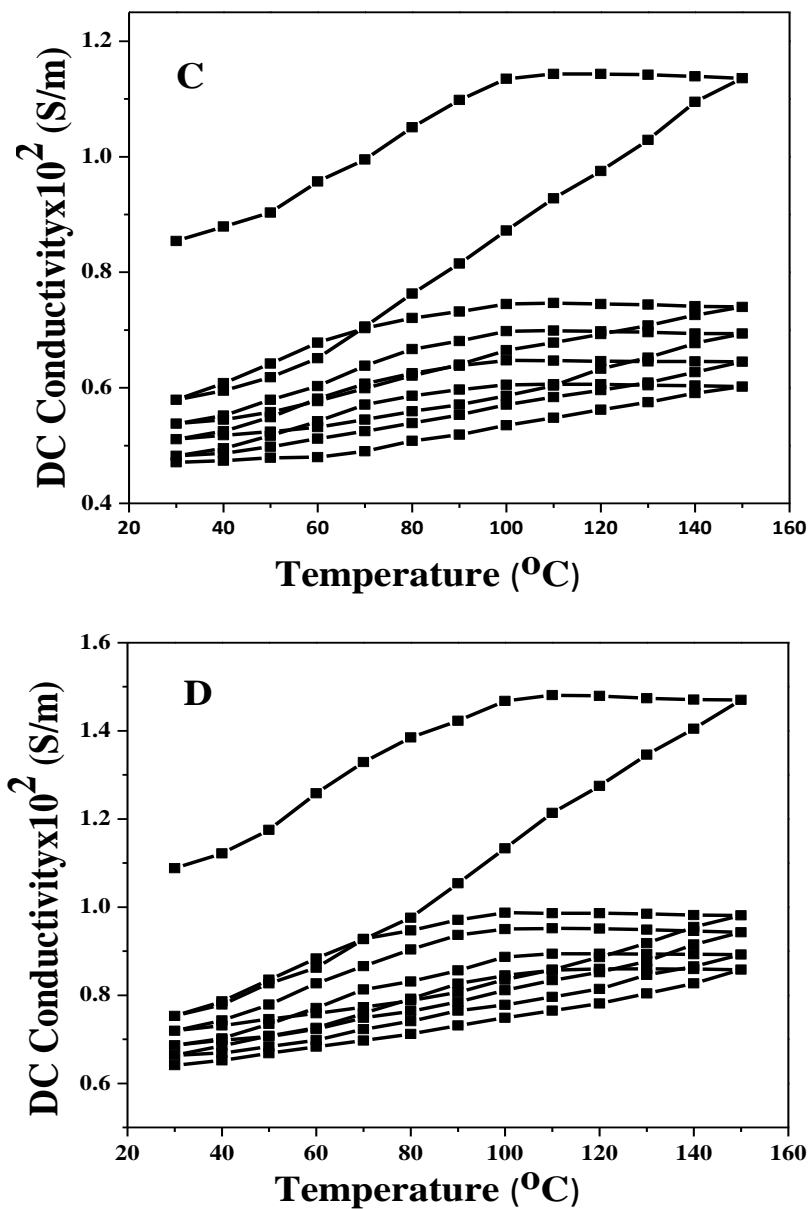**Fig. 3.10:** **The temperature dependence of DC conductivity under cyclic ageing up to 150°C for (C) PANI-TSA and (D) PANI-NSA**

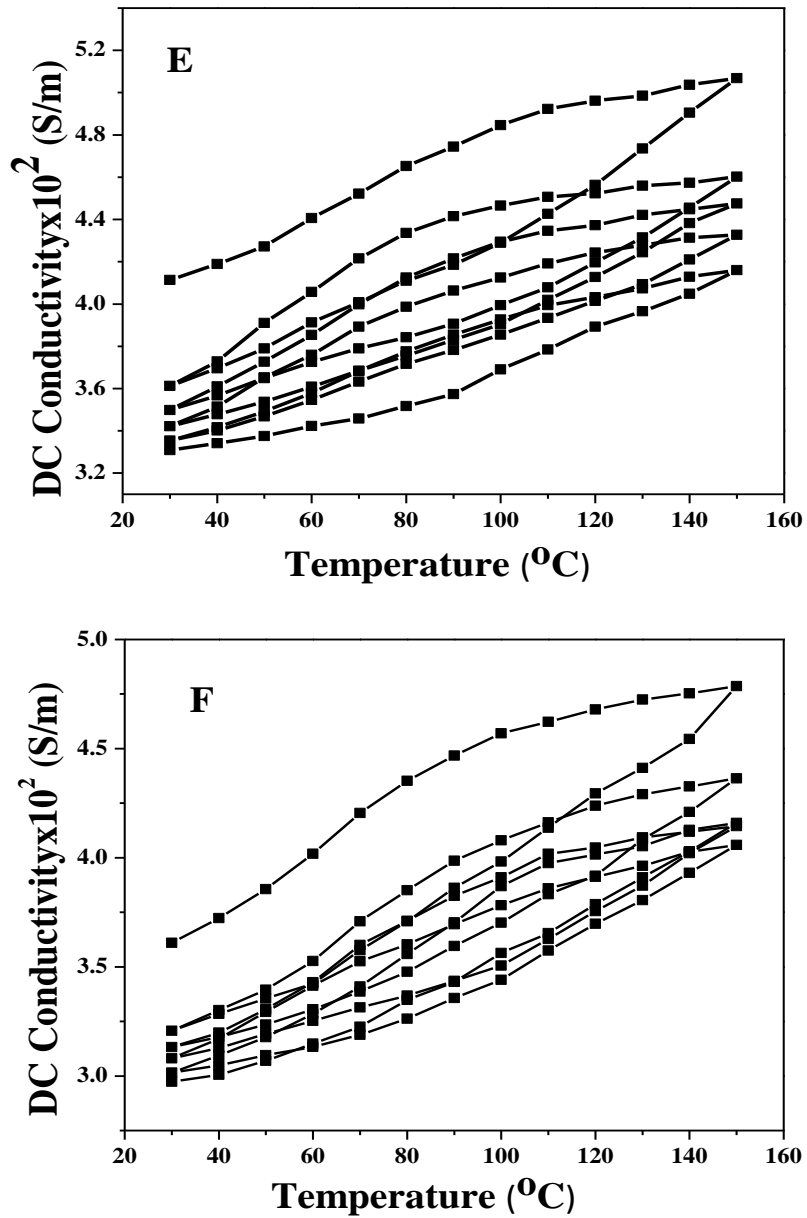**Fig. 3.10: The temperature dependence of DC conductivity under cyclic ageing up to150°C for (E) PANI-HCl/FMWCNT and (F) PANI-H₂SO₄/FMWCNT**
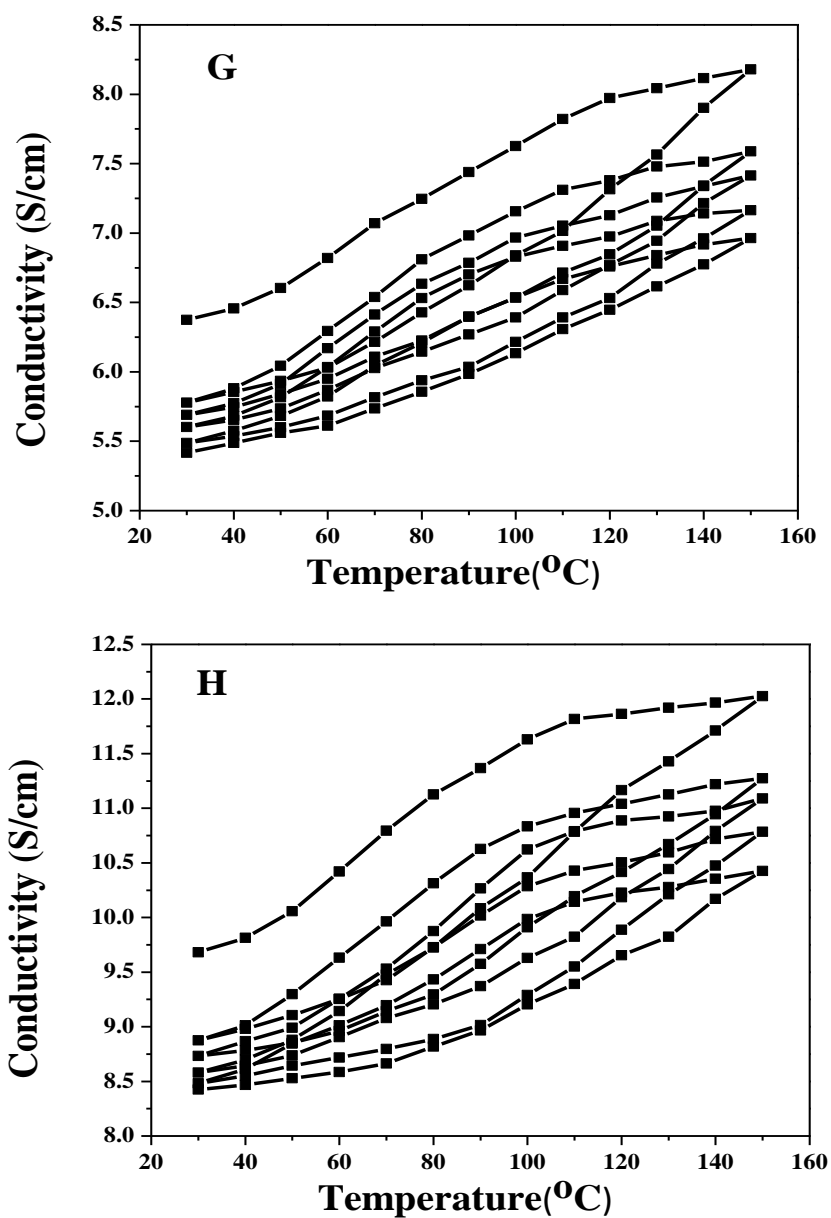
Fig. 3.10: The temperature dependence of DC conductivity under cyclic ageing up to 150°C for (G) PANI-TSA/FMWCNT and (H) PANI-NSA/FMWCNT

Figure 3.11A, reveals that after the first cycle, the percentage retention of conductivity of PANI-HCl, PANI-H$_2$SO$_4$, PANI-TSA and PANI-NSA at 30°C are 62.936, 66.04, 67.799 and 69.21, respectively. At the end of fifth cycle, the corresponding values are 41.99, 48.58, 53.98 and 58.92, respectively for these samples. Sulphonic acid doped samples show the best values of conductivity retention compared to inorganic acid dopants with HCl recording the least values. An unusual ability to retain DC conductivity is shown by PANI/CNT composites. All composites exhibit good retention of conductivity after the first cycle. The values for percentage retention of conductivity after the first cycle for PANI-HCl/CNT, PANI-H$_2$SO$_4$/CNT, PANI-TSA/CNT, PANI-NSA/CNT are 87.82, 88.84, 90.64 and 91.68, respectively. The reduction in DC conductivity is negligible compared to that of neat PANI. The performance of sulfonic acid doped samples is found to be superior to that of HCl and H$_2$SO$_4$. After five cycles, the percentage retention values are 80.43, 82.38, 85.16and 86.4 which reveal their excellent capability to retain DC conductivity at higher temperatures. When the value of PANI-NSA and PANI-NSA/CNT are compared, conductivity of PANI-NSA is decreased to 69.2% while that of composite remained almost unaffected with 86.4%. Similarly for PANI-HCl and PANI-HCl/CNT, conductivity of PANI-HCI rapidly decreased to 42% of its initial value while that of PANI-HCl/CNT decreased to only 80.43%. Here the contribution of sulphonic acid dopants to conductivity retention with values of 85.16% and 86.4% require special mention. In general during cyclic ageing, the loss in conductivity is maximum after the first cycle; thereafter the percentage of reduction is not that significant. From the data furnished, a striking difference observed is that the loss in conductivity of pure PANI is much larger

compared to composites. In composites, the loss in conductivity after the first cycle is negligible and from second cycle onwards conductivity remains more or less the same. So performance-wise, pure PANI samples seem inferior to composites.
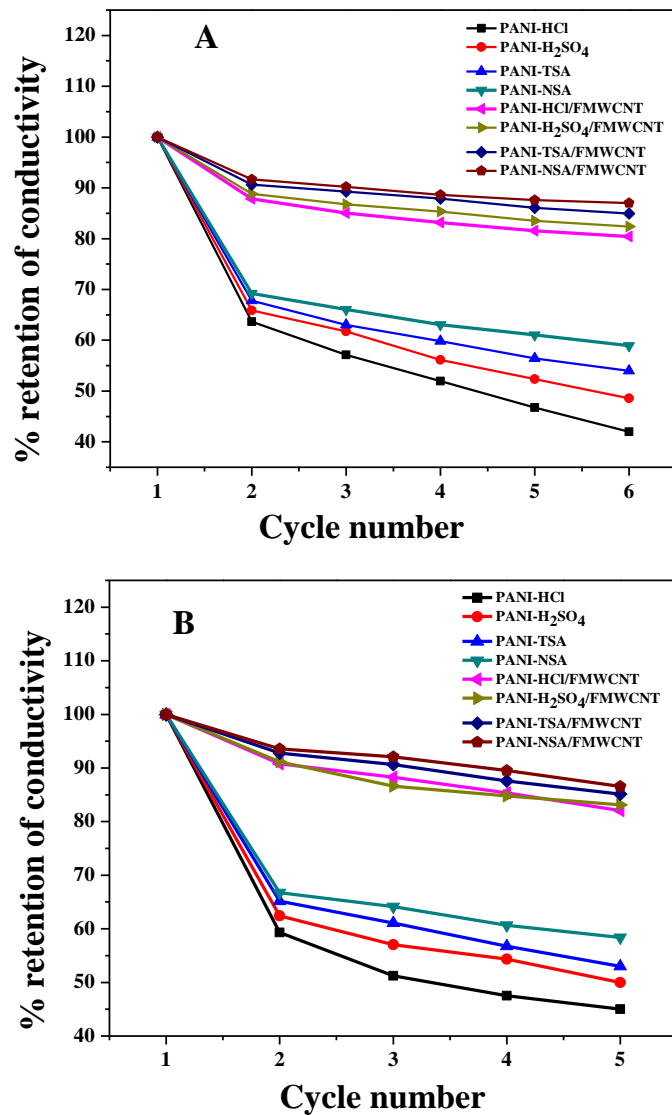

Fig. 3.11: **Percentage retention in DC conductivity of various samples (A) at 30°C and (B) at 150°C for each cycle under cyclic aging conditions**

The conductivity value at 150°C was examined for each cycle and percentage retention is depicted in Figure 3.11(B). After the first cycle, the conductivity retention percentage is found to be 59.31, 62.41, 65.14 and 66.73. For the fifth cycle, their values are seen to have decreased to 45.03, 50, 52.99 and 58.36. In all these experiments, PANI-NSA has the best value for high temperature retention followed by PANI-TSA, PANI-H_2SO_4 and the least value obtained for PANI-HCl. For composite samples, the study reveals that all of them behave in almost a similar manner. Their percentage retention at 150°C is more than 90%. When the percentage retention of conductivity is compared for each cycle, there is excellent consistency in their conductivity at 150°C. Sulfonic acid doped samples show only 15% and 14% reduction in DC conductivity even for the fifth cycle. Thus the use of bulky sulphonic acid dopants enhances the high temperature retention of DC conductivity of samples. When the behaviour of PANI and PANI/CNT composites is compared during heat treatment to 150°C, PANI/CNT exhibit unique capacity to increase its conductivity to high values. In literature, decrease in conductivity is attributed to deterioration of polymer structure as there are many changes occurring at high temperature. According to Rannou et al. (23), chemical processes and structural changes in PANI occurs when temperature is elevated, leading to degradation of conductivity. The reason for the same is explained as dedoping, chemical cross-linking, ring chlorination, ring sulphonation, oxidation etc. The temperature range of the study is not supposed to lead to chemical changes other than deprotonation and slow aerial oxidation of PANI chains. In order to investigate conductivity degradation mechanism, the well-accepted theory in conducting polymer system (24,25) which describes the system as semi crystalline with conducting

regions separated by insulating region can be adopted. Accordingly, neat PANI consists of conducting phase composed of long sequence of protonated PANI units across a non-conducting phase created by short sequences of chains containing structural defects. They proposed that at high temperatures the de-protonation of some PANI units results in the reduction of long sequence of PANI units. Thus, conducting polymer phase is converted into the damaged phase, thereby decreasing the conducting regions and reducing the electrical conductivity. The TGA studies of the samples reveal that there is a weight loss at about 100°C which is attributed to the loss of dopants and moisture. Being relatively more volatile, HCl loss is faster and hence, the HCl doped PANI has the highest decrease in conductivity. For other samples, the loss of dopant is relatively slower and hence they exhibit improved retention in conductivity during cyclic ageing. PANI-NSA sample (Fig. 3.11) shows highest stability. Here the interaction of π electrons of the conjugated naphthalene ring with the π conjugation system of PANI is providing extra stability to the system and retains the dopant to the polymer chain.

The cyclic ageing studies reveal the exceptional high temperature DC conductivity stability performance of PANI-FMWCNT samples. From TGA thermograms of PANI-FMWCNTs, the elevated thermal stability of nanocomposites as well as the delay in loss of dopant after introduction of FMWCNTs has been revealed. The role of stabilising interactions which are responsible for binding dopants to the system due to which their release is delayed has already been discussed. Thus, the retention of dopants to the polymer chain can aid in conductivity stability of composites during cyclic ageing studies. But a remarkable change observed is the relatively small

difference in the percentage reduction in conductivity of various composite samples compared to pure samples. This indicates that the conductivity degradation is not solely due to deprotonation, i.e., the ability of all composite samples to retain conductivity after thermal cycling, to maintain stable conductivity at elevated temperatures and how it is retained in subsequent cycles seeks further investigation into the interactive forces between PANI chains and nanotubes. In this interfacial polymerisation process, PANI chains are growing along the surface of nanotubes in a highly ordered way and are strongly held to nanotubes through covalent grafting and π-π interaction. The interaction between π bonded surface of nanotubes and conjugated surface of PANI is responsible for such an ordering in the chain packing of PANI (26). Thus a highly extended and orderly aligned polymer backbone chain structure is obtained on CNT surface. Thus in composites the PANI chain is growing along the surface of CNTs resulting in polymer chains which are highly ordered and crystalline domains are present in PANI shell around the nanotube shell. This unique structure on CNTs can remain intact and unperturbed upon heating. The interface that constitutes the polymer chain covalently grafted to CNTs is also of importance here. The strong interaction between CNTs and conjugated polymer chain is not disturbed upon heating to 150°C and the electronic conduction in this phase remains unaltered. Even if the outer PANI layer is degrading this phase can retain the level of conductivity at elevated temperatures. The improved stabilisation in conductivity for all composites at higher temperatures can be due to this new phase and improved crystallinity of the samples. In the next section isothermal accelerated ageing of these samples is carried out in order to investigate possibility of factors contributing to conductivity ageing phenomenon.

3.3.6.2 Isothermal ageing studies

Table 3.2: Isothermal DC conductivity ageing data of various samples

Temperature.	Time (min.)	DC Conductivity of (S/m)							
		PANI- HCl	PANI-H$_2$SO$_4$	PANI- TSA	PANI-NSA	PANI-HCl/ FMWCNT	PANI-H$_2$SO$_4$/ FMWCNT	PANI-TSA/ FMWCNT	PANI-NSA/ FMWCNT
50°C	0	26.2	24.1	90.5	116.0	430.3	382.7	662.8	1009.5
	15	27.4	25.6	92.3	118.9	436.4	386.8	670.4	1018.3
	30	28.1	26.5	93.7	120.5	439.2	389.6	671.9	1021.7
	45	28.0	26.1	93.5	121.6	442.4	391.3	672.5	1022.8
	60	28.5	26.7	94.2	122.8	443.3	392.1	673.3	1023.4
80°C	0	30.2	26.8	98.5	132.4	472.5	429.2	713.2	1084.3
	15	32.0	27.9	99.7	136.0	479.7	435.0	722.5	1101.2
	30	32.7	28.1	102.3	139.1	481.5	438.1	728.9	1102.9
	45	32.5	29.5	103.1	139.7	486.3	440.6	730.5	1103.5
	60	33.1	29.7	103.1	140.8	488.4	441.1	731.1	1104.0
110°C	0	26.6	25.4	96.3	118.8	481.6	453.3	756.8	1131.3
	15	25.7	24.9	95.8	117.5	481.9	454.2	757.1	1132.5
	30	24.0	24.1	92.7	115.7	481.2	454.2	757.9	1132.5
	45	23.1	23.7	91.5	115.1	480.9	454.5	758.3	1132.9
	60	22.3	23.3	90.2	114.2	480.7	454.3	758.5	1133.4
140°C	0	21.4	22.7	76.8	92.9	479.0	458.0	757.4	1130.5
	15	19.5	21.3	72.1	90.2	473.5	454.3	756.2	1129.4
	30	18.1	20.5	70.9	89.3	471.0	452.2	755.9	1128.5
	45	15.8	19.3	69.3	87.1	469.3	449.7	754.6	1128.3
	60	15.2	17.7	68.2	85.5	468.5	449.2	754.0	1128.1

The isothermal stability of samples with respect to DC conductivity is studied with isothermal accelerated ageing at 50, 80, 110 and 140°C at 15 minute intervals. The DC conductivity ageing data is given in Table 3.2. The relative conductivity of samples is obtained by dividing conductivity at 0,15,30,45 and 60 minutes with the one at zero minute. The relative conductivity of samples at 0, 15, 30, 45 and 60 minutes is plotted as a function of time in Figure 3.12. For pristine PANI samples, as expected, conductivity increases and stability is achieved at 50 and 80°C. From 110°C onwards there is a gradual reduction in conductivity with increase in time. A noticeable observation is for isothermal ageing at 140°C where the conductivity keeps on decreasing. Though the degree of aging is comparatively less in NSA doped and TSA doped PANI, the drop in conductivity is observed here also. These phenomena points to the possibility of damage in conjugated PANI chain structure by atmospheric agents. The relationship between aerial oxidation and conductivity deterioration is studied by Tansley and Maddison (27). They have reported that oxygen absorption occurs on the surface of polymers followed by its diffusion into the bulk. This could lead to incorporation of oxygen into the polymer chain causing discontinuity in conduction pathways and thus decreasing the conductivity of polymer. As discussed earlier, this observation substantiate the possibility of conducting polymer phase getting converted into the damaged phase and thus decreasing the conducting regions. In PANI-FMWCNT composites improved thermal stability of DC conductivity is observed. These samples exhibit increase in conductivity at 50°C and 80°C and though there is no further increase, consistency in conductivity is achieved at 110°C. At 140°C the conductivity decreases and there is a stabilisation for conductivity.
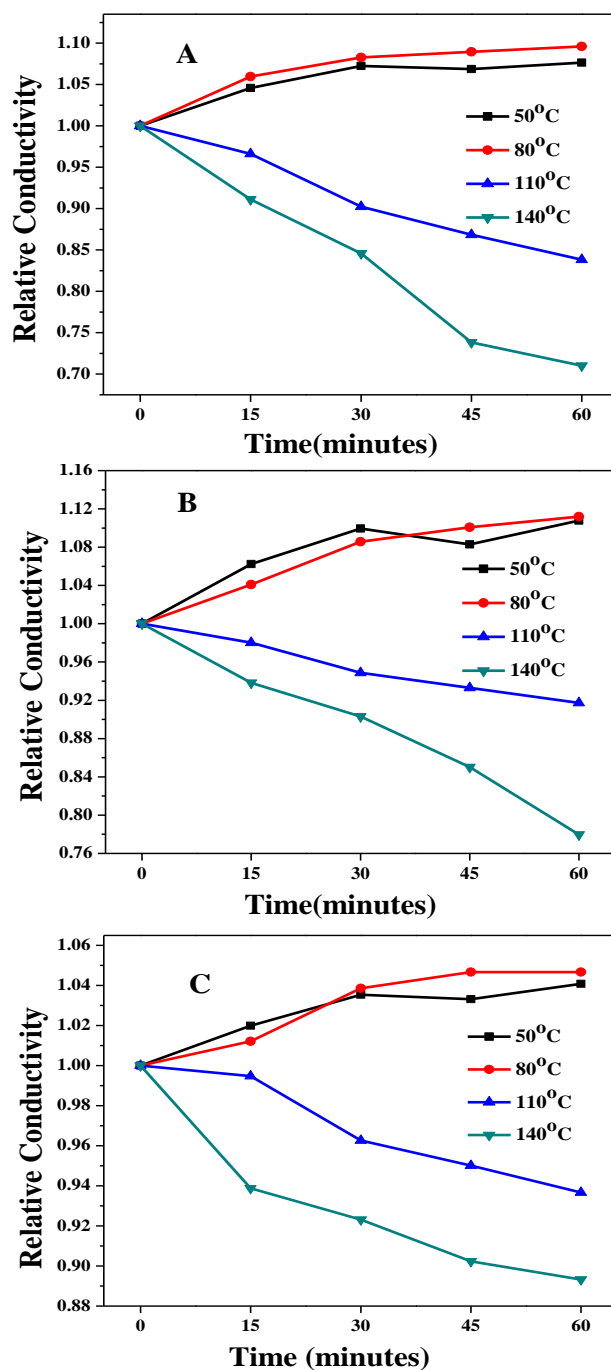
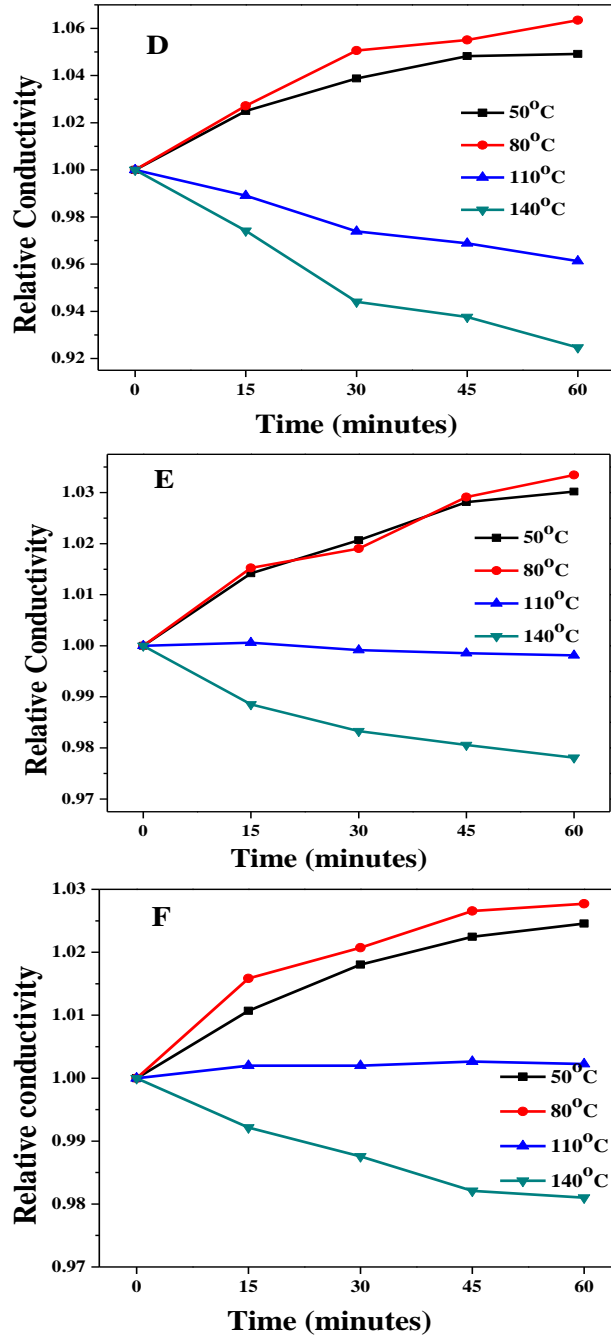**Fig. 3.12: Relative conductivity as a function of time for (A) PANI-HCl, (B) PANI-H2SO4, (C) PANI -TSA**

Fig. 3.12: Relative conductivity as a function of time for (D) PANI - NSA, (E) PANI – HCl/ FMWCNT, (F) PANI-H$_2$SO$_4$/FMWCNT
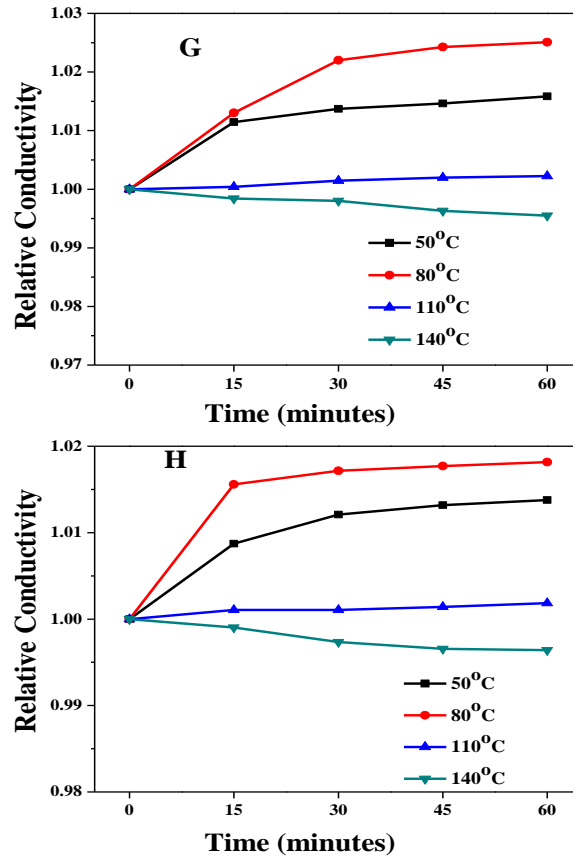
Fig. 3.12: Relative conductivity as a function of time for (G) PANI-TSA/ FMWCNT and (H) PANI – NSA/ FMWCNT

The stabilisation in more pronounced in sulphonic acid doped composite samples. Among PANI-FMWCNT composites also NSA doped and TSA doped composites exhibit superiority in conductivity stability. The deterioration in conductivity of composites at 140°C denotes that the polymer phase is on the verge of conductivity ageing. On the basis of this study, the conductivity stability of doped PANI and doped PANI/FMWCNTs can be rated as follows PANI-HCl < PANI-H2SO4 <PANI-TSA < PANI-NSA <

PANI < HCl/FMWCNT < PANI-H2SO4/FMWCNT <PANI-TSA/FMWCNT < PANI-NSA/FMWCNT.

The above observation ascertains that CNTs are preventing the polymer phase from degradation and the polymer-CNT interface is responsible for retaining the conductivity at elevated temperature. In this context, role of FMWCNT in protecting the polymer chain from atmospheric oxidation needs further investigation. It is reported that functionalisation of CNTs can prevent diffusion of oxygen through the polymer chain (8) which inhibits oxidation by atmospheric oxygen. When polymer chain oxidation occurs it can reduce π electron delocalisation due to decrease of protonation level and ES sequence and hence destruction of polaron structure (28). In composites, it can be presumed that when polymer chain oxidation is prevented, conducting region within the polymer phase is protected from ageing. Thus PANI-CNT interface and strong interaction between these two lead to synergistic properties to the composites. These properties are responsible for high conductivity of composites and their retention up to a temperature of 140°C. The grafting of FMWCNTs to the polymer chains is actually locking the CNTs to the polymer chains which is exceptionally stable and prevents the ageing of DC conductivity of composites. Among the dopants TSA and NSA, due to their efficient delocalisation of PANI chains exhibit best conductivity retension at high temperature. The impact of FMWCNTs in dynamic interfacial polymerisation of aniline is revealed by its conductivity retention at high temperature. So a wider range of applications can be considered for these composites at high temperature.

3.7 Conclusions

Different FMWCNT loadings were used to fabricate PANI/FMWCNTs through interfacial polymerization. With 12.9% of CNT content, nanocomposites of thin, uniform PANI encapsulation on CNTs are obtained. SEM and TEM images show PANI coated uniformly on the surface of the FMWCNTs and shows highest improvement in DC conductivity. The sample is doped with dopants like HCl, H_2SO_4, TSA and NSA. TGA analysis confirms the covalent grafting and strong interaction between polymer chains and nanotubes. FTIR spectra reveal effective site-selective interactions between the quinoid ring of PANI and CNTs, facilitating charge-transfer processes between the two components. These results suggest that interfacial polymerisation in presence of FMWCNT is an effective way for improving DC conductivity and thermal stability. Cyclic and iso-thermal ageing studies reveal the improved high temperature retention in conductivity of the composite. When PANI and composites are doped with TSA and NSA there is further improvement in conductivity as well as conductivity retention. The order of high-temperature stability of DC conductivity is PANI-HCl < PANI-H_2SO_4 < PANI-TSA < PANI-NSA < PANI-HCl/FMWCNT < PANI-H_2SO_4/FMWCNT < PANI-TSA/FMWCNT < PANI-NSA/FMWCNT. Deprotonation and polymer chain degradation by atmospheric oxygen are the prime reasons for conductivity ageing at high temperature. The well-aligned PANI chain structure on CNTs remains unperturbed upon heating. This leads to high temperature retention of DC conductivity of composites compared to pure PANI and this excellent property of composites may imply their potential application in the high temperature range.

References

[1]   P. Rannou, M. Nechtschein, J.P. Travers, D. Bernera, A. Walter, D. Djurado, *Synth. Met.*, 101, 1999, p. 734.

[2]   J. Prokes, M. Trchova, D. Hlavata, J. Stejskal, *Polym. Degrad. Stab*., 78, 2002, p. 393.

[3]   I.S. Edenkova, J. Prokes, M. Trchova, J. Stejskal, *Polym. Degrad. Stab*., 93, 2008, p. 428.

[4]   H.J. Lee, S.W. Han, Y. Kwon, L.S.Tan, J.B. Baek, *Carbon*, 46, 2008, p. 1850.

[5]   I.Y. Jeon, L.S.Tan, J.B. Baek, *J. Polym. Sci. Part A: Polym. Chem*., 48, 2010, p.1962.

[6]   H. Hiura, T.W. Ebbesen, K. Tanigaki, H. Takahashi, Chem. Phys. Lett., 202, 1993, p. 509.

[7]   J.L. Hudson, M.J. Casavant, J.M. Tour, J. Am.Chem.Soc., 126, 2004, p. 11158.

[8]   B. Gao, Q. Fu, L. Su, C. Yuan, X. Zhang, Electrochim. Acta., 55, 2010, p. 2311.

[9]   J. Huang, R.B. Kaner, *Angew. Chem., Int. Ed.,* 43, 2004, p. 5817.

[10]   G.M. Nascimento, P.Y.G. Kobata, M.L.A. Temperini, *J. Phys. Chem. B.,* 112, 2008, p.11551.

[11]   R.V. Salvatierra, M.M. Oliveira, A.J.G. Zarbin, *Chem. Mater*., 22, 2010, p. 5222.

[12]   B. Gao, Q. Fu, L. Su, C. Yuan, X. Zhang, *Electrochimica Acta*., 55, 2010, p.2311.

[13]   F. Yilmaz, Z. Kucukyavuz, *J. Appl. Polym. Sci*. 111, 2009, p. 680.

[14] M.I. Boyer, S. Quillard, E. Rebourt, G. Louarn, J.P. Buisson, A. Monkman, S. Lefrant, *J. Phys. Chem. B* 102, 1998, p. 7382.

[15] P. Saini, V. Choudhary, B.P. Singh, R.B. Mathur, S.K. Dhawan, *Mater Chem. Phys*. 113, 2009, p. 919.

[16] H. Zengin, W. Zhou, J. Jin, R. Czerw, D.W. Smith Jr., *Adv. Mater.* 14, 2002, p.1480.

[17] E.N. Konyushenko, J. Stejskal, M. Trchova, J. Hradil, J. Kovarova, J. Prokes, M. Cieslar, J.Y. Hwang, K.H. Chen, I. Sapurina, *Polymer*, 47, 2006, p. 5715, *Adv. Mater*., 14, 2002, p.1480.

[18] W. Feng, A. Fujii, M. Ozaki, K. Yoshino, *Carbon*, 43, 2005, p. 2501.

[19] J.C. Chiang, A.G. MacDiarmid, *Synthetic Met*., 13, 1986, p. 193.

[20] X.S. Du, M. Xiao, C. Meng, *Eur. Polym. J*., 40, 2004, p.1489.

[21] Z. Ping, G.E. Nauer, H. Neugebauer, J. Theiner, A. Neckel, *J. Chem. Soc. Faraday Trans*., 93, 1997, p. 121.

[22] M. Cochet, W.K. Maser, A.M. Benito, M.A. Callejas, M.T. Martínez, J.M. Benoit, J. Schreiber, O. Chauvet, *Chem. Commun*., 16, 2001, p. 1450.

[23] P. Rannou, M. Nechtschein, J.P. Travers, D. Bernera, A. Walter, D. Djurado, *Synth. Met*., 101, 1999, p.734.

[24] S. Sakkopoulos, E. Vitoratos, E. Dalas, *Synth. Met*., 92, 1998, p.63.

[25] B. Sixou, J.P. Travers, Y.F. Nicolau, *Synth. Met*., 84, 1997, p.703.

[26] J. Xu, P. Yao, Y. Wang, F. He, Y. Wu, *J. Mater. Sci: Mater. Electron.*, 20, 2009, p. 517.

[27] T.L. Tansley, D.S. Maddison, *J. Appl. Phys*., 69, 1991, p. 7711.

[28] S. Bhadra, N.K. Singha, D. Khastgir, *Synth. Met*., 156, 2006, p. 1148.

.....೪೧.....

SYNTHESIS OF FMWCNT-PANI COMPOSITES BY DIFFERENT METHODS AND STUDY OF THERMOELECTRIC PROPERTIES AND THERMAL STABILITY OF DC CONDUCTIVITY[*]

Nanocomposites consisting of FMWCNT and PANI were prepared by traditional single phase (SP) polymerization and dynamic interfacial polymerisation (IF) methods. Morphological and structural analysis showed that synthesis by interfacial polymerisation resulted in a well-ordered coating of PANI with a uniform core-shell structure, while single phase polymerisation resulted in thick core shell structure with many protrusions. IF composite showed better electrical conductivity and Seebeck coefficient as compared to SP composite. However, there was no corresponding increase in thermal conductivity of the composite. The introduction of a large number of nano-interfaces that scatter phonons very effectively leads to the development of composites with enhanced power factor making it suitable for thermoelectric applications.

The composite was further characterized by Raman, FTIR, UV-Vis spectroscopy, XRD and TGA. The thermal stability of electrical conductivity of the composites was investigated over a temperature range of 30-150°C by cyclic and isothermal ageing. On cyclic thermal ageing, the conductivity of the IF composites showed 87% retention while the conductivity of the SP composites registered 62.38% after five cycles. On isothermal ageing for 3h at 140°C, 99.8% conductivity was maintained by IF samples while the SP samples could retain only 92% conductivity.

[*]A.P.Sobha and Sunil K. Narayanankutty, "Electrical and Thermoelectric Properties of Functionalized Multiwalled Carbon Nanotube/ Polyaniline Composites Prepared by Different Methods", *IEEE Transactions on Nanotechnology,* DOI: 10.1109/TNANO.2014.2323419, (Volume:13, Issue 4) 835— 841, July 2014.

A.P. Sobha and Sunil K. Narayanankutty, "DC Conductivity Retention of Functionalised Multiwalled Carbon Nanotube/Polyaniline Composites", *Materials Science in Semiconductor Processing,* DOI:10.1016/ j.mssp.2015.06.018,Volume 39, November 2015, Pages 764—770

A.P.Sobha and Sunil K. Narayanankutty, "A study on the DC conductivity and thermoelectric Properties of Carbon Nanotube based Polyaniline Composites, IEEE - International Conference on Power, Signals, Controls and Computation (EPSCICON) 2012, VAST, Thrissur, Kerala, India.

A.P.Sobha and Sunil K. Narayanankutty, "An elegant way of improving the electrical conductivity and thermoelectric property of MWCNT/PANI nanocomposites, 4th International Conference on Advanced Nano Materials(ANM) 2012,IIT Madras, Tamilnadu, India.

4.1 Introduction

Thermoelectrics are promising materials having high energy efficiency. Being 'greener' and leaving very little or no carbon emission, these materials are gaining increased attention among researchers. The performance of thermoelectric materials is determined by a dimensionless quantity called the figure of merit ZT,

$$ZT = S^2 \sigma T / k$$

Where S is Seebeck coefficient (thermoelectric power, the change in voltage per unit temperature difference in a material), σ is the electrical conductivity, T is the temperature in Kelvin and k is the thermal conductivity.

Studies on the TE properties of PANI/CNT composites have suggested that they can be promising candidates for the development of lightweight and low-cost polymeric composites for TE applications (1). Strong π–π interaction between CNTs and PANI achieved through in situ polymerisation creates a well ordered chain structure improving the electrical properties of the composites (2). In the previous chapter it has been described that interfacial polymerisation of aniline in presence of CNT at an aqueous-organic interface is an efficient method for meeting the above requirement.

In this study, PANI/FMWCNT nanocomposite was synthesised through dynamic interfacial polymerisation. The composite was also synthesised through single phase dynamic polymerisation for comparison. The influence of polymerisation method on the morphology and crystallinity was investigated by means of SEM, TEM and XRD. The interaction between PANI chain and CNTs was studied through spectroscopic and

thermogravimetric analysis. Thermoelectric properties (electrical conductivity, seebeck coefficient and thermal conductivity) of the as-prepared PANI/ FMWCNT nanocomposites were studied and correlated with the structure of composites. Also, the thermal stability of electrical conductivity of the composites was investigated over a temperature range of 30-150°C by cyclic and isothermal ageing.

4.2 Experimental Procedure

4.2.1 Synthesis of PANI and FMWCNT-PANI composite by in-situ dynamic interfacial polymerisation method

Synthesis of PANI-FMWCNT composite involves polymerization of aniline in a water/chloroform interface with aniline and nanotubes in the organic phase and APS in the aqueous phase. 0.6g of FMWCNT was dispersed in 100mlof CHCl$_3$ by sonication for 30 minutes and 4.65g aniline was added and sonication was continued for another 30 minutes. 11.25g APS was dissolved in 200ml. of 1M HCl. The organic solution was kept in a 500ml. beaker at 0-5°C and the inorganic solution was added to the organic solution kept in the beaker. The reaction mixture was kept under constant stirring. The mixture turned green, indicating formation of the polyaniline emeraldine salt. The two phase solution was kept at 0-5°C for 12h. Afterwards, the aqueous phase is transferred to another beaker. The organic phase is removed by repeated treatment with fresh quantities of chloroform for five times. The composite was filtered, washed repeatedly with distilled water and finally with acetone, and then dried at 800°C for 24h. The PANI/FMWCT composite thus prepared was de-doped using large excess of 0.5 M NH$_4$OH to obtain the corresponding base. The solution containing

PANI/FMWCNT composite was kept overnight under stirring and then filtered. The residue was washed with 500 ml of 0.5M NH_4OH. The de-doped PANI/FMWCNT samples were dried for 48 h under vacuum at 80^oC. The samples thus obtained were protonated with 1.5M NSA dopant. The weight percentage of CNTs was calculated from the weight of the starting materials and the weight of the products after polymerization. As the NT remains in the composite, the final yield will be the sum of NT and aniline polymerized. From this the weight percentage of NT was calculated. The weight percentage of FMWCNT in S_1 was found to be 24.5%. Let this composite sample be S_1. The weight percentage of FMWCNT in S_1 was estimated and found to be 24.5%.

4.2.2 Synthesis of PANI and FMWCNT-PANI composite single phase polymerisation method

0.6g. of FMWCNT was dispersed in 100ml. of 1M HCl by sonication for 30 minutes. 4.65 g aniline was added and sonication was continued for another half an hour.11.25g of APS dissolved in 200ml. 1M HCl was slowly added to the reaction mixture which is kept under constant stirring. The polymerisation reaction was continued for 12h. at $0\text{-}5^oC$. The product was filtered, washed repeatedly with distilled water and acetone, dried at 800^oC for 24h. The product was de-doped and re-doped with NSA as in S_1. Let this composite sample be S_2. The weight percentage of FMWCNT in S_2 was estimated and found to be 18.2%.

4.2.3 Characterisation

The morphology of the samples was probed by SEM and TEM. XRD, FTIR, UV-Vis and Raman spectroscopy were used to carry out the

structural characterization of the samples. The DC conductivity as well as the cyclic thermal ageing and isothermal ageing studies were performed as described in section 2.2.6. Seebeck coefficient and thermal conductivity measurements were done as described in section 2.2.7 - 2.2.8. TGA were performed on a Q50, TA instruments thermogravimetric analyser with a programmed heating of 10°C/min starting at room temperature and proceeding up to 800°C in an air atmosphere.

4.3 Results and Discussion

4.3.1 Morphology studies

The SEM and TEM images obtained for samples S_1 and S_2 are shown in figure 4.1. The SEM images (Fig. 4.1A.) of both composite samples show tubular morphology with carbon nanotubes as core encapsulated by the PANI coating forming core-shell nano structure. Thus it seems that the polymerisation is beginning at the surface of nanotubes, nanotubes acting both as core and template resulting in PANI encapsulated nanotubes. The striking difference noticed in the images of the composite samples is that in S_1 the PANI coating is highly uniform while it is thicker in S_2 with many protrusions. For S_1 the core shell structure is seen to be thin, homogeneous and well-aligned with an average diameter of 93nm (diameter varying from 78 to 110nm.). The images of S_2 reveal that the PANI coating is non-uniform as there are aggregates of PANI formed on CNTs. The non-homogeneity is evident from the diameter distribution i.e., here the average diameter is 175nm (diameter varying from 115 to 190nm). The thickness and uniformity of PANI coating is confirmed using TEM images. Figure 4.1b shows TEM of sample $S_1$and S_2 where single tubes are visible.
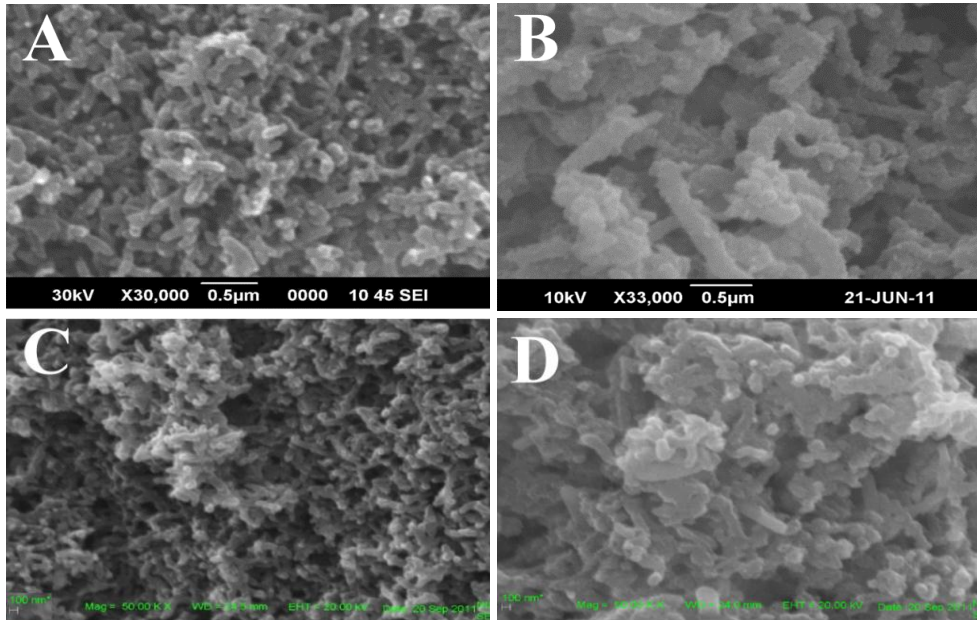
Fig. 4.1: (A) SEM images of Composites S_1 (A and C) and S_2. (B and D). Scale bar is 500nm and 100nm.
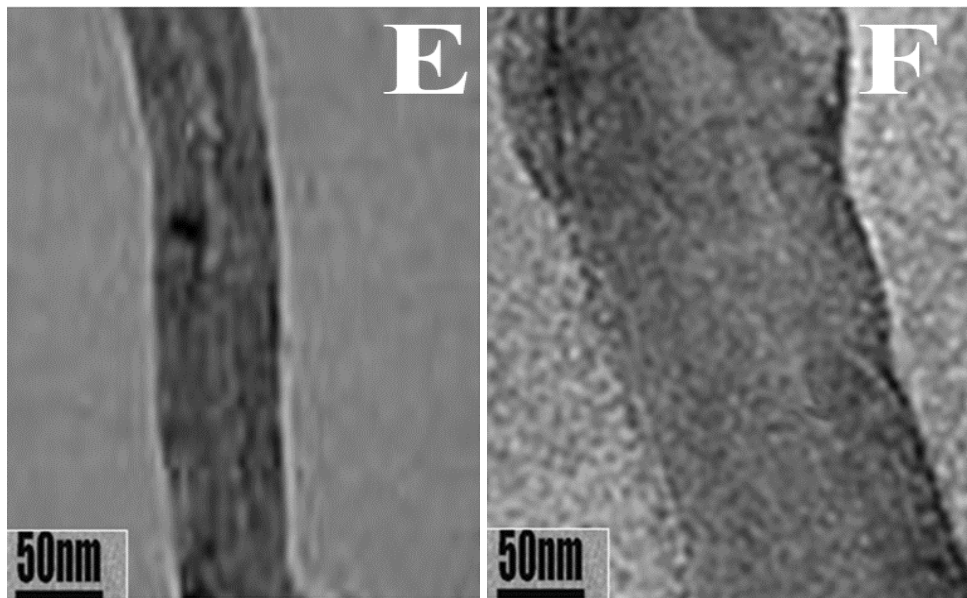

Fig. 4.1: (B) TEM image of S_1 (E) and S_2 (F).

The formation mechanism of S_1 and S_2 composites is responsible for this drastic change in morphology. In sample S_1 the CNTs along with adsorbed aniline molecules is present in the droplets of organic phase and they migrate to the water-chloroform interface. During polymerisation with APS, two initiation sites are available i.e. aminobenzoyl radical grafted on CNTs and aniline radical adsorbed on CNTs. Aniline gets polymerised on the surface of CNT at the water-chloroform interface and diffuses gradually into the aqueous phase avoiding secondary growth. As secondary growth is suppressed here, non-uniform and thicker PANI coating is prevented. This special advantage of interfacial polymerisation contributes to narrow size distribution of PANI chains in core-shell structures. As PANI chains are formed along nanotubes due to strong π-π attraction between the hexagonal surface lattice of the CNT and the planar structured molecules of PANI, the general compacted coil conformation and random molecular arrangement of PANI is avoided here (3). Instead interfacial polymerisation induces a greater polymer chain ordering on nanotubes resulting in highly extended, ordered and well aligned polymer chain in the composite structure. This result reveals the possibility of better control of the polymer coating thickness on nanotubes through interfacial polymerisation.

Contrary to this, in S_2, as the polymerisation is proceeding in single phase, more and more aniline gets polymerised on the nanotube surface. Though nanotubes are there to act as template, after formation of a few initial layers, the π-π interaction becomes weaker and cannot retain the ordering in chain packing along the nanotubes. Thus secondary growth is possible leading to coiled and random arrangement of PANI chains

resulting in a thick and non-uniform polymer shell on CNTs. Deposition of PANI lumps occur which is seen as projections in SEM and TEM images. The proposed scheme for formation of composites S_1 and S_2 is shown in figure 4.2.
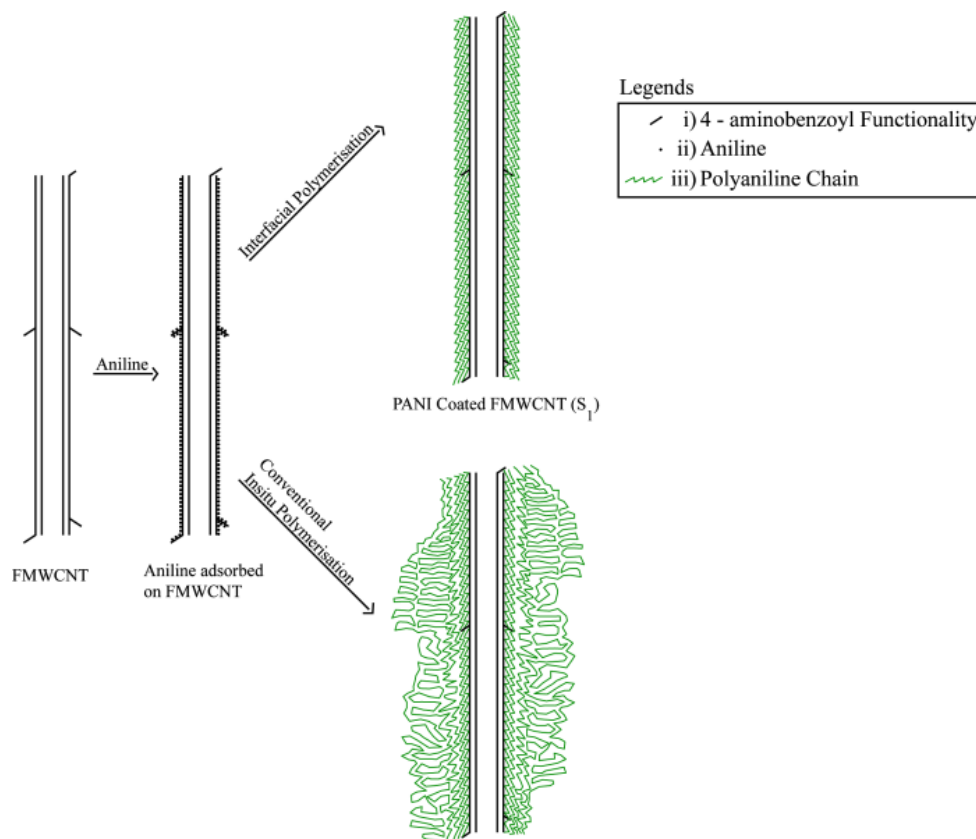

Fig. 4.2: Schematic representation of polymerisation process for composite formation.

4.3.2 Spectroscopy

In order to understand the interfacial interaction between CNTs and PANI, Raman, FTIR and UV Visible Spectra studies were conducted.
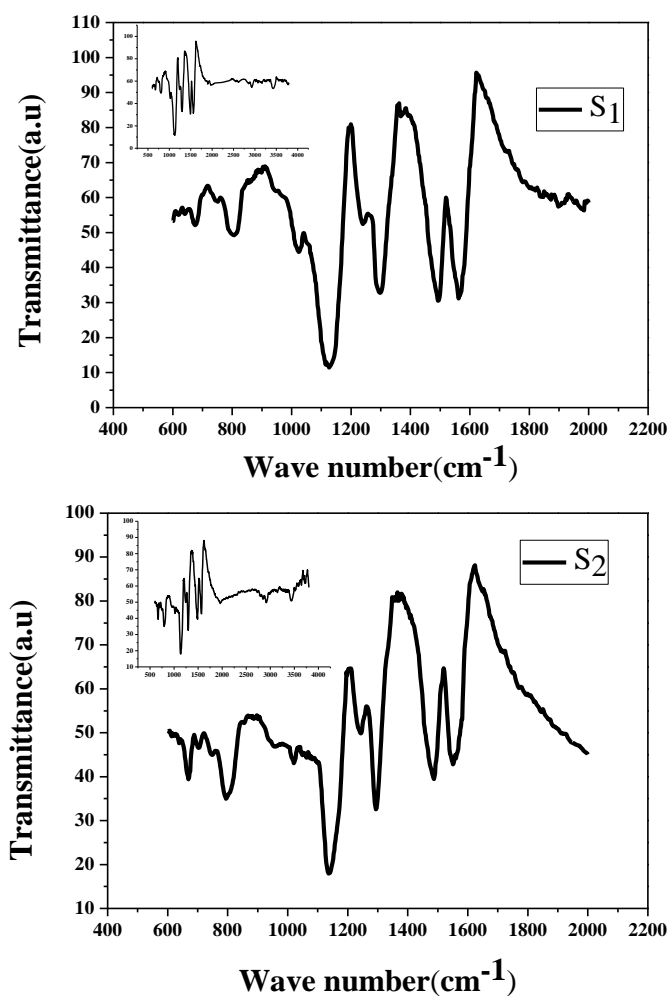
4.3.2.1 Fourier Transform Infrared Spectroscopy

Fig. 4.2: FTIR spectra of S_1 and S_2 (inset – FTIR in the range 500–3700cm^{-1}).

Figure 4.2 shows the FTIR spectra for S_1 and S_2. All characteristic absorptions of PANI are reflected in PANI-CNT composites. The peak around 1130 cm^{-1}, described as the "electron-like band", is considered to be a measure of delocalisation of electrons (4). This peak is observed at 1138 cm^{-1} in S_2 and at 1126 cm^{-1} for S_1. It is also noted that the intensity

of the peak is higher for S_1. This may be ascribed to better π-π interaction between the conjugated surface of CNT and PANI in the case of S_1.

The characteristic bands around 1562 and 1486 cm^{-1} correspond to the C=C stretching vibrations of quinoid and benzenoid rings, respectively. The spectrum of S_1 shows a higher ratio of these intensities (I_Q/I_B), indicating quinoid-rich PANI layer. Usually, aromatic structures interact strongly with the basal plane of graphitic surfaces through π stacking (5,6). The site-selective interactions between the quinoid ring of the PANI and NTs are likely to promote the stabilization of the quinoid ring structure in the composite. This leads to more conductive bipolaronic structure which is confirmed by DC conductivity results.
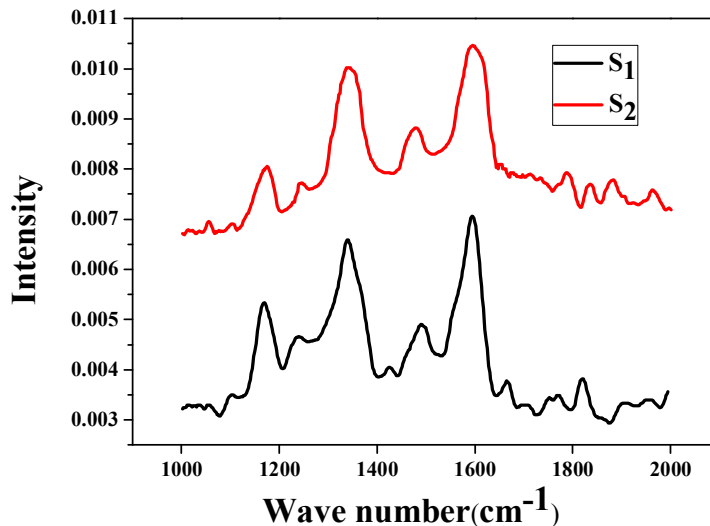
4.3.2.2 Raman Spectroscopy

Fig. 4.3: Raman spectra of composites S_1 and S_2.

In fig 4.3 Spectra of S_1 and S_2 show the typical bands of coated PANI on CNTs which includes C–H bending of quinoid ring at 1,169 cm-1, C–H bending of

benzenoid ring at 1,260 cm^{-1}, C–N^{+} stretching at 1,339 cm-1, C=N stretching vibration at 1,484 cm^{-1} and C–C stretching of the benzene ring at 1,600 cm^{-1}. These observations reveal the presence of the doped PANI-ES structure and formation of core–shell nanocomposite (7). With respect to composite S_2, new peaks at 1425 and 1639 cm^{-1} appear in S_1. This is an implication of improvement of the ordering degree of the PANI chains in S_1. Also in the spectrum of S_1, C-H bending of the benzenoid ring at 1175 cm^{-1} has shifted to 1166 cm^{-1}. These support the fact that PANI chains are highly ordered along CNT axis in S_1 and the polymer coating is enriched with microcrystalline domains.

4.3.2.3 UV Visible Spectra

The UV-Visible spectra (Fig. 4.4) of both samples in NMP exhibit two characteristic peaks - (a) at 328nm (S_1) and 337nm (S_2) corresponding to π-π* transition (b) at 715nm (S_1) and 682nm (S_2) due to n-π* transition (8). Compared to S_2, the spectrum of S_1 exhibits a slight blue shift for π-π* transition. This can be suggested to be due to the site-selective interaction between the quinoid ring of the PANI and CNTs (9) and when PANI coats over the CNTs, the interfacial interaction between the two causes the π–π* transition to shift to a lower wavelength. The spectrum in the wavelength 682nm in S_2 is red shifted to 715nm in S_1. This is indicative of an increased delocalization of charge carriers resulting from the presence of CNTs in composite (9). This again confirms strong interaction between CNTs and quinoid ring of PANI resulting in enhanced charge transfer from quinoid unit of PANI to nanotubes.
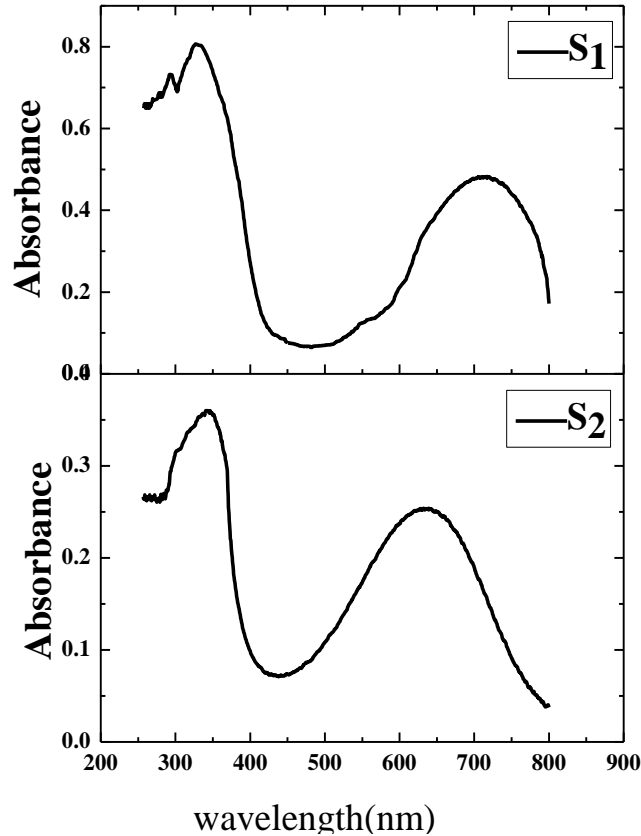
Fig. 4.4: UV–visible spectra of S_1 and S_2.

4.3.3 X-Ray Powder Diffraction Analysis

X-ray diffraction (XRD) analysis was done to assess crystallinity and molecular ordering which can influence electrical transport properties in composites. Figure 4.5 presents the XRD patterns of FMWCNT and nanocomposites S_1 and S_2. For FMWNTs, an intense diffraction peak is observed at 25.1^o and low intense peaks at $42\text{-}43^o$, corresponding to a graphite-like structure. The diffractograms of S_1 and S_2 clearly indicate that amorphous state of pristine PANI is changed significantly by the introduction of CNTs. Both composites present crystalline peaks approximately at 15.2^o, 20.7^o and

25.8^{o}. Many authors (10-12) have reported the increased order of polymer chains in the PANI coatings on CNTs in composites. Yao et al. (10) reported the peak sharpening in PANI/SWCNT composites. They related this to the monodistribution of the periodicity between the polymer backbone chains, revealing that polymer chains in the composites have a more ordered arrangement and that the composites are more crystalline.
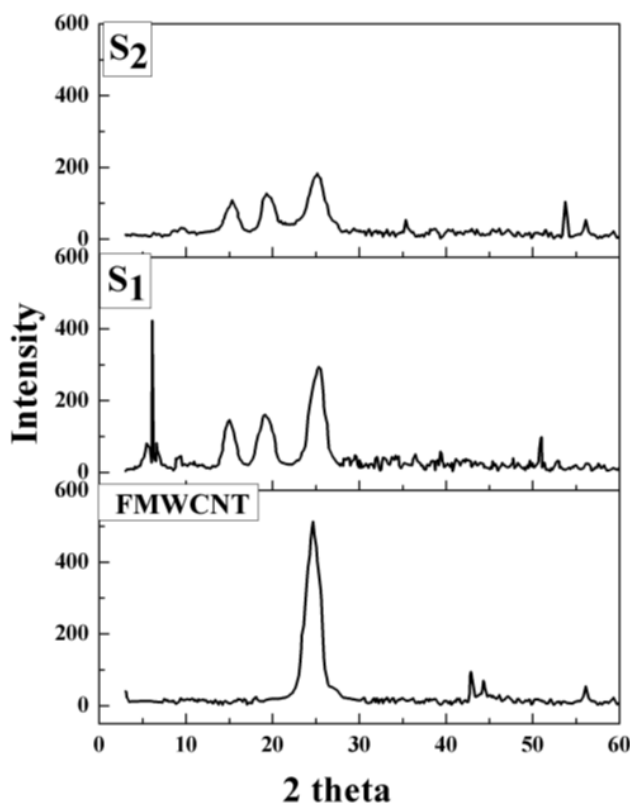

Fig. 4.5: XRD patterns of FMWCNT, Composites S_1 and S_2.

All these peaks especially the one at 25° in composite S_1 is more intense and sharper compared to S_2. This can be ascribed to the fact that interfacial polymerisation promotes order and alignment in polymer chain confirmation

along nanotubes leading to an integrated crystalline structure. Even more promising observation for S_1 composite is the presence of a sharp and intense peak at 6.47^o. This peak is characteristic of nanostructured polyaniline (11,13), whereas such a peak is absent in S_2. This confirms the fact that polyaniline chains are ordered along CNT axis in S_1 and the polymer coating is enriched with microcrystalline domains. In conventional polymerisation process, more and more PANI is deposited on nanotubes forming large aggregates. As the distance from NTs increases, it is not possible to distribute the polymer chains on nanotubes with the same order of periodicity as seen in S_1. As a result amorphous regions increase in composite S_2. Thus XRD studies provide strong evidence that there is enhanced structural ordering of PANI chains in composite S_1 compared to S_2.

4.3.4 Thermogravimetric Analysis

The TGA thermograms of S_1 and S_2 composites from room temperature to800°C at a heating rate of 5°C/min in an air atmosphere is illustrated in figure 4.6. The delay in the loss of dopant in composite S_1 is evident from its TGA thermograms. For S_1 the loss of dopant starts from 227^oC and for S_2 it starts from 190^oC. In S_1, the dopant molecules are more easily confined and stabilized among compact and well-aligned CNTs. These stabilising interactions are responsible for binding dopants to the system due to which their release is delayed. These strong interactions is reflected as improved DC conductivity and DC conductivity retention of S_1 composites during cyclic ageing and isothermal ageing studies which will be discussed in later section. Regarding the polymer chain degradation, three observations are made (1). T_{onset} for PANI degradation gets delayed in S_1 by 35^oC (2). The

maximum degradation temperature (T_{max}) for PANI is increased by 30°C in S_1 compared to S_2. This increase in Tmax is indicative of high thermal stability of PANI in the composite S_1. This result also suggests that there is a good interaction between PANI and nanotubes and nanotube surface is uniformly coated by PANI. This strong interaction is possible through charge transfer mechanism from conjugated polymer chain to nanotubes (9,14). (3) Another interesting observation is the delay in the degradation of nanotubes in S_1 compared to S_2. There is an additional weight loss at about 610°C in S_1. Though this weight loss is not characteristic of either PANI or nanotubes, this confirms additional thermal stability of S_1 compared to S_2.
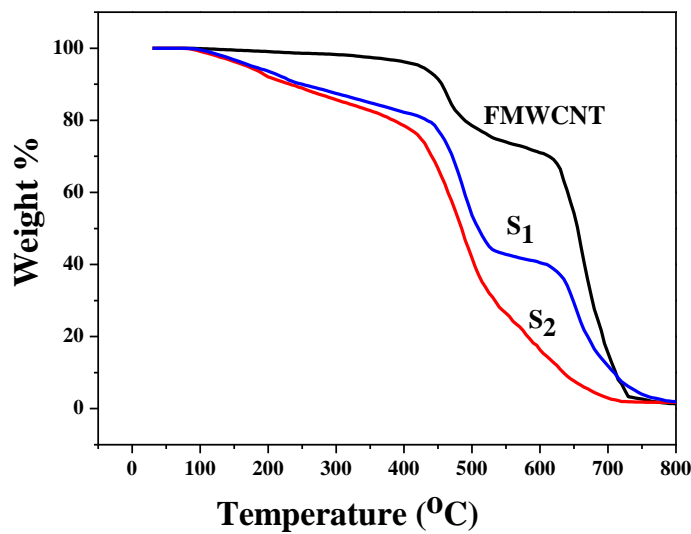

Fig. 4.6: TGA of FMWCNT, S_1 and S_2.

4.3.5 Thermoelectric properties

4.3.5.1 DC Conductivity

The electrical conductivities of the composites were measured from 295 to 355K which is depicted in figure 4.7. The following observations are

noted. (i) The room temperature DC conductivity of S_1 (960S/m) is more than ten times that of S_2 (76.3 S/m). (ii) With increasing temperature, there is a steady increase in conductivity for both samples indicating a semiconducting behaviour. The electrical conductivity of a semiconductor is given by the equation $\sigma = ne\mu$, where n, e, μ are carrier concentration, electric charge and carrier mobility, respectively.
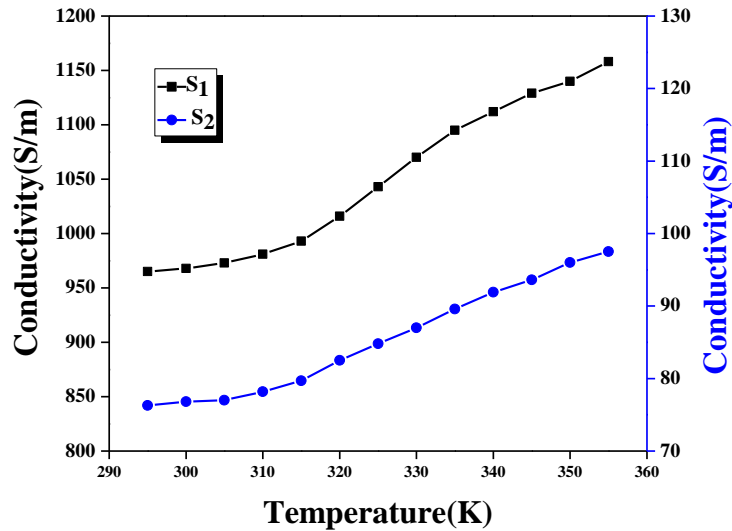

Fig. 4.7: Tenfold increase in electrical conductivity for the composite S_1 compared to S_2.

In order to explain this remarkable difference in conductivity between the samples of composites S_1 and S_2, the transport mechanism in these composites has to be investigated. Generally introduction of CNT to PANI enhances the electrical conductivity of composites by facilitating the interaction between PANI chains and nanotubes through charge transfer between the two (16). More importantly, with their excellent transport properties and high aspect ratio, CNTs can interconnect efficiently with the

conducting channels for carrier transport in various conducting grains of the PANI coated over them (17). In such carrier transport through hoping mechanism of conducting particles, the reduction in the interfacial contact and tunneling resistance plays an important role in facilitating conductivity. Both morphology and XRD studies reveal that due to the efficient templating effect of CNTs in the composite formation of S_1, highly oriented and extended polymer chains with improved crystallinity results here. It is well-known that such ordered molecular structure increases the effective degree of electron delocalization between polymer chains and CNTs and therefore lowers the carrier hopping barrier (16). Also this increased ordering degree of the PANI chains on nanotubes makes the nanotubes interconnect efficiently to the polymer chains by countering the interfacial contact and tunneling resistance (17, 18). It can be understood that such structures can facilitate the transport of charge carriers, by providing them a smooth pathway leading to improved carrier mobility as well as increased electrical conductivity. Thus in sample S_1, the PANI chains remain strongly bonded to the tubes and act as an effective "conducting bridge" leading to improved DC conductivity. While in S_2 the thick, randomly coiled and entwined PANI chains on CNTs can hamper the nanotubes from bridging the carrier paths. Such polymer coating on CNTs cannot stabilise the PANI - CNT interaction in composites and thereby increase DC conductivity. Contrary to what is seen in S_1, thick PANI layers in S_2 are acting as tunneling barriers between adjacent nanotubes inhibiting carrier transport. Thus the remarkable difference in conductivities of the composites S_1 and S_2 is attributed to the alignment and confirmation of PANI chains on CNTs. This is substantiated from the conductivity values of

dedoped samples. When composite S_2 was dedoped, the room temperature conductivity was reduced to 9 S/m while that of S_1 reduced only to 323 S/m.

4.3.5.2 Thermal Conductivity

The room temperature thermal conductivity of composites was measured. MWCNTs have high thermal conductivity (19) while PANI has an extremely low thermal conductivity of 0.43 W/m/K. Another promising result from this study is that the thermal conductivity of composite samples is seen to be reduced to that of PANI (Table 4.1). Previous studies have reported that the thermal conductivity of CNT/polymer composites is relatively insensitive to the CNT concentration (10, 20, 21). In this aspect they are found to be much superior to that of inorganic thermoelectric materials. Many studies on thermal conductivity of conductive polymer composites reveal that the charge carrier contribution to the thermal conductivity is generally small while phonon contribution is dominant (21, 22). These investigations have indicated that the nanostructures, including nano inclusions and nano interfaces in composites, can scatter phonons and reduce thermal conductivity. The prepared composites consist of numerous nanointerfaces which act as effective scattering centers of phonons. As the phonons are highly scattered, thermal transport in these composites is impeded. Thus the thermal conduction behaviour and electrical conduction behaviour of composites are different. In sample S_1, there is further reduction in thermal conductivity and this is attributed to the fine PANI layers on nanotube surface as a result of interfacial polymerisation. It is in agreement with earlier reports which reveal that the advantage of polymer composites is in the improvement of electrical conductivity while the thermal conductivity remains comparable to typical polymeric materials.

4.3.5.3 Seebeck coefficient

Figure 4.8 shows variation of seebeck coefficient, S of composites with temperature. S values are positive which confirms that the composites are of P-type materials (23). Both composites exhibit an increase in Seebeck coefficient with increasing temperature over the measured range from 295K to 355K. In the present study, room temperature Seebeck coefficient of sample S_1 (27.9 µV/K) is significantly improved compared to S_2 (18.23 µV/K) i.e., 53% higher than that of S_2. Interestingly, the remarkable improvement of DC conductivity in S_1 doesn't result in decrease of its Seebeck coefficient. Usually when there is an improvement in electrical conductivity through charge carrier concentration, it has a detrimental effect on Seebeck coefficient (24). As Seebeck coefficient relies on the energetic carrier transport and the electrical conductivity depends on the transport of all mobile charges increased carrier concentration enhances electrical conductivity, but causes decrease in the Seebeck coefficient (25).
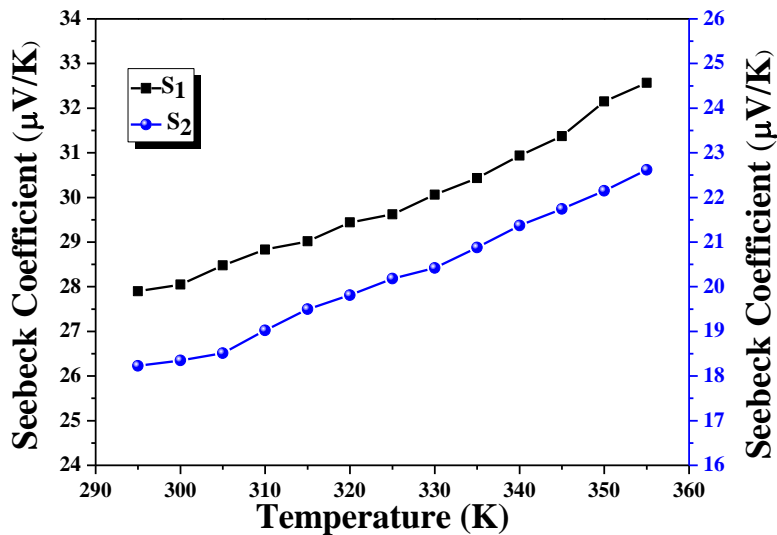

Fig. 4.8: Seebeck coefficient of S_1 compared to S_2.

In studies of conducting polymer based thermoelectric materials, where there is a simultaneous increment in both electrical conductivity and Seebeck coefficient, the enhancement was attributed to the improvement of charge carrier mobility (26, 27). The authors state that the improved carrier mobility is a consequence of improved molecular ordering in polymer chains. As far as thermoelectrics are concerned, the most successful route to achieve improved TE properties is the above mentioned route as it avoids the unpleasant depreciation of Seebeck coefficient with increasing electrical conductivity. The explanation put forward by Meng et al. (22) is important in our experiment also. They relate the improvement of thermoelectric properties of the composite to the size dependent energy-filtering effect caused by the nanostructured PANI coating layer enwrapped over the CNTs. Owing to the efficient templating effect of FMWCNTs during interfacial polymerisation, an exceptional order in chain packing state is acquired. As in the case of electrical conductivity in S_1, the more aligned and extended confirmation of polymer chain on nanotubes is allowing smooth passage of energetic charge carriers also. Thus it can be ascertained that if increased carrier mobility is achieved through improved molecular ordering of polymer chains, both electrical conductivity and seebeck coefficient can be improved.

Table 4.1: Thermoelectric properties of composites.

Sample	Electrical Conductivity σ (S/m)	Thermal Conductivity k(W/m K)	Seebeck Coeff S(μ V/K)	Figure of merit ZT (300K)
S_1	960	0.49	27.9	457.6×10^{-6}
S_2	76.3	0.516	18.25	14.77×10^{-6}

A comparison of thermoelectric properties of composites at 300K is given in the Table 4.1. Based on the measurement results, the performance of a thermoelectric material is evaluated by its dimensionless figure of merit, $ZT=S^2 \sigma T/k$. The figure of merit of S_1 is more than 25 times that of S_2 which shows the improvement brought about by the molecular ordering of polymer chains in composites. As the composites have comparable thermal conductivity, comparison of thermoelectric performance is also done on the basis of power factor ($S^2\sigma$).
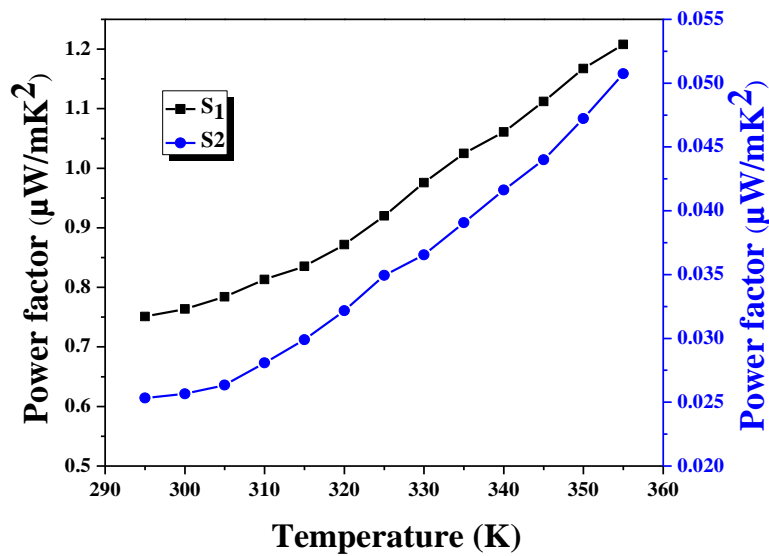

Fig. 4.9: Improved power factor for composite S_1compared to S_2.

The PF of composite samples is plotted against temperature and is depicted in figure 4.9. The thermoelectric power factor of composites is at par with the figure of merit. This study suggests a simple method for achieving unique combination of high electrical conductivity, good seebeck coefficient and low thermal conductivity in CNT based PANI composites. Though, ZT of the composite is currently too low to be

considered as a good thermoelectric material, the results show the possibility of tuning the thermoelectric properties of the conductive polymer and for fabricating efficient thermoelectric devices based on CNT based PANI composites.

4.3.6 Thermal stability of DC conductivity

Cyclic thermal ageing (Fig. 4.8) and isothermal ageing (Fig 4.10) methods were used to study the DC conductivity retention of composites. Earlier reports have revealed the role of MWCNT on the electrical conductivity of MWCNT/PANI composites (28, 29). On cyclic thermal ageing process, electrical conductivity increases with increase in temperature pointing to a semiconductor behavior of both composites. During the first cycle, conductivity steadily increases up to $120^{o}C$ for S_1 samples and up to $110^{o}C$ for S_2 and then the rate of increase diminishes. A significant drop in conductivity is observed after the first cycle, with Sample S_2 showing a larger decrease. After the completion of one cycle, the samples again show increase in conductivity in subsequent cycles. While sample S_1 is capable of achieving a higher conductivity, the extent of increase is low for sample S_2. The values for percentage retention of conductivity after each cycle at $30^{o}C$ and $150^{o}C$ are given in figure 4.9. It shows that the percentage retention in conductivity of S_1 and S_2 at $30°C$ is 91.7 and 70.5 respectively. The corresponding values at the end of the fifth cycle are 87% and 62.38%, respectively. So it is seen that S_1 has better capability to retain DC conductivity at higher temperatures compared to S_2.
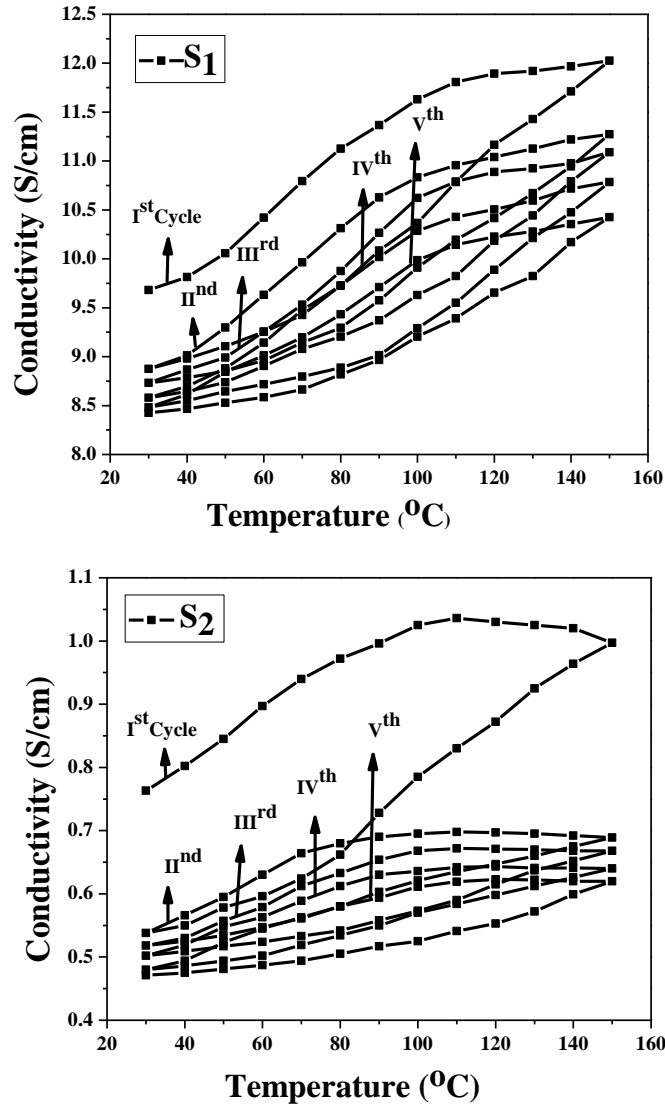
Fig. 4.8: The temperature dependence of DC conductivity under cyclic ageing up to 150°C for S₁ and S₂.

A similar behavior is observed at 150°C (Fig. 4.9b.) with S_1 showing more retention than S_2. In chapter 3, the conversion of conducting polymer phase into the damaged phase resulting in decreased electrical conductivity was discussed. TGA thermograms of sample S_1 has revealed the elevated

thermal stability and the delay in loss of dopant for this sample. Spectroscopic studies indicated the role of stabilising interaction between PANI and CNTs in S_1. XRD analysis revealed that S_1 has ordered polymer chain structure with improved crystallinity. This unique structure on nanotubes stands almost unaffected upon heating. So S_1 is more resistant to damage under elevated temperature. S_2 samples are devoid of such structural ordering, crystallinity and interaction. Hence there is large conductivity degradation. For conducting polymers like PANI, carrier transport is very sensitive to confirmation and ordering of polymer chains along CNT. Wang et al. (26) reported that arrangement of the PANI chains on CNTs reduced the $\pi-\pi$ conjugated defects in the polymer backbone besides increasing the effective degree of electron delocalization and therefore enhanced the carrier mobility in PANI. It can be inferred that to retain conductivity at elevated temperature, the structure and alignment of PANI chains on nanotubes should be retained.
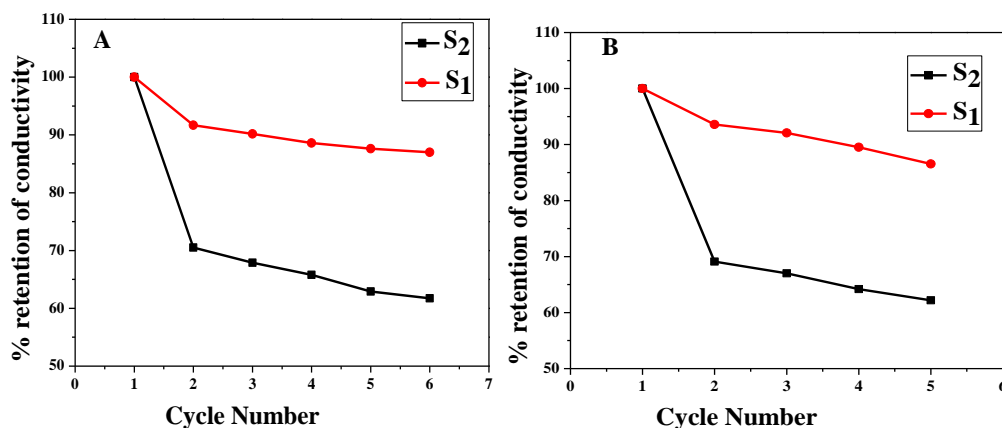

Fig.4.9: Percentage retention in DC conductivity of S_1 and S_2 (A) at 30^0C (B) at 150^0C for each cycle under cyclic aging conditions.

Isothermal stability of samples with respect to DC conductivity is studied with isothermal ageing at 50, 80, 110 and 140°C at 30 minutes intervals. The relative conductivity of samples is obtained by dividing conductivity at 0,30,60,90,120,150 and 180 minutes with the one at zero minute. The relative conductivity is plotted as a function of time in figure 4.10. For sample S_1 improved thermal stability of DC conductivity is observed. These samples exhibit increase in conductivity at 50°C and 80°C and though there is only slight increase, consistency in conductivity is achieved at 110^0C. At 140°C, after an initial decrease, stabilisation for conductivity is achieved. For S_2 sample, as expected, conductivity increases and stability is achieved at 50 and 80°C. From 110°C onwards there is a gradual reduction in conductivity with increase in time. For isothermal ageing at 140°C, the conductivity of the sample keeps on decreasing. After three hours, the conductivity reduced to 92% of the initial value. These observations substantiate the results from cyclic ageing. Apart from this, the phenomenon also reveals the possibility of oxygen absorption on the surface of polymers followed by its diffusion into the bulk (30). Tansley et al. (31) reported that oxygen absorption occurs on the surface of polymers followed by its diffusion in to the bulk. This could lead to incorporation of oxygen into the polymer chain transforming the semiconducting state into an oxidized one. This oxidation can lead to discontinuity in conduction pathways and thus decrease the conductivity of polymer. From the previous discussions regarding the structural and interactive forces operating in S_1 and S_2 composites, it is clear that S_1 can resist the diffusion and the attack of atmospheric oxygen on polymer chains. But in S_2, the thick but loose polymer chains allow the diffusion of oxygen into the polymer chains and causes oxidation of polymer

chains. This disruption in conjugated chain structure hinders conductivity as is evident from the ageing studies on S_2 samples. Based on the above discussion, deprotonation and polymer chain degradation by atmospheric oxygen lead to conductivity ageing at high temperature.
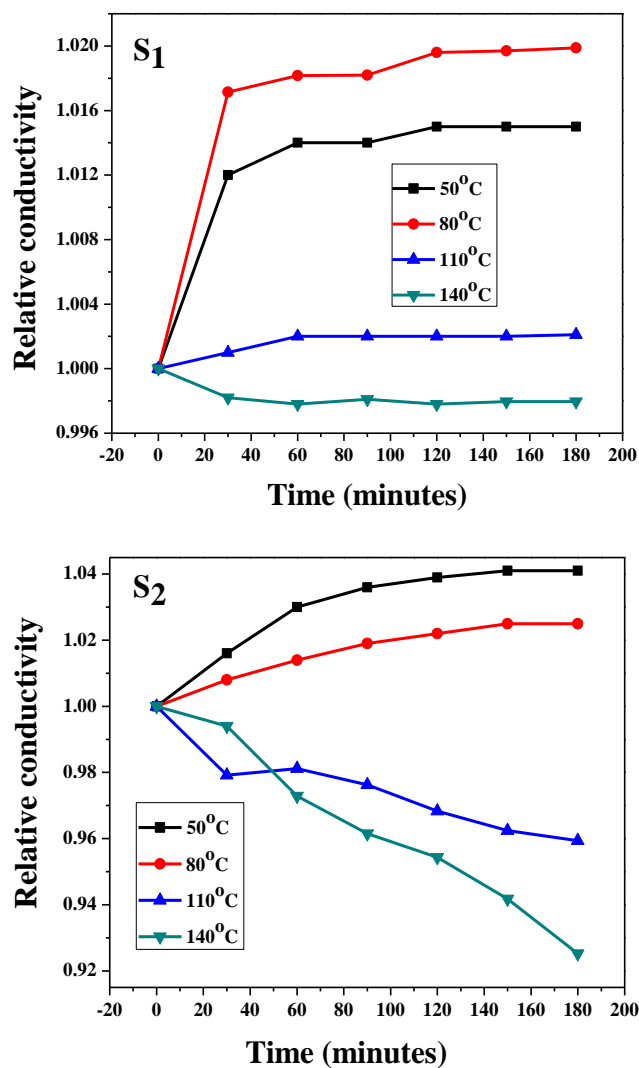

Fig. 4.10. Relative conductivity as a function of time for S_1 and S_2.

The morphology and interaction between PANI and CNTs are crucial in deciding the extent of degradation. Thus the excellent properties of S_1 composite are very promising for electronic applications.

4.4 Conclusions

PANI/FMWCNT composites were prepared by single phase (SP) polymerisation and interfacial polymerisation (IF) methods. By proceeding with dynamic interfacial polymerisation, remarkably enhanced electrical conductivity, improved seebeck coefficient and ZT are obtained in PANI/FMWCNT composites. The XRD, SEM and TEM results of this sample showed that this composite possess an extended and ordered molecular structure as secondary growth is avoided here. This polymer chain with ordered molecular structure formed on the surface of nanotubes increased the carrier mobility resulting in an electrical conductivity of 960 S/m and Seebeck coefficient 27.9 µV/K. Though this process allows for thermoelectric performance improvement, it maintains the low thermal conductivity of PANI Thus we have demonstrated an effective synthetic route which lead to favorable improvement in seebeck coefficient, electrical conductivity and thermal conductivity which makes this composites more attractive for thermoelectric applications.

When subjected to cyclic thermal ageing for five cycles, the IF composite shows 87% retention while the conductivity of SP sample retains only 62.38%. The composite synthesised through interfacial polymerisation maintains 99.8% conductivity on isothermal ageing for three hours at 140°C, while the other sample retains 92% conductivity. Morphology, XRD, FTIR, Raman, UV-Visible spectroscopy and TGA studies reveal the role of interfacial

polymerisation in the formation of highly ordered polymer backbone on CNTs, improved crystallinity and strong PANI-NT interactions in the composites.

References

[1]   Y. Du, S.Z. Shen, K. Cai, P.S. Casey, *Prog. Polym. Sci.,* 37,2012, p. 820.

[2]   W. Feng, X.D. Fai, Y.Q. Lian, J. Liang, X.G. Wang, K. Yoshino, *Carbon*, 41, 2003, p. 1551.

[3]   R.V. Salvatierra, M.M. Oliveira, A.J.G. Zarbin, *Chem. Mater.* 22, 2010, p.5222.

[4]   S. Quillard, G. Louarn, S. Lefrant, A.G. MacDiarmid, *Phys. Rev. Lett.*, 59, 1987, p. 1464

[5]   C. Dhand, S.K. Arya, S.P. Singh, B.P. Singh, M. Datta, B.D. Malhotra, *Carbon*, 46, 2008, p. 1727.

[6]   P. Kar, A. Choudhury, *Sensor Actuat. B-chem.*, 183, 2013, P. 25.

[7]   T.M. Wu, Y.W. Lin, *Polymer*, 47, 2006, p. 3576.

[8]   Z. Ping, G.E. Nauer, H. Neugebauer, J. Theiner, A. Neckel, *J. Chem. Soc. Faraday Trans.*, 93,1991, p.21.

[9]   M. Cochet, W.K. Maser, A. M.Benito, M.A. Callejas, M.T. Martínez, J.M. Benoit, J. Schreiber, O. Chauvet, *Chem. commun.*, 16, 2001, p. 1450.

[10]   Q. Yao, L .Chen, W. Zhang, S. Liufu, X. Chenm, *ACS Nano*, 4, 2010, p.2445.

[11]   R. Chan Yu King, F. Roussel, J.F. Brun, C. Gors, *Synth. Met.*, 162, 2012, P. 1348.

[12] K.R. Reddy, B.C. Sin, C. Yoo, D. Sohn, Y. Lee, *Journal of Colloid and Interface Science*. 340, 2009, p.160.

[13] Z.M. Zhang, Z.X. Wei, M.X. Wan, *Macromolecules*, 35, 2002, p. 5937.

[14] J. Yun, J.S. Im, H. Kim, Y.S. Lee Applied Surface Science 258, 2012, p.3462.

[15] L.Li, Z. Qin, X. Liang, Q. Fan,Y. Lu, W. Wu, M.Zhu, J. Phys. Chem. C,113, 2009, p.5502.

[16] E.N. Konyushenko, J. Stejskal, M. Trchova, J. Hradil, J. Kova´ rova´, J. Prokes, M. Cieslar, J.Y. Hwang, K.H. Chen, I. Sapurina, *Polymer*, 47, 2006, p. 5715.

[17] P. Saini, V. Choudhary, B.P. Singh, R.B., Mathur, S.K. Dhawan, *Mater Chem Phys*., 113,2009, p.919.

[18] H. Zengin, W. Zhou, J. Jin, R.Czerw, D.W. SmithJr, *Adv. Mater*.,14, 2002, p.1480.

[19] S. Berber, Y.K. Kwon, D. Tomanek, *Phys. Rev. Lett*. 84, 2000, p.4613.

[20] C. Yu, Y.S. Kim, D. Kim, J.C. Grunlan, *Nano lett.*, 8, 2008, p. 4428.

[21] C.A. Hewitt, D.L. Carroll, Carbon Nanotube-Based Polymer Composite Thermoelectric Generators, ACS Symposium Series, Vol. 1161.

[22] C. Meng, C. Liu, S. Fan, *Adv. Mat.*, 22, 2010, p. 535.

[23] S.C.K. Mishra, S. Chandra, *Indian J. Chem.*, 33, 1994, p. 583.

[24] A.F. Loffe, Semiconductor Thermo elements and Thermoelectric Cooling, London, 18. A. Eucken and G. Kuhn, 1957.

[25] N. W. Ashcroft and N. D. Mermin, Solid State Physics, New York, Holt, Rinehart and Winston, 1976.

[26] Q. Wang, Q. Yao, J. Chang, L. Chen, *J.Mater.Chem.*,22, 2012, p.17612.

[27] Y.Du, S.Z. Shen, W. Yang, R. Donelsonb, K. Cai, P.S. Casey, *Synth. Met.,* 161, 2012, p. 2688.

[28] M.O. Ansari, F. Mohammad, *Compos. Part B-Eng.,* 43, 2012, p.3541.

[29] A.L. Cabezas, Y. Feng, L.R. Zheng, Z.B. Zhang, *Carbon*, 59,2013, p.270.

[30] B. Gao, Q. Fu, L. Su, C. Yuan, X. Zhang, *Electrochim. Acta*, 55, 2010, p. 2311.

[31] T.L. Tansley, D.S .Maddison, 69, 1991), J. Appl. Phys., p.7711.

.....๛๛.....

Chapter 5

IMPROVED STRAIN SENSING PROPERTY OF FUNCTIONALISED MULTIWALLED CARBON NANOTUBE/POLYANILINE COMPOSITES IN TPU MATRIX*

PANI / FMWCNT based conductive thermoplastic polyurethane (TPU) films were prepared to study their strain sensing property. The composites were prepared by solution casting method using FMWCNT coated with polyaniline. The coating was done by in-situ and ex-situ polymerization of aniline. The composites thus prepared were designated as FMWCNT-PANI/TPU (I) and FMWCNT-PANI/TPU (E), respectively. The electrical resistivity and resistivity – strain behaviour of these composites were measured. The percolation threshold and the strain sensitivity of these films depended on the dispersion of conductive fillers in the polymer matrix. The well-dispersed filler in FMWCNT-PANI/TPU (I) composites resulted in low percolation threshold and improved strain sensitivity. The composite with 2weight % filler content, showed a gauge factor of 1075 at 100% strain and exhibited high reversibility in resistivity upon elongating to 20%. A coating of PANI on FMWCNT reduced its entanglement and enhanced the interfacial interaction between the nano fillers and TPU, leading to improved strain sensitivity. The experimental data for strain sensing was in good agreement with the theoretical equations derived from a model based on the tunneling theory by Simmons.

5.1 Introduction

The ability to change the electrical conductivity when tensile strain is applied is considered as a potential requisite for a strain sensor. Recently, significant advances have been made in building highly sensitive strain sensors using CNT/ polymer composites (1-3). When an elastomer is used as matrix, strain sensors with high surface area and wide strain range can be produced. Due to their better stretchability, bendability, mechanical robustness, light weight, and low-cost of fabrication, they find application in many areas where conventional strain sensors cannot be used (4). The CNT based elastomeric sensors developed have higher sensitivity compared to conventional strain sensors such as metal-foil strain gauges (4-7). The higher sensitivity observed in these strain sensors is attributed to factors such as formation of conductive network, variation in internal conductive network, tunneling effect of conductive particles and piezoresistivity. The electrical conductivity in these CPCs is provided by conductive filler which forms a network within the polymer matrix. A low filler content is to be maintained as the amount of conductive fillers reduces the recovery rate (8). However, the efforts to develop strain sensors with low percolation threshold, low filler content, high sensitivity, good repeatability, low hysteresis and excellent durability has not fully succeeded yet. Infrastructures like buildings, bridges etc., are expected to stay for centuries. In the case of vehicles they are expected to serve for years. So the stability of conductive network under harsh conditions is essential. In our earlier studies it was reported that the composites of FMWCNT and PANI prepared through interfacial polymerisation exhibited improved electrical properties as well as high temperature stability in electrical conductivity (9). Recent works on thermoplastic polyurethane (TPU)

composites showed that they can sustain very large deformations and possess excellent thermo physical properties. No systematic study on the strain sensitivity of FMWCNT-PANI/TPU composites has been reported yet. In this chapter the dependence of electrical conductivity on the strain level of composites based on FMWCNT-PANI/TPU is reported. The FMWCNT with a surface layer of PANI was prepared through in-situ polymerisation and ex-situ polymerisation methods. FMWCNT without PANI were also used for comparison. The observed difference in electrical and electromechanical properties was examined based on their morphology and distribution of the conductive component within the insulating matrix. The experimental data was compared with theoretical equations derived from a model based on the variation of the tunneling distance between conducting particles under strain.

5.2 Experimental

5.2.1 Synthesis of FMWCNT-PANI/TPU composites FMWCNT-PANI/TPU composites were prepared by the following methods.

(i)   Synthesis of FMWCNT-PANI/TPU (I) composite films

FMWCNT-PANI filler was synthesised through interfacial polymerisation of aniline in presence of FMWCNTs as per section 4.2.1. The procedure involved polymerisation of 0.465g of aniline in a water/chloroform interface with aniline and nanotubes in the organic phase and APS in the aqueous phase. The composite sample was dedoped and redoped with 1.5M naphthalene sulphonic acid (NSA) dopant. FMWCNT-PANI/TPU(I)composites were prepared as follows. A fixed quantity(4g)

of TPU was dissolved in 100ml THF under vigorous stirring. Different weight percentages of FMWCNT-PANI filler (0.25, 0.50, 0.75, 1.00, 1.25, 1.50, 2.00, 2.50, and 3.00 weight %) were dispersed in 100ml THF through sonication for 1 hour at room temperature. These two solutions were mixed together by ultra sonication for 1 hour and the mixed solution was transferred into a Petri dish and kept in an oven at 60°C under vacuum for 10 hours to remove the solvent. The polymer composite films were collected and cut into the required dimensions for further measurements. These FMWCNT-PANI/TPU (I) composites are designated as NC_{11}, NC_{12}, NC_{13}, NC_{14}, NC_{15}, NC_{16}, NC_{17} and NC_{18}.

(ii)   Synthesis of FMWCNT-PANI/TPU (E) composite films

Polyaniline was synthesised through interfacial polymerisation of aniline in absence of FMWCNTs. Appropriate quantity PANI is mixed with FMWCNT and the mixture (0.25, 0.5, 0.75, 1, 1.25, 1.5, 2, 2.5, and 3 weight %) were dispersed in 100ml THF through sonication for 1 hour at room temperature. The remaining procedure is the same as in (i). These composites FMWCNT-PANI/TPU (E) composites are designated as NC_{21}, NC_{22}, NC_{23}, NC_{24}, NC_{25}, NC_{26}, NC_{27} and NC_{28}.

(iii)   Synthesis of FMWCNT/TPU composite films

Different quantity of FMWCNT (0.25.0.5.0.75, 1, 1.25, 1.5, 2, 2.5, and 3 weight %) were dispersed in 100ml THF through sonication for 1 hour at room temperature. The remaining procedure is the same as in (i). These composites FMWCNT/ TPU composites are designated as NC_{31}, NC_{32}, NC_{33}, NC_{34}, NC_{35}, NC_{36}, NC_{37} and NC_{38}.

5.2.2 Characterization

The microstructure of the composites was observed using Hitachi SU6600 Variable Pressure FESEM and JEOL 300 KV HRTEM. To study the electrical and electromechanical properties, samples of the size of 60mm × 10 mm × 1 mm were cut from the composite films. The DC conductivity of the composites was measured by a standard two-probe electrode configuration using a Keithley 2400 nanovoltmeter as described in section 2.2.5. The strain sensitivity measurements were performed on a Shimadzu Universal Testing Machine (model AG-I) coupled with the Keithley 2400 nanovoltmeter as per section 2.2.8.

5.3 Results and analysis

5.3.1 Electrical properties of unstrained samples

Figure 5.1 presents the measured DC electrical conductivity of the composite films at filler concentrations up to 3 weight percentage. Virgin TPU film is reported to have an electrical conductivity of the order of 10^{-14} S/cm(11). FMWCNT-PANI/TPU (I) composite exhibits more pronounced enhancement in conductivity than the other two composites (Fig. 5.11). In this case the conductivity increases by 10 orders at a CNT loading of 0.75%. This sharp increase in conductivity to 1.1×10^{-4} S/m indicates the formation of infinite conductive networks by the filler particles (12). In the case of FMWCNT/TPU and FMWCNT-PANI/TPU (E) the conductive network formation occurs at 1% filler concentration. At high filler loadings all the composites show a stabilization effect. It is observed that FMWCNT with a uniform coating of PANI greatly improves the conductivity of TPU films.
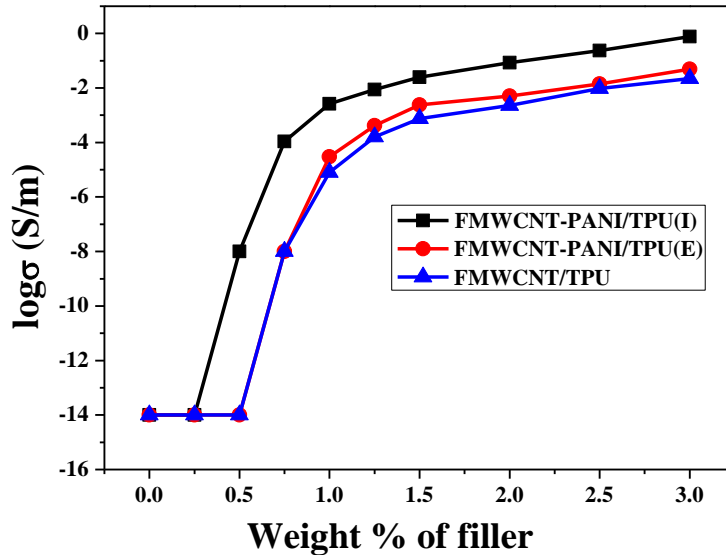
Fig. 5.1: Electrical conductivity of various composites as a function of the weight % of the filler.

According to the classical percolation theory

$$\sigma = \sigma_0 \, (v\text{-}v_c)^t \quad \dots\dots\dots\dots\dots\dots\dots\dots\dots\dots\dots\dots\dots\dots\dots\dots (5.1)$$

for $v > v_c$

where σ is the electrical conductivity of the composite, σ_0 is a constant for a particular filler–polymer combination, v is the filler's volume fraction, v_c is the percolation threshold, the exponent 't' is related to sample dimensionality, i.e., t = 1, 1.33, or 2.0 for one, two, or three dimensions, respectively (12,13). By getting the logarithm from both sides of Eq. (5.1), this equation can be written in the following format,

$$\log \sigma = \log \sigma_{0 +} t \log (v\text{-}v_c) \quad \dots\dots\dots\dots\dots\dots\dots\dots\dots\dots\dots\dots (5.2)$$

Eq. 5.2 can be used to find the percolation threshold and the critical exponent via linear regression of log (σ) versus log (v-v_c). By fitting the experimental

data to a plot of log σ versus log(v- v_c/v_c), as shown in figure 5.2a,b and c, the percolation threshold values for FMWCNT-PANI/TPU(I), FMWCNT-PANI/TPU (E) and FMWCNT/TPU composites are found to be 0.6, 0.9 and 0.95 weight% respectively (0.42, 0.6 and 0.63 volume percentage). Critical exponent values of the FMWCNT-PANI/TPU (I), FMWCNT-PANI/TPU (E) and FMWCNT/TPU composites found in this study are 2.97, 2.28 and 2.11, respectively. The fitted value for the critical exponent deviates from the theoretical universal scaling value t = 2. This can be explained by multiple percolations in conducting polymer systems, as proposed by Levon et al. and Grimaldi et al. (14,15). According to the authors, the electrical conductivity of a polymer system is determined by the morphology of filler particles also in addition to the filler loading. In the case of tunnelling percolation network, such a large exponent indicates a broad distribution of the tunnelling resistance and hence a broad distribution of the inter particle distance (15). In this experiment, the results prove that PANI coated nanotubes can improve the conductivity and decrease percolation threshold. From the above discussion it can be inferred that the low percolation threshold value for FMWCNT-PANI/TPU(I) results from its well-dispersed and high-aspect ratio filler components. The dispersion of various filler particles in TPU matrix and its effect on effective aspect ratio is discussed in the section of morphology studies.
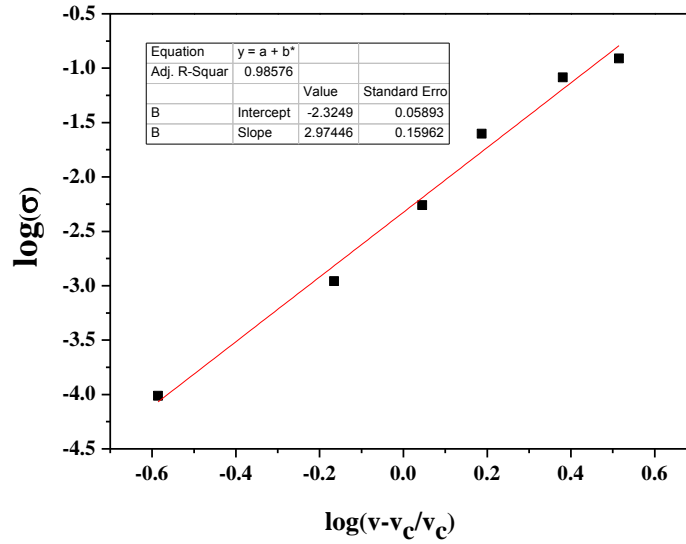
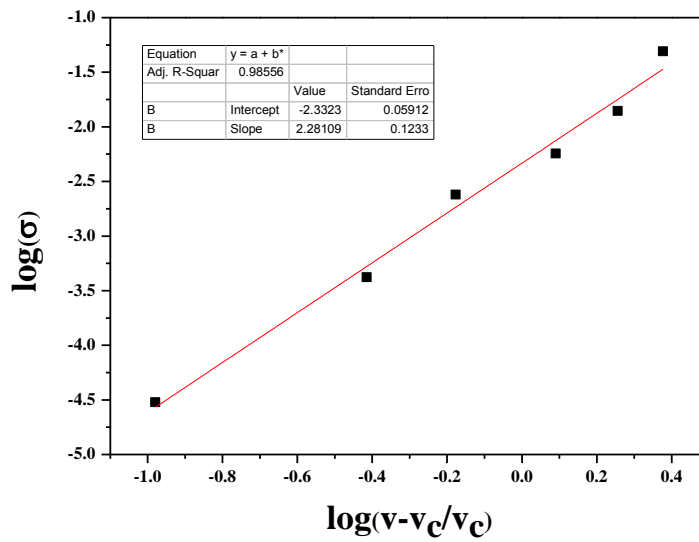**Fig. 5.2a: Log-log plots of σ_{DC} and v-v$_c$/v$_c$ of FMWCNT-PANI/TPU(I).**

Fig. 5.2b: Log-log plots of σ_{DC} and v-v$_c$/v$_c$ of FMWCNT-PANI/TPU(E).
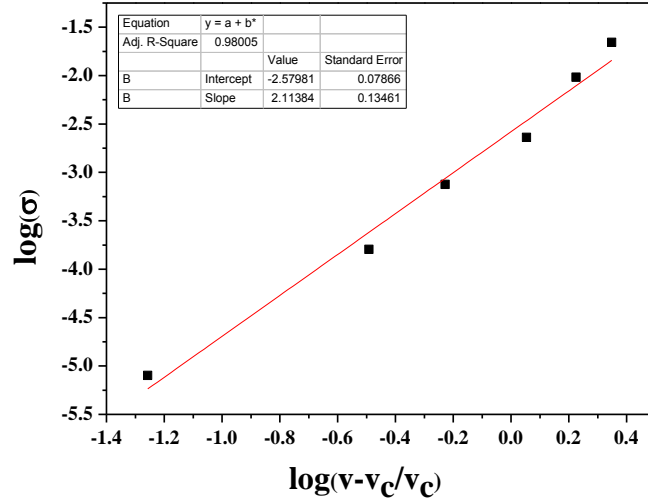
Fig. 5.2c: Log-log plots of σ_{DC} and $v\text{-}v_c/v_c$ of FMWCNT/TPU.

5.3.2 Morphology

The FESEM micrographs in figure 5.3 show the surface morphology of the FMWCNT, PANI coated FMWCNT, FMWCNT-PANI/TPU(I), TPU/PANI/FMWCNT(E) and FMWCNT/TPU samples.
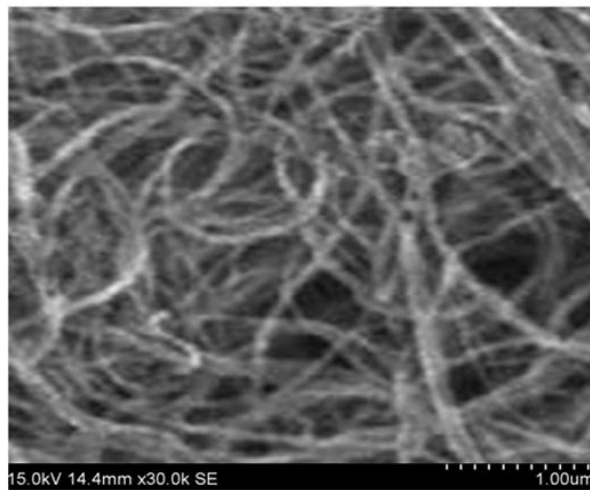

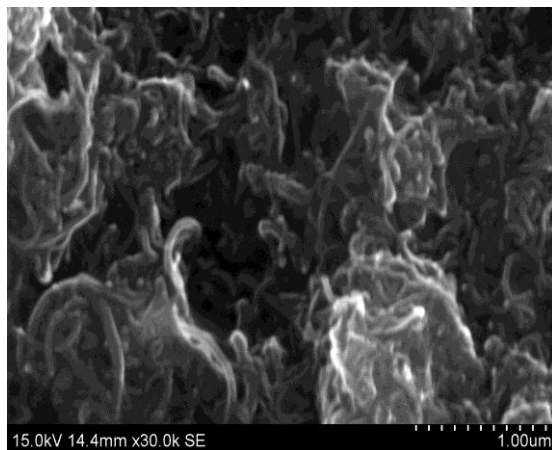**Fig. 5.3a: FESEM image of FMWCNT.**

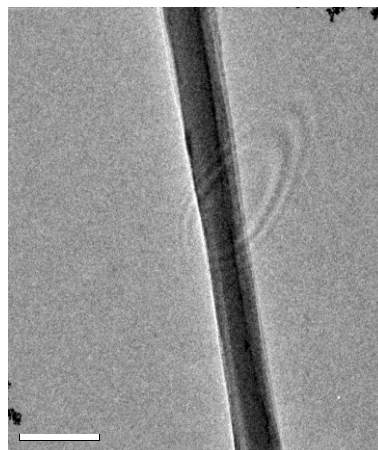**Fig. 5.3b: FESEM image of PANI coated FMWCNT.**

Fig. 5.3c: TEM image of PANI coated FMWCNT.

The FESEM image of FMWCNT (Fig.5.3a) shows that its average diameter is 20nm. FESEM images of the PANI coated FMWCNT and TEM image of the same (Fig.5.3b and c) confirm that the outer surface of the individual CNTs is coated uniformly by a thin PANI layer of thickness about 10nm. The image of FMWCNT-PANI/TPU(I) composite(filler loading of 2 weight%)in figure 5.3d shows that PANI coated FMWCNTs remain fairly straight, non-entangled and homogeneously dispersed in the polymer matrix. The average diameter of these PANI coated nanotube fillers is about 80nm in TPU matrix, indicating that a layer of TPU is formed on its surface. The large surface area of the CNTs increases the van der Waals intermolecular interactions leading to a strong tendency to aggregate when dispersed within the polymer matrix. This aggregation is detrimental to the conductive network formation (16). So, CNTs though possessing a high aspect ratio, its flexibility and tendency for aggregation reduces its effective aspect ratio. This reduction in actual aspect ratio is an obstacle for acquiring high conductivity and low percolation threshold. In FMWCNT-PANI/TPU(I) composites, the tendency for

agglomeration is reduced and effective aspect ratio of nanotubes is retained because of the presence of a uniform coating of PANI on the CNT surface. It is assumed that the numerous bonding sites between PANI encapsulated FMWCNTs and TPU polymer chains are leading to an enhanced dispersion of these filler particles in the polymer matrix. Even with a low percentage loading of PANI/ FMWCNT, the composite seems capable of forming an efficient network. This efficiency in network formation leads to low percolation threshold and high conductivity in FMWCNT-PANI/TPU(I) composites. In the other two composites (Fig. 5.3e and f) FMWCNT and PANI are seen as curled, entangled and randomly oriented, aggregates. There is poor adhesion between CNTs and polyurethane. The aggregation of CNTs suggests that the functionalisation of CNTs do not aid in dispersion of CNTs in TPU matrix. Even the presence of PANI does not modify the dispersion of CNTs in FMWCNT-PANI/TPU(E) samples. Thus the poor adhesion and heterogeneous dispersion of conductive fillers in TPU matrix is responsible for the relatively high percolation threshold and low electrical conductivity of these composites.
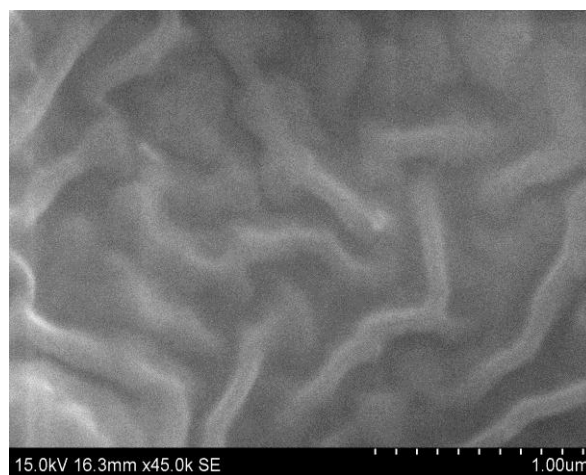

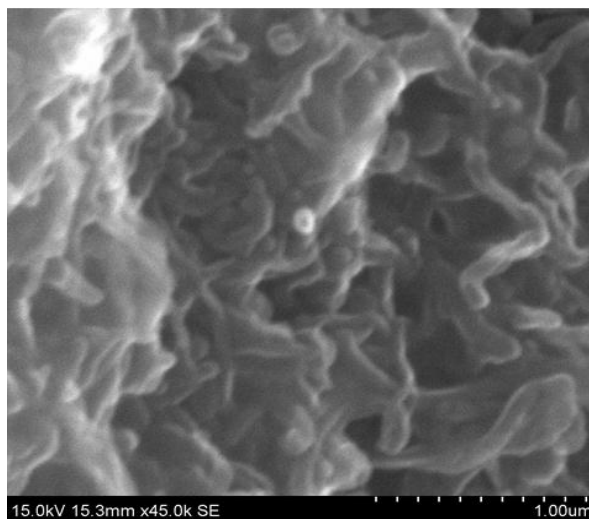**Fig. 5.3d: FESEM image of FMWCNT- PANI/TPU(I).**

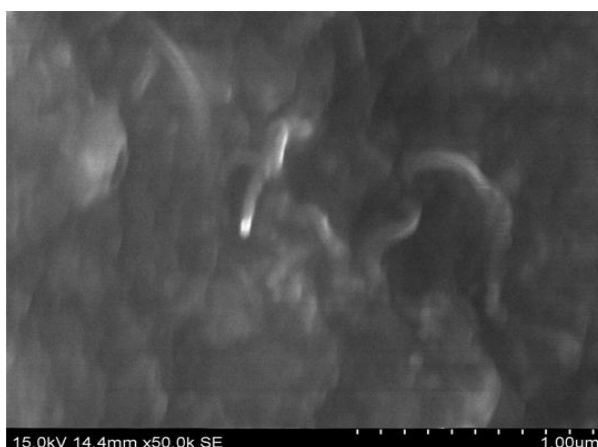**Fig. 5.3e: FESEM image of FMWCNT-PANI/TPU(E).**

Fig. 5.3f: FESEM image of FMWCNT/TPU.

5.3.3 Strain sensing

Generally the variation of the effective electrical conductivity of strain sensing nanocomposites is more sensitive to an applied strain when the conducting filler concentration is close to the value of the percolation

threshold (17, 18). At this concentration, any distortion of the conductive network generates a change in potential barrier that makes the transport of charge carriers difficult. As a consequence, a significant change in resistance will be produced (19). But, once the applied strain reaches a critical value, the separation between MWCNTs is so large that the electrically percolating network breaks down and electrical ''depercolation'' occurs (7, 20). At this stage, measurement of the resistance of the composites to an applied strain can be difficult due to the extremely high values in the non-conducting regime. Therefore, an optimum value near the percolation threshold has to be chosen, which doesn't cross the measurable limit of resistivity. In order to acquire detailed information about the behaviour of the conductive network during mechanical deformation, composites containing 2 weight % of filler concentrations are chosen.

Figure 5.4 shows the change in resistivity of the TPU composite film with respect to applied strain up to 100%. All the samples present a definitive trend where resistivity increases proportionally with increasing tensile strain. Up to 2.5% strain there is only a slight increase in resistivity in all these composites. During elongation, two phenomena occur simultaneously in the composite films i.e. breakdown of existing conductive networks and formation of new conductive networks. These two phenomena compete with each other during the whole process (21- 23). When there is hardly any increase in resistivity, it reveals that the number of the formation and breakdown of the conductive paths formed by filler particles are balanced. At 5% strain, the relative resistivity reaches 2.6, 1.14 and 1.05 for FMWCNT-PANI/TPU(I), FMWCNT-PANI/TPU(E) and FMWCNT/TPU respectively. From there onwards a linear relationship can be observed

between resistivity and strain. Here the breakdown of conductive networks is more predominant than its formation. Though the behaviour of all composites follow the same pattern, a steeper slope for FMWCNT-PANI/TPU(I) is noticed. During the 100% deformation, FMWCNT-PANI/TPU(I) composite records an increase of three order while for the other two composites it is of one order only. Generally for a conductor-filled polymer to be electrically conductive, the filler particles must either be in contact, or be sufficiently close to each other to enable conductance through ''tunnelling effect'' (24,25). Conductivity of the system therefore is dependent on the number of contact points and the distance between neighbouring particles. In our experiment, for FMWCNT-PANI/TPU(I) film, the homogeneity in dispersion aids in the formation of an efficient conductive network and high conductivity. The strong interfacial interaction between TPU matrix and PANI coated CNTs leads to a linear alignment of the filler particles. When an external strain is applied, the alignment of polymer chains in the direction of the stretch increases the average distance between the conductive filler particles. This corresponds to a decrease in effective filler particle concentration, as suggested in a number of studies. Here the filler particles are already at an optimum distance contributing maximum to the electrical conductivity. Consequently there will be a hike in the electrical response of the composite film. This will result in highest strain sensitivity for this sample.

For TPU/PANI/FMWCNT(E) and for FMWCNT/TPU the increase in resistivity with elongation is relatively less. In both of these composites CNTs are in an entangled and coiled state. Upon elongation, the uncoiling of CNTs occur which can induce formation of new conductive paths. i.e.,

breakdown of existing conductive networks and formation of new conductive networks take place simultaneously, though the former process predominates. Thus the increase in resistivity during the tenure of 100% elongation is comparatively less in these composites.
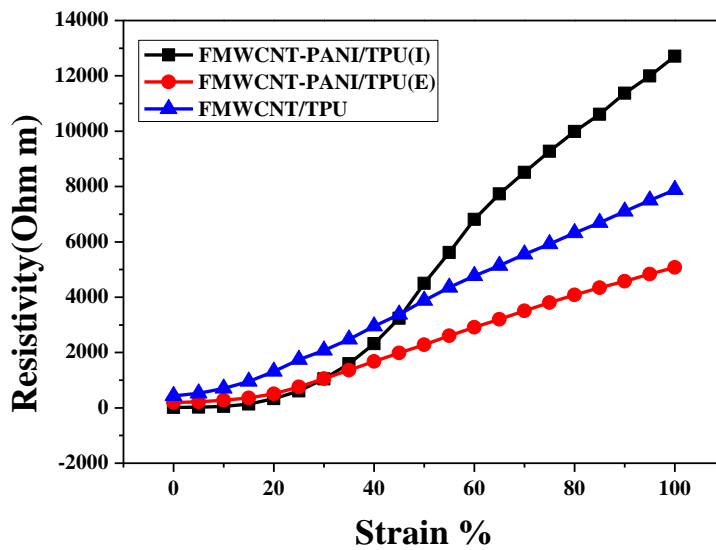

Fig. 5.4: Resistivity Vs. Strain percentage for the composite films.

To estimate the strain sensitivity of these composites quantitatively, the gauge factor has been calculated. It is defined as the relative change in electrical resistance due to an applied mechanical deformation. It is thus a dimensionless parameter, which can be obtained from

$$\text{GF} \ = \ \frac{\frac{dR}{R}}{dl/l} \quad \dots \dots \dots \dots \dots \dots \dots \dots \dots \dots \dots \dots \dots \dots \dots \dots \dots \dots (5.3)$$

where R is the steady-state electrical resistance of the material without deformation and dR is the resistance change caused by the change dl in length (l) (25).
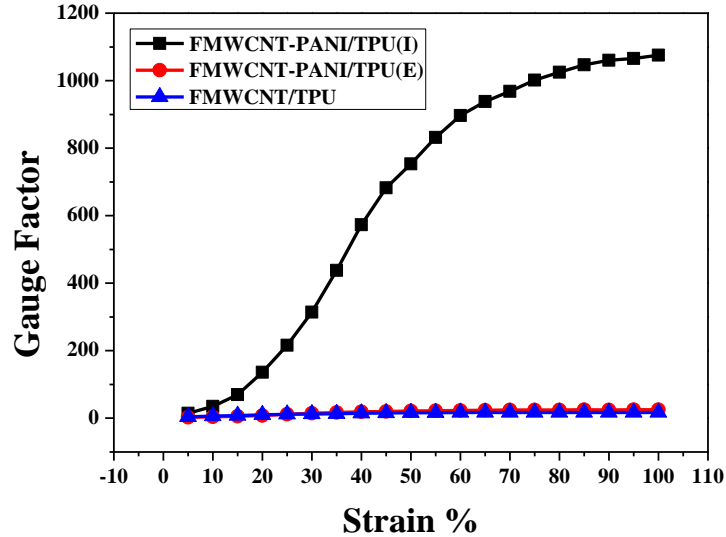
Fig. 5.5: Gauge factor as a function of strain percentage for the composite films.

The calculated GF values are given in figure 5.5. As expected, FMWCNT-PANI/TPU(I) is the most strain sensitive with a gauge factor of 14 at 5% strain which jumps to 896 at 60% strain. From there onwards, the rate of increase is rather small and GF reaches to 1075 at 100% strain. On the other hand, for the other two composites GF values are, 24 and 17 at 100% for FMWCNT-PANI/TPU (E) and FMWCNT/TPU, respectively. Enhanced sensitivity (GF > 50) is usually difficult to achieve in CNT based TPU composites due to inhomogeneous mixing, irregular particle/CNT bundle sizes, wide distribution of tunnel gaps etc. (4). As discussed in section 3.1, FMWCNT-PANI/TPU(I)has high effective aspect ratio, uniform dispersion and low resistivity. These geometrical and resistivity factors contribute to the high gauge factor obtained. L. Lin et al. (4) has demonstrated the use of mixed carbon fillers and functionalized carbon nanotubes in TPU based strain sensors and reported of large strain-sensing capability and a wide

range of strain sensitivity. They compared the range of tunable sensitivity with some other results reported in literature. They noted that a GF of 5 to 140238 (220% strain) obtained in their study with 10% filler content, is much larger than the results reported previously. But reducing the filler content is also very important as it determines the portion of unrecoverable elongation in TPU. In the case of filled TPU composites, it was also reported (27) that almost complete recovery (up to 98%) after elongation can be reached in pure polyurethane. However, the presence of the conductive filler reduces the recovery rate down to 70% when the load is above the percolation threshold. Hence achieving good strain sensitivity along with low filler content is highly desirable. In our experiment a gauge factor of 1075 at 100% strain with 2% filler concentration is achieved.

Usually mechanical deformation of the elastomeric composite leads to deformation and disruption of the electrical percolation network. The extent of this deformation is evident from the relative conductivity changes when samples are subjected to elongation/contraction cycles (9,28). As the deformation in practical use is usually under 15%, the samples were stretched to a 20% strain and then the strain was released. Figure 5.6 reveals the resistance changes during the elongation/contraction cycle. All samples exhibit hysteretic behaviour. E. Hrehorova et al. (29) pointed out that, the portion of unrecoverable electrical conductivity in polyurethane elastomer/ polyaniline (PU/PANI-HCl) composite films is probably due to micro-heterogeneity of PU/PANI-HCl composite. They explained that some places previously occupied by PANI-HCl clusters became micro-pores ("free volume places") and might be filled with polymer segments or PANI-HCl clusters during mechanical unloading. The probability of their complete

healing was negligible considering the very small content of the PANI phase in the composite. According to them, intermolecular interactions would promote diffusion of flexible and chemically similar chain segments of the elastomer matrix rather than reversion of dissimilar and hard fragments of PANI-HCl into these vacant ''free volume places'' of the PU matrix. In our experiment, the same reason can be applied for FMWCNT-PANI/TPU (E) and FMWCNT/TPU composites. But for FMWCNT-PANI/TPU (I) composite, the film resistivity increases from 11.8 to 334 ohm-m at 20% elongation and returns to 40.5 ohm-m after elongation. This composite exhibit excellent sensitivity as well as high reversibility of conductivity after deformation. Because of the well-distributed inter connections of conducting paths existing between PANI coated CNTs and TPU chains, even with 100% elongation, some of the conducting networks are retained. This is seen from the FESEM images of the 100% strained samples given in figure 5.7. The high effective aspect ratio and strong adhesion between the filler particles allows them to align in the direction of elongation and return to previous state without much damage. In earlier reports (28-30) the irreversible component of resistance in TPU/PANI composites were very large as in the case of FMWCNT-PANI/TPU (E) and FMWCNT/TPU composites. In CNT based elastomeric composites, there should be good interaction between polymer chains and nanotubes to counter this irreversible portion. In FMWCNT-PANI/TPU (I) composite, the PANI coated FMWCNTs are well bound to the TPU chains. When a stretching force is applied, the filler particles are dragged along the line of stretch. On retraction, the contacts between filler particles are restored. As a result, high GF combined with excellent reversibility is obtained. For FMWCNT-PANI/TPU

(E) and FMWCNT/TPU composite films, due to the strong attraction, CNTs form rigid aggregates which in turn restrict its mobility. Thus relatively weak bonding between CNTs and TPU chains results in poor strain sensitivity and reversibility.
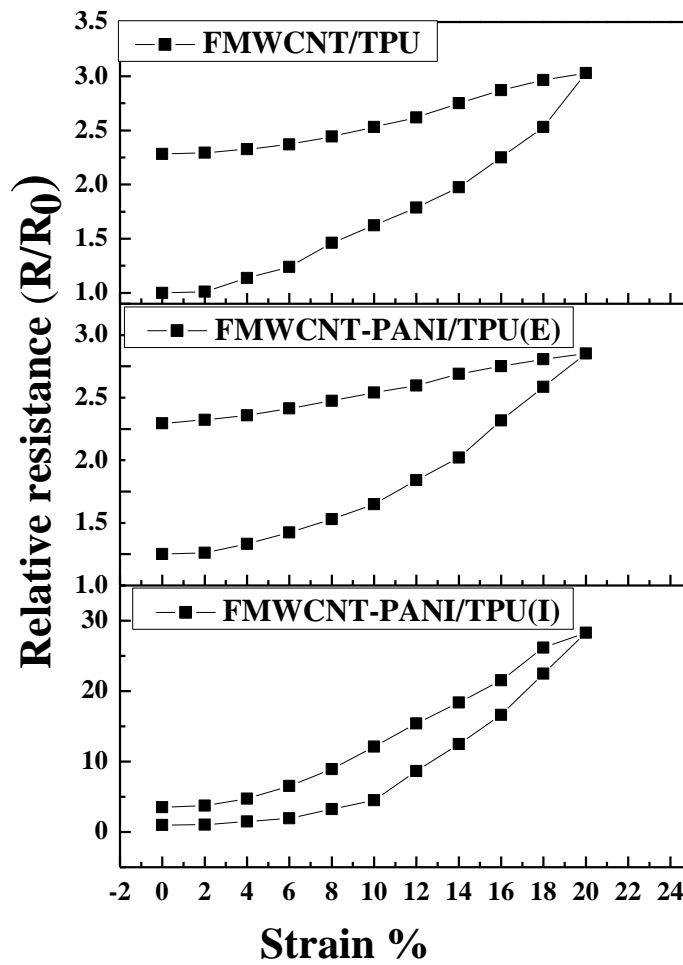

Fig. 5.6: R/R$_0$ for the first elongation/contraction cycle with a maximum strain of 20% for the composite films.
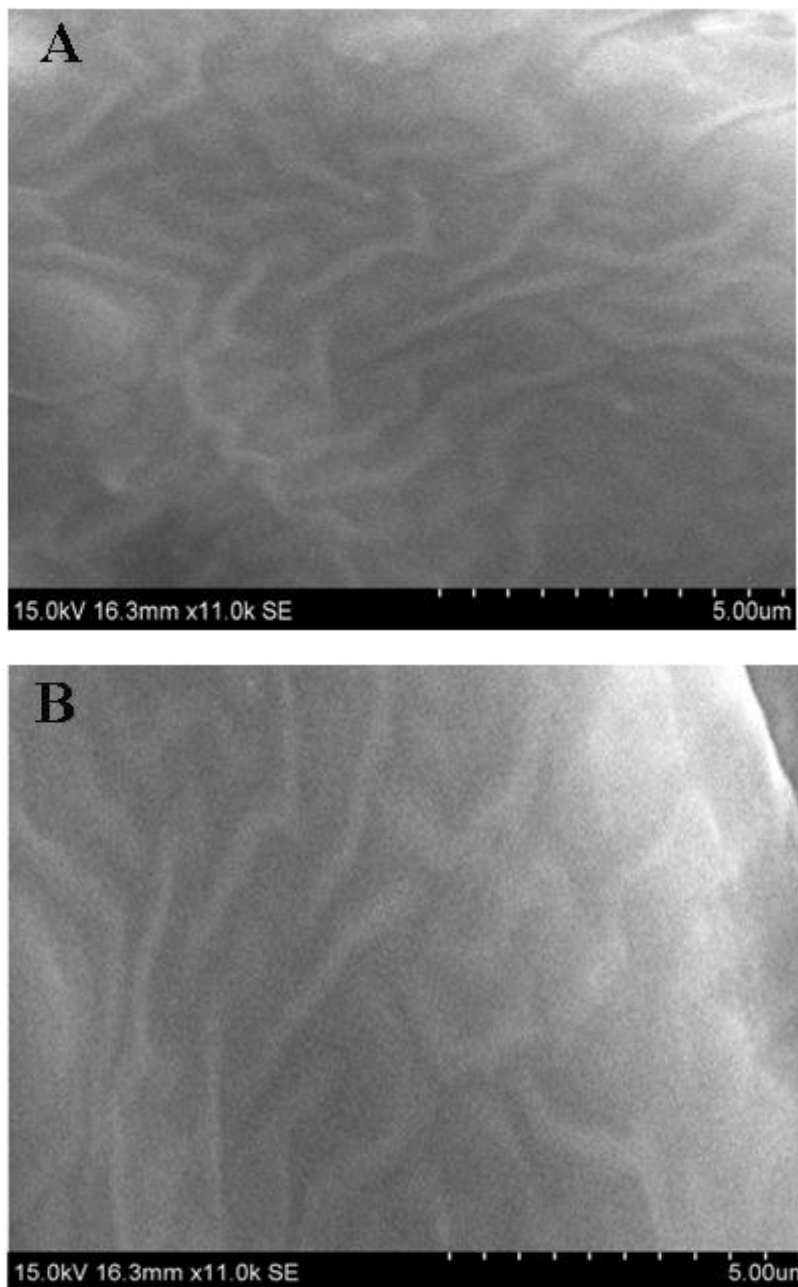
**Fig.5.7: FESEM image of FMWCNT- PANI/TPU(I) composite (A) Unstrained
condition (B) after 100% elongation**

The bonding between polymer chains and filler particles is best revealed from the cyclic straining studies of the composites. Generally, during the first ten cycles, the resistance drops to lower values which then tend to stabilize (29, 30). Hence the reversibility of the change in electrical resistance at elongation was tested under continuous cycles up to 20% for 20 cycles. Figure 5.8 shows the plot of resistance change ratio after each cycle for 5%, 10%, 15% and 20% for the three composites.

All the composites exhibit hysteresis behaviour as the electrical conductivity is not completely recoverable under loading /unloading cycles. However, after 5-7 cycles, the strain-dependent resistance responses were almost stabilized. It is seen that all the three composites exhibit good reversibility in conductivity up to 5% elongation/contraction cycles. As the strain percentage increases, the irreversible component also increases. From the resistance change ratios given in the figure 5.8, it is clear that FMWCNT-PANI/TPU(I) composite film exhibits minimum hysteresis during these cyclic elongation/contraction cycles. This indicates the stability in resistivity during the cyclic straining of the film. The conductive networks formed by CNTs with high effective aspect ratio is capable of reconstructing the conductive pathways i.e., such a network is beneficial in avoiding the fracture of conductive path. This rearrangement of CNTs results in an efficient conductive network along the stretching direction after every cycle. It can be observed that variation in structure and bonding of conductive fillers in TPU matrix, results in different strain sensing behaviour as well as its reproducibility.
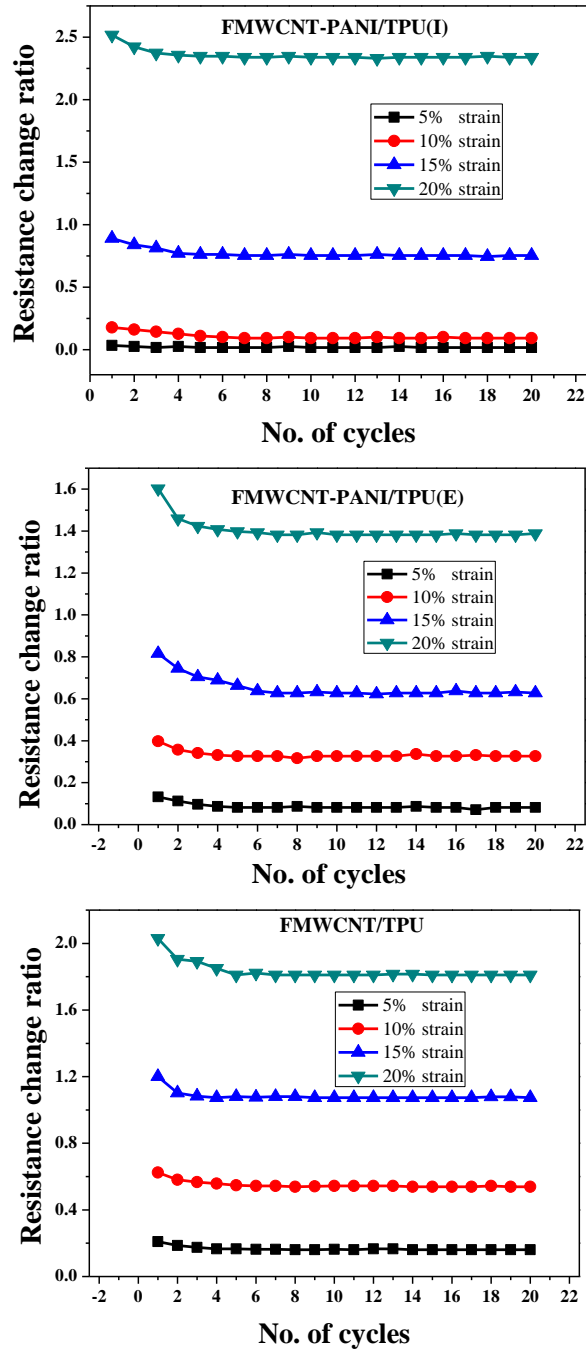
Fig. 5.8: Resistance change ratio for each elongation/contraction cycle with a maximum strain of 20% for the composite films.

Figure 5.9 shows the plot of relative resistance of the composites for each cycle plotted as a function of time under 20% strain. During these cycles, shoulder peaks are seen for all the composites. This might be originating from the competition between destruction and reconstruction of conducting pathways during loading-unloading cycles (31).
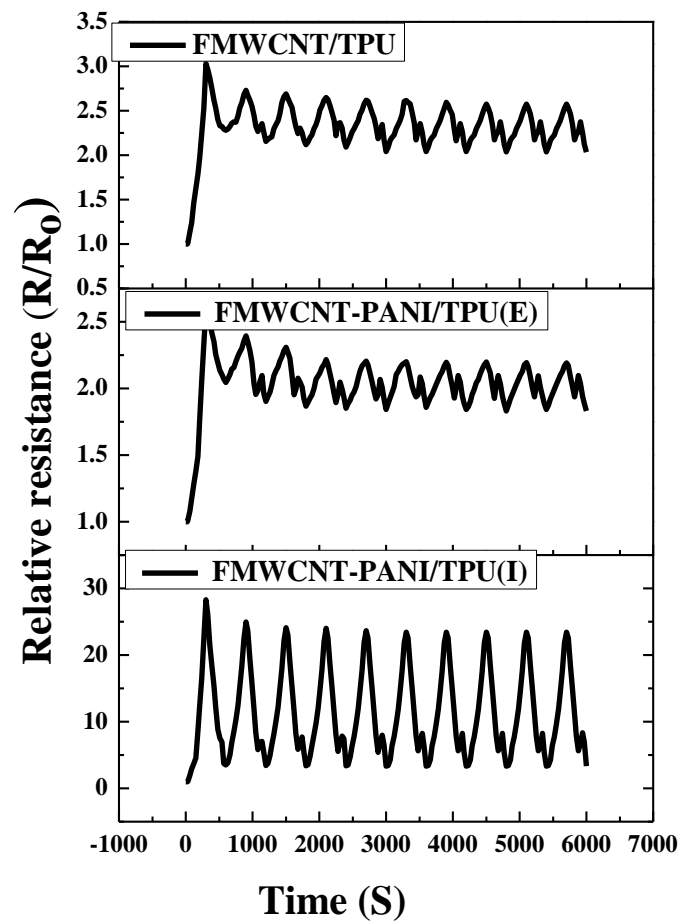

Fig.5.9: R/R$_0$ for each cycle plotted as a function of time under 20% strain for the composites.

5.3.4 Origin of strain sensitivity

The origin of high strain sensitivity of FMWCNT-PANI/TPU(I) composite films is investigated. The strain sensing response of the CPC films arises from the dimension-dependent change in the intrinsic resistivity of the composite. It has been reported that parameters such as geometry of the percolative network, the CNT nano-structure and the relative contribution of the tunneling resistance to the total electrical resistance decide the strain sensitivity of such composites (32,33)

In order to investigate the origin of strain sensitivity, Zhang et al. (34) carried out a modeling study based on the tunneling theory by Simmons (35). According to the model derived in, the total electrical resistance R of the composite is

$$R = \left(\frac{L}{N}\right)\left(\frac{8\pi hs}{3a2\gamma e2}\right)\exp(\gamma s) \quad\text{.................................(5.4)}$$

where Lis the number of particles forming a single conducting path, N the number of conducting paths, h the Plank's constant, s the least distance between conductive particles, a^2 the effective cross-section, where tunneling occurs, e the electron charge, and γis calculated as

$$\gamma = \frac{4\pi(2m\varphi)^{0.5}}{h}\gamma = \frac{4\pi\sqrt{2m\varphi}}{h}\quad\text{.................................(5.5)}$$

where m is the electron mass and φ the height of potential barrier between adjacent particles.

If strain is applied to the composite film, the resistance will be altered due to the change in particle separation. At low strains (<10%), the following assumptions are followed (1). The inter-particle distance changes proportionally with increased strain from s_0 to s. (2) The height of the potential barrier changes linearly with applied strain, from ϕ_0 to ϕ. (3) The number of conducting pathways decreases linearly with strain.

The inter particle distance s is given

$$s = s_0(1 + C\varepsilon) = s_0 \left[1 + C \left(\Delta l/l_0\right)\right] \dots\dots\dots\dots\dots\dots\dots\dots (5.6)$$

$$\phi = \phi_0(1 + D\varepsilon) = \phi_0 \left[1 + D \left(\Delta l/l_0\right)\right] \dots\dots\dots\dots\dots\dots\dots (5.7)$$

$$N = N_0(1 - E\varepsilon) = N_0 \left[1 - (E \,\Delta l/l_0)\right] \dots\dots\dots\dots\dots\dots\dots (5.8)$$

where s_0 is the initial inter-particle distance at zero strain, N_0 is the initial number of conducting paths, ϕ_0 is the initial potential barrier when no strain is applied, ε is the tensile strain of the elastomer matrix, l is the deformation of a composite sample, l_0 is the initial length of a sample, and *C, D* and *E* are constants. The total number of conducting particles (n) is constant, expressed as follows:

$$n = L \times N \dots\dots\dots\dots\dots\dots\dots\dots\dots\dots\dots\dots\dots\dots\dots\dots (5.9)$$

Substitution of Eqn. (5.5)–(5.9) into Eqn. (5.4) yields

$$R = \left[\frac{B(1+Cx)}{\sqrt{1+Dx(1-Ex^2)}}\right] \exp \left[A(1+Cx)(1+Dx)^{0.5}\right] \dots (5.10)$$

where x = ε, A = γ s_0, B = $8\pi nhs_0/3\gamma_0 N_0^2 a^2 e^2$ and n is the total number of conducting particles.
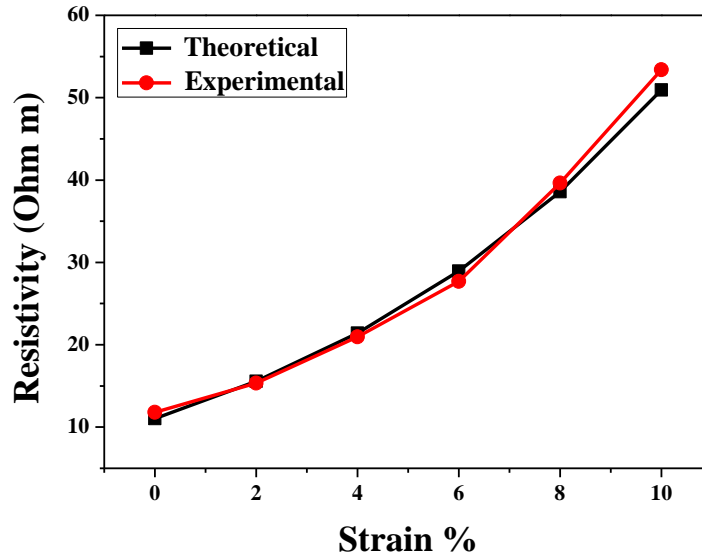
Fig. 5.10: **Experimental and theoretical data of strain dependent resistance for FMWCNT-PANI/TPU (I) composites with strain less than 10%.**

The plot of resistance versus strain based on this model as well as experimental data points at 10% strain are also shown in figure 5.10. Good agreement between the theoretical and experimental data suggest that the model of tunneling currents quite well suitable for this system. The fitting parameters are A = 1.003, B = 4.064, C = 8.9045, D = 0.0243, E= 0.000043. Usually tensile elongation increases the distance between the conducting particles, increasing the resistivity of the composite film. The low rate of resistivity hike with strain indicates that the number of conducting paths remains almost the same at strain below 10%, i.e. conductive networks are only slightly affected.

It is assumed that for larger strains (>10%), the inter-particle distance changes linearly and proportionally with increased strain from s_0 to s. The high rate of the increase of R/R_0 at larger deformations l/l_0 is related to

destruction of the conducting network. As the number of conducting paths N decreases, corresponding increase in resistivity is also observed.

For an elastomeric composite, the separation s under tensile strain is calculated as

$$s = s_0 (1 + C\varepsilon) = s_0 [1 + C (\Delta l/l_0)] \quad .... (5.11)$$

Due to the high rate of resistivity increase at larger strains, it is assumed that the number of conducting pathways changes at a much higher rate, and can be expressed as follows[40]

$$N = N_0/exp (M\varepsilon + W\varepsilon^2 + U\varepsilon^3 + V\varepsilon^4) \quad ....(5.12)$$

Where M, W, U and V are constants. Substituting Eqns (5.11) and (5.12) into Eqn (5.4) yields

$$R = B (1 + Cx) exp [A + (2M + AC) x + 2Wx^2 + 2Ux^2 + 2Vx^2] \quad ... (5.13)$$

where $x = \varepsilon$, $A = \gamma s$ and $B = 8\pi nhs_0/2\gamma_0 N_0^2 a^2 e^2$

The plot of experimental and theoretical resistance data at strain levels above 10% is shown in figure 5.11. This indicates that the model of tunneling currents describes the experimental data quite well at relatively large deformation. The fitting parameters are, A = 10.785, B = 0.000915, C = 0.7322, M = 1.8347, W = -5.7966, U = 1.526 and V = 1.2091.
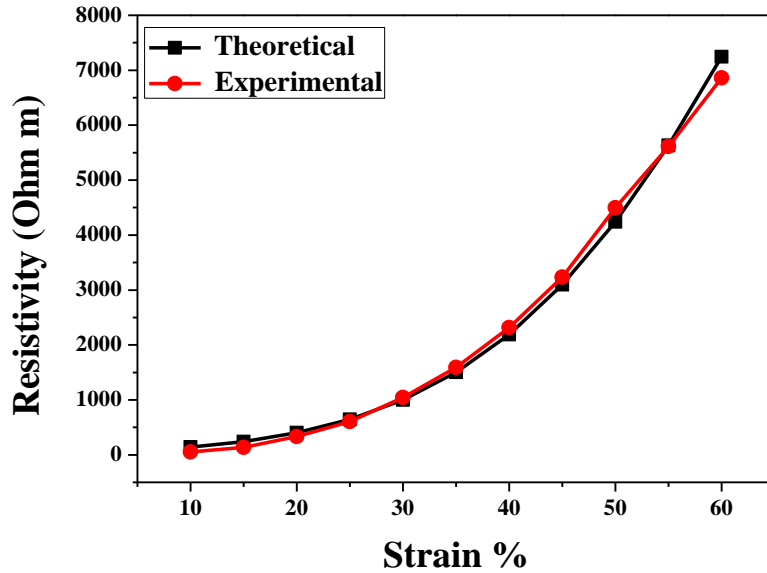
Fig. 5.11: **Experimental and theoretical data of strain dependent resistance for FMWCNT-PANI/TPU (I) composites with strain greater than 10%.**

The high rate of increase in resistance observed with large deformations is due to the extensive destruction of conducting networks. With deformation, the number of CNT-to-CNT contact reduces, resulting in an increase in the electrical resistance. In the case of FMWCNT-PANI/TPU (I), uniform dispersion and high effective aspect ratio of the conductive inclusions lead to maximum number of filler contacts in the composite providing it with minimum percolation threshold and high conductivity (section 3.1). For this composite film, the reduction in the number of break downs of CNT-CNT contact (conducting path, N) is very large resulting in a drastic reduction in conductivity.

5.4 Conclusions

Conductive TPU composite films are prepared by adding in-situ and ex-situ polymerised PANI-FMWCNT as conductive filler. The in-situ polymerised PANI-FMWCNT filler particles are able to decrease the percolation threshold for electrical conductivity of the composite film. The electrical and strain sensing properties of this composite film are significantly higher than the other composites, confirming the advantage of the in-situ polymerised PANI-FMWCNT as effective conductive fillers. With a filler content of 2%, the composite shows the highest gauge factor of 1075 on 100% straining. Also, the composites exhibit excellent reversibility in resistivity after cyclic deformation. In this composite, homogeneous dispersion of Polyaniline coated FMWCNT filler particles in TPU matrix keeps the conductive fillers as individual tubes increasing its interfaces with the matrix. Electrical and strain sensing properties of the composite films strongly depend on the dispersion and interfacial interaction of the filler particle with the TPU matrix. The experimental data for strain sensing can be described based on the theoretical equations derived from a model based on the tunneling by Simmons.

References

[1]   Z. Li, P. Dharap, S. Nagarajaiah, E.V. Barrera, J.D. Kim, *Adv.Mater.*,16, 2004, p.640.

[2]   M. Park, H. Kim, J.P. Youngblood, *Nanotechnology*, 19, 2008, p.055705.

[3]   M.Knite, V.Teteris, A.Kiploka and J.Kaupuzs, *Sensor Actuat. A-Phy.,*110, 2004, p.142–149.

[4]   L. Lin, S. Liu, Q. Zhang, X. Li, M. Ji, H. Deng, Q Fu, *ACS Appl. Mater. Inter.*, 5, 2013, p. 5815-5824.

[5]   I. Kang, M.A. Khaleque, Y. Yoo, P.J. Yoon, S.Y. Kim, K.T. Lim, *Compos. Part A: Appl. Sci.*, 42, 2011, p. 623- 630.

[6]   P. Slobodian, P. Riha, P. Saha, *Carbon*, 50, 2012, p. 3446- 3453.

[7]   J.R. Bautista-Quijano, F. Aviles, J.V. Cauich-Rodriguez, *J Appl Polym Sci.*, 130, 2013, p. 375-382.

[8]   F. Li, L.Qi, M. Xu and D. Ma, *J. ApplPolym Sci.*,75, 2000, p. 68-77.

[9]   J.H. Kong, N.S. Jang, S.H. Kim and J.M. Kim, *Carbon*, 77, 2014, p. 199.

[10]   A.P. Sobha, S.K. Narayanankutty, *IEEE Trans. Nanotechnol.*, 13, 2014, p. 835–841.

[11]   J. Masanoto and T.Iwamot, Polymer data handbook. London: Oxford University, 1999.

[12]   D. Stauffer and A. Aharony, Introduction to Percolation Theory, Second ed. London, Taylor & Francis; 1992, p. 17-30.

[13]   M. Weber and M.R. Kamal, *Polym Compos*. 18, 1997, p.711-725.

[14]   K. Levon, A. Margolina and A.Z. Patashinsk, *Macromolecules*, 26, 1993, p. 4061.

[15]   C.Grimaldi and I.Balberg, *Phys. Rev.Lett.*, 96, 2006, p. 066602.

[16]   Y. Yang, M.C. Gupta, K.L. Dudley, R.W. Lawrence, *Nanotechnology,* 15 2004, p. 1545.

[17]   M. Knite, V. Teteris, A. Kiploka, J. Kaupuzs, *Sensors and Actuators A: Physical,* 110, 2004, p. 142.

[18]   N.C. Das, T.K. Chaki, D. Khastgir, *Polym Int*. 51, 2002, p.156.

[19]   G.T. Pham, Y.B. Park, Z.Y. Liang, C. Zhang, B. Wang, *Compos. Part B,*39, 2008, p.209.

[20]   L. Flandin, A. Hiltner and E. Baer, *Polymer*, 42, 2001, p. 827.

[21] L. Flandin, Y. Brechet and J.Y. Cavaille, *Compos. Sci. Technol.*, 61, 2001, p. 895.

[22] L. Lin, S. Liu, Q. Zhang, X. Li, M. Ji, H. Deng, Q Fu, *ACS Appl. Mater. Inter.*, 5,2013, p.5815.

[23] K.P. Sau, T.K. Chaki, D. Khastgir, *Compos Part A –Appl Sci Manuf.*, 29, 1998, p. 363.

[24] W.S. Bao, S.A Meguid, Z.H. Zhu, G.J. Weng, *J Appl Phys*, 111, 2012, p. 093726.

[25] G.J. Simmons, *J. Appl Phys.*, 34, 1963, p. 1793.

[26] P. Costa, J. Silva, V. Sencadas, R. Simoes, J.C. Viana and S. Lanceros-Méndez, *J. Mater Sci*, 48, 2013, p. 1172.

[27] F. Li, L. Qi, J. Yang, M. Xu, X, Luo, D. Ma, *J. Appl Polym Sci.*, 75, 2000, p. 68.

[28] M.K. Shin, J. Oh, M. Lima, M.E. Kozlov, S.J. Kim, R.H. Baughma, *Adv Mater.*, 22, 2010, P. 2663.

[29] E. Hrehorova, V.N. Bliznyuk, A.A. Pud, V.V. Shevchenko, K.Y. Fatyeyeva, *Polymer*, 48, 2007, p. 4429.

[30] R. Zhang, H. Deng, R. Valenca, J. Jin, Q. Fu, E. Bilotti and T. Peijs, *Compos Sci Technol.,* 74, 2013, p. 1.

[31] L. Lin, H. Deng, X. Gao, S. Zhang, E. Bilotti, T. Peijs, Q. Fu, *Polym Int.*, 62, 2013, p. 134.

[32] A.I. Oliva-Avilés, F. Avilés, V. Sosa, *Carbon,* 49, 2011, p. 2989.

[33] N.Hu, Y. Karube, M. Arai, T. Watanabe, C. Yan, Y. Li, Y. Liu, H. Fukunaga, *Carbon*, 48, 2010, p. 680.

[34] X.W. Zhang, Y. Pan, Q. Zheng, X.S. Yi, *J. Polym Sci B: Polym Phys*, 38, 2000, p. 2739.

…..୭ଓ…..

Chapter **6**

ELECTRICAL, THERMAL, MECHANICAL AND ELECTROMAGNETIC SHIELDING PROPERTIES OF PANI/FMWCNT/TPU COMPOSITES[*]

Thermoplastic polyurethane (TPU) composites based on Polyaniline (PANI) and functionalised multiwalled carbon nanotubes (FMWCNT) were prepared by in-situ polymerization of aniline in TPU solution assisted by ultra sonication (PANI/ FMWCNT/TPU). Composites without polyaniline were also prepared by the same method (FMWCNT/TPU). Field emission scanning electron microscopy and transmission electron microscopy images of these composites showed good dispersion in the case of PANI/FMWCNT/TPU composites. The electrical and electromagnetic shielding properties of the prepared composites were studied as a function of weight percentage of FMWCNTs. In-situ polymerisation reduced the aggregation of FMWCNTs and improved its dispersion as well as interfacial interaction with TPU matrix. Thus a low percolation threshold (0.58 wt %) was obtained in PANI/FMWCNT/TPU composites. It displayed a conductivity of 28.6 S/m and SE of 31.35dB in X band region at 8% filler concentration. For FMWCNT/TPU composites, the values were 1.52s/m and 19.65dB respectively. Absorption, rather than reflection, was found to be the major shielding mechanism. Enhanced thermal and mechanical properties of the currently synthesised composites were confirmed by TGA, DMA and tensile analysis.

6.1 Introduction

With the introduction of high operating frequency and band width in electronic systems, concerns about the ill effects on the environment due to EMI are being raised. The signal strength and the quality of functioning of electronic equipments are affected by these electromagnetic waves. EMI can interfere with the functioning of any electronic equipment – from cell phone, medical devices to the high security military equipments (1-3). This led to studies on the development of materials with the capacity to absorb or to reflect these radiations ie: shielding. Microwave absorber in the field of stealth technology gives the object a capacity to evade radar detection (4). Microwave absorbers can also be used for the reduction of electromagnetic interference problems. So a microwave absorber with a wide absorption frequency, high absorption capability, and good thermal stability is aimed here. Because of low density, design flexibility, ease of processing and high conductivity at low filler loading, polymer nanocomposites based on high aspect ratio conductive nanofillers are promising materials for EMI shielding. It was evident that polymers filled with high aspect ratio nanofillers exhibit higher EMI shielding effectiveness (SE) than polymers filled with the conventional microfillers. High strength and stiffness, extremely high aspect ratio, and good electrical conductivity of CNT make it a filler of choice for shielding applications (4, 5). Despite these advantages, a homogeneous dispersion of CNTs in a polymer matrix devoid of entanglement is difficult to attain. This results in low electrical conductivity of these nanocomposites. Many groups have attempted strategies to improve the dispersion of CNTs and thereby improve electrical conductivity (4-7). According to them, parameters such as aspect ratio, conductivity, orientation,

dispersion and concentration of CNTs influence percolation threshold, conductivity and EMI SE of the polymer composites. The Processing method also has a crucial influence on these parameters. The improved dispersion and low electrical percolation of polyaniline coated FMWCNT in TPU matrix has been demonstrated in chapter 5. Better dispersion of CNT in the polymer matrix can improve its dispersion stability and connectivity, which in turn will increase the EMI shielding effectiveness of the composite.

In the present chapter, we report the synthesis of nanocomposites of PANI coated FMWCNT in TPU matrix through in-situ polymerisation of aniline in TPU matrix containing FMWCNTs. The polymerisation process was accompanied by ultra sonication. FMWCNT in TPU matrix were also synthesised by dispersing FMWCNT in TPU matrix through sonication. The EMI shielding efficiency of the composites was studied over a frequency range of 8-12 GHz in the X band.

6.2 Experimental

6.2.1 Synthesis of FMWCNT-PANI/TPU Composite films

FMWCNT-PANI/TPU composites were prepared by the following methods. (i) Ultra sonically assisted in-situ polymerisation of aniline in TPU matrix containing FMWCNTs. Composite samples containing different weight % (0.25, 0.5, 0.75, 1, 1.5, 2, 4, 6 and 8) of FMWCNTs were synthesized by one-step in-situ polymerization of aniline with APS as the oxidant in TPU solution. 4gm TPU was dissolved in 100ml THF. Different weight percentages of FMWCNTs (0.25, 0.5, 0.75, 1, 1.25, 1.5, 2, 4, 6 and 8) and 0.093gm of aniline were dispersed in 100ml 1M PTSA solution through

sonication for 30 minutes. The reaction mixture was kept at 0-5°C. 4gm TPU was dissolved in 100 ml THF through magnetic stirring and was added to the above reaction mixture and sonication was continued. 10ml 1M APS solution was added drop wise and sonication was continued for another half an hour. The solution was again stirred at room temperature for 30 minutes. The reaction mixture was filtered and washed. Then the composites were dissolved in THF and cast into films with thickness of about 1mm. The polymer composite films were collected and cut into the required dimensions for further measurements. These FMWCNT-PANI/TPU composite films (2, 4, 6 and 8 wt %) are designated as NC_{12}, NC_{14}, NC_{16}, and NC_{18} (Sample NC_1).

6.2.2 Synthesis of FMWCNT/TPU composite films

Composite films of FMWCNT/TPU samples were also synthesised by introducing FMWCNTs (0.25, 0.5, 0.75,1, 1.5,2,4,6 and 8 weight %) into the TPU matrix. The FMWCNTs were dispersed in THF by sonication for 30 minutes. 4gm TPU was dissolved in 100ml THF. The two solutions were mixed thereafter and sonication continued for another 30 minutes. The FMWCNT/TPU composite films (2, 4, 6 and 8 wt.%) are designated as NC_{22}, NC_{24}, NC_{26}, and NC_{28} (Sample NC_2).

6.2.3 Characterization

The microstructure of the composite was   observed using a Hitachi SU6600 Variable Pressure Field Emission Scanning Electron Microscope (FESEM) and transmission electron microscopy (TEM) (JEOL JEM 120 KV). The DC conductivity of the composite films was measured by a standard two-probe electrode configuration using a Keithley 2400 nanovoltmeter.

Dynamic mechanical properties of composite films were measured by dynamical mechanical analyser (DMA) (800, TA Instruments). The tensile properties of the samples were performed according to ASTM D 142 using a Shimadzu Universal testing Machine (model AG 1) with a testing velocity of 150mm/min. Thermo gravimetric investigations (TGA) were performed using a Q 50, TA Instruments Thermo Gravimetric Analyser in the temperature range between 40 and 700°C in nitrogen gas with a heating rate of 10°C/min. The EMI shielding efficiency (SE) measurement was performed with a ZVB20 vector network analyzer in the frequency range of 8to 12 GHz (X-band) as described in section 2.2.11.

6.3 Results and Discussion

6.3.1 Morphology

The electrical properties and EMI SE of composites are determined by the dispersion state of CNTs in the polymer matrix (8). Therefore, to investigate the dispersion state of CNTs in the TPU matrix, FE-SEM and TEM were used. Morphology of the composites is shown in figure 6.1(a-f) Figure 6.1a showing FMWCNTs are of diameter 15-30 nm. The image shows that some of them have diameter greater than 30nm, indicating bundling of the nanotubes. The FESEM image of NC_1 composites (Fig. 6.1 b,d and e) shows uniform dispersion of PANI coated FMWCNTs embedded in the TPU matrix. A tubular morphology for PANI coated FMWCNTs in TPU matrix is noted here. The nanotubes are devoid of tangling and agglomerates are minimal. Such uniform dispersion results because of the strong interfacial adhesion existing between CNTs and TPU matrix. In contrast, the FESEM image of NC_2 reveals the distribution of CNTs with

entwined agglomerates. This morphology is indicative of weak interfacial interaction between CNTs and TPU matrix. This difference in morphology is due to the difference in the mechanism of formation of composites. In the NC_1 composites, aniline is adsorbed on the CNT surface and these CNTs are dispersed in TPU matrix through sonication. During in-situ polymerisation of aniline assisted by ultra sonication, anilinium ions are formed on the CNT surface. These ions repel each other and get polymerised on the CNT surface resulting in formation of PANI coated individual CNTs. When CNTs along with aniline is dispersed in TPU matrix, the polymerisation results in the formation of thin and uniform PANI encapsulation. The PANI coated CNT interact with TPU matrix through hydrogen bonding. Thus PANI coating on CNT can cause (1) reduction in Van der Waal's force among nanotubes (2) interfacial bonding of PANI and TPU matrix. This better compatibility between polyaniline and TPU allows homogeneous distribution of filler particles. These filler particles as suggested by TEM form a thorough network which is helpful for improving the electrical conductivity and shielding efficiency of these composites. At the same time, morphology of NC_2 reveals that sonication helps little in overcoming the Van der Waal's force between CNTs. Repulsion happens during sonication in this case also, but there is bundling of CNTs during solidification, as revealed by FESEM analysis. As a result, the distance between the conducting particles is increased. This microstructure can have detrimental effect on the formation of conductive network, resulting in reduced conductivity and shielding efficiency.
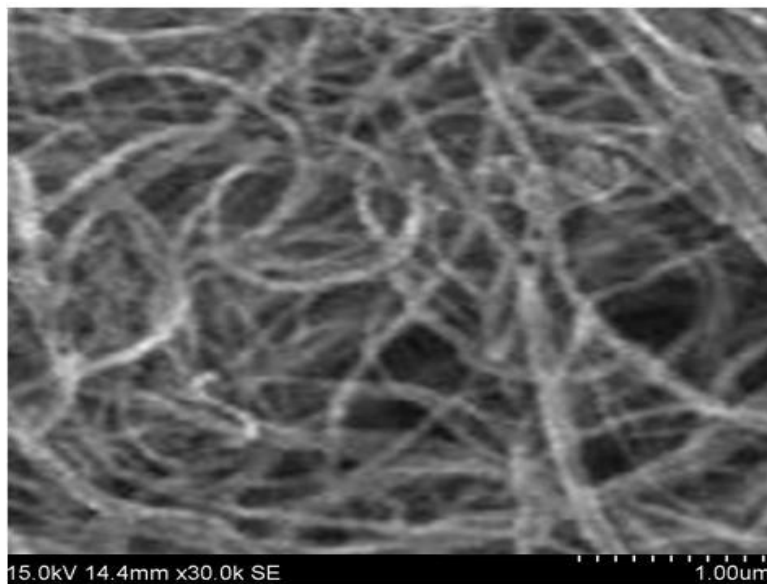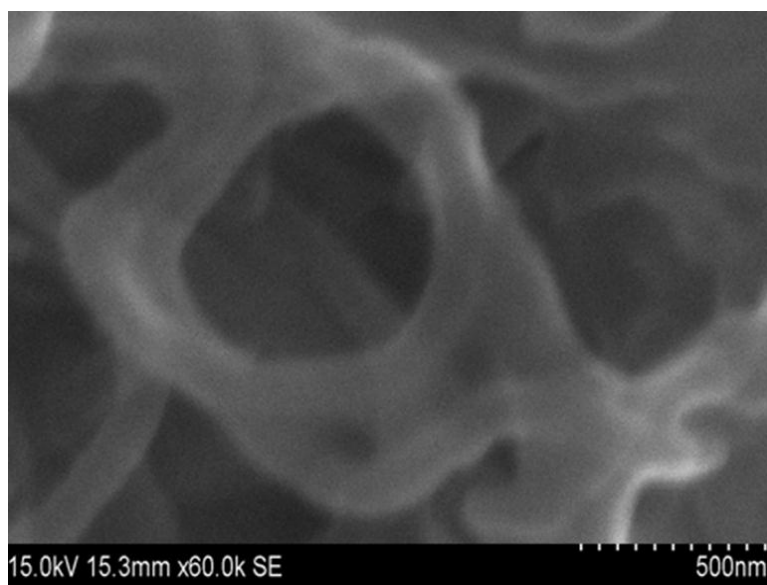
Fig. 6.1a: FESEM of FMWCNT

Fig. 6.1b: FESEM of NC$_{16}$
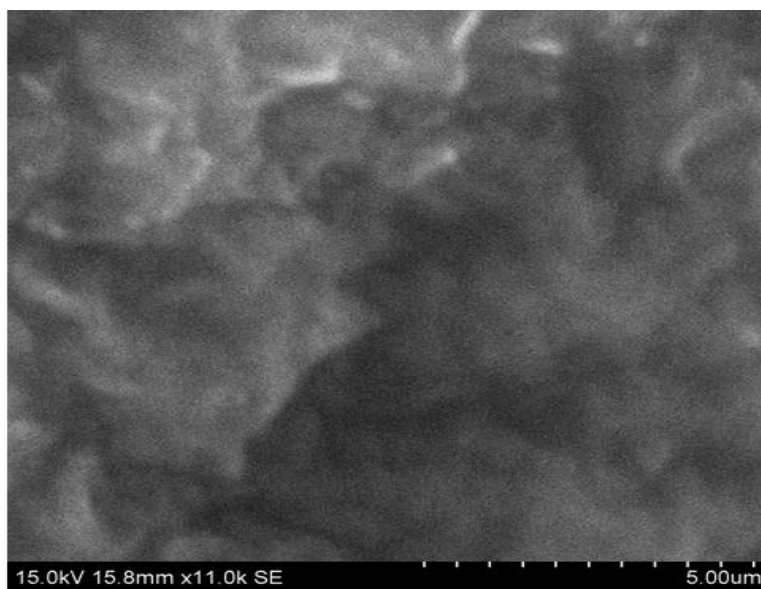
Fig. 6.1c: FESEM of NC$_{26}$
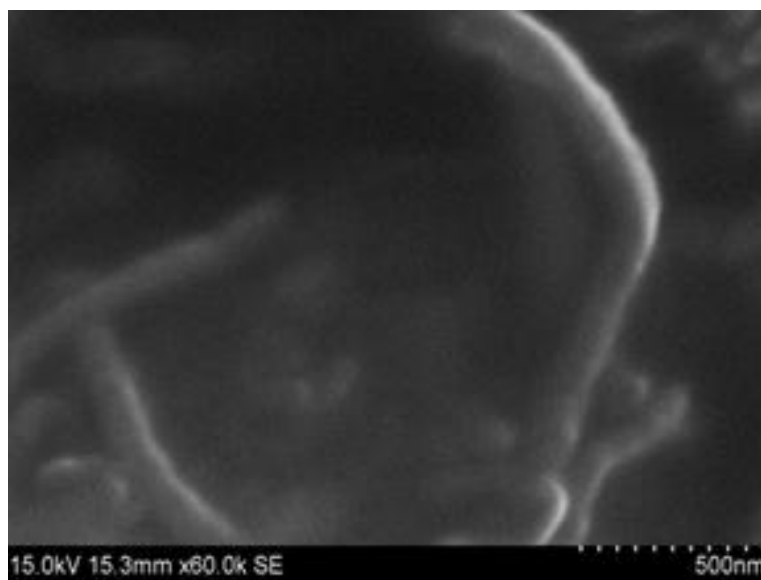
Fig. 6.1d: FESEM of NC$_{18}$
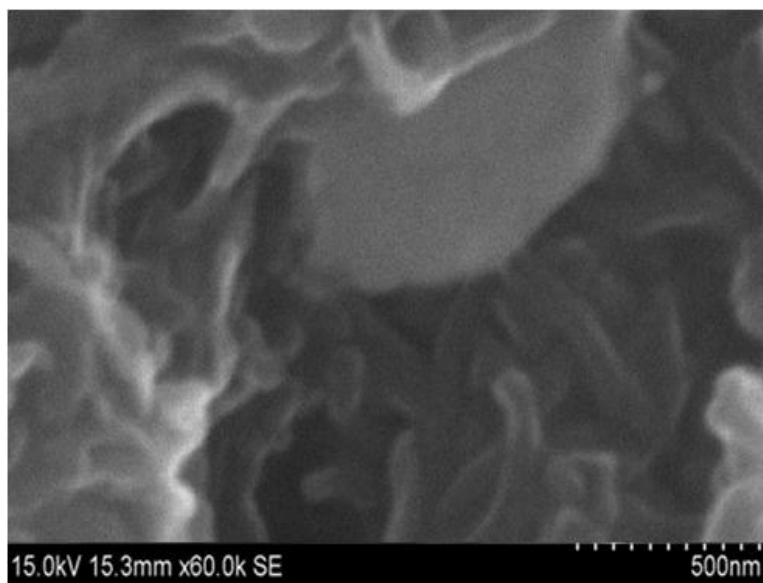
Fig. 6.1e: FESEM of NC$_{28}$

Fig. 6.1f: TEM of NC$_{18}$

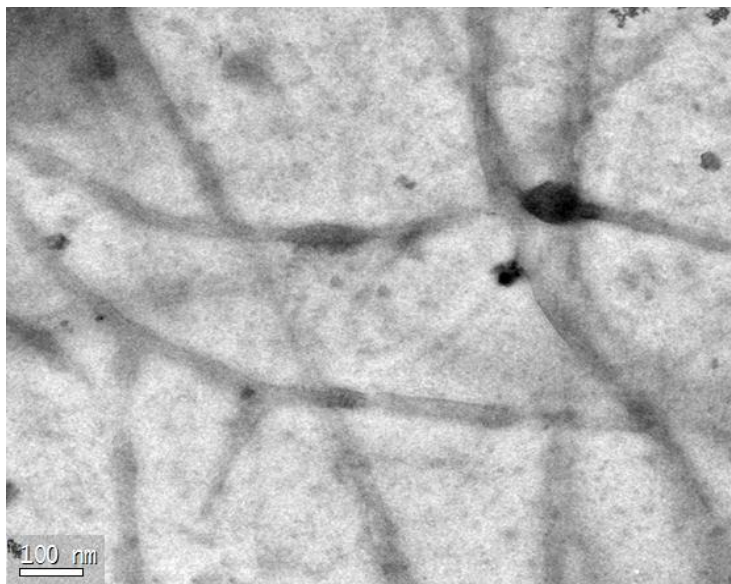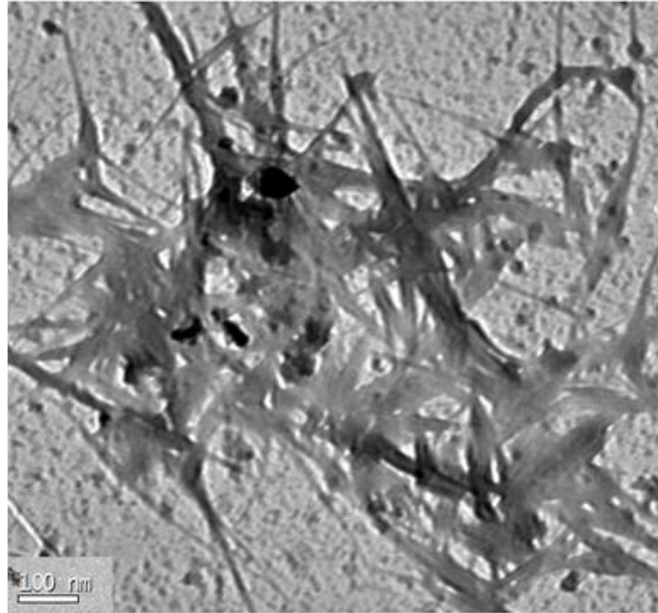**Fig. 6.1f: TEM of NC$_{18}$**
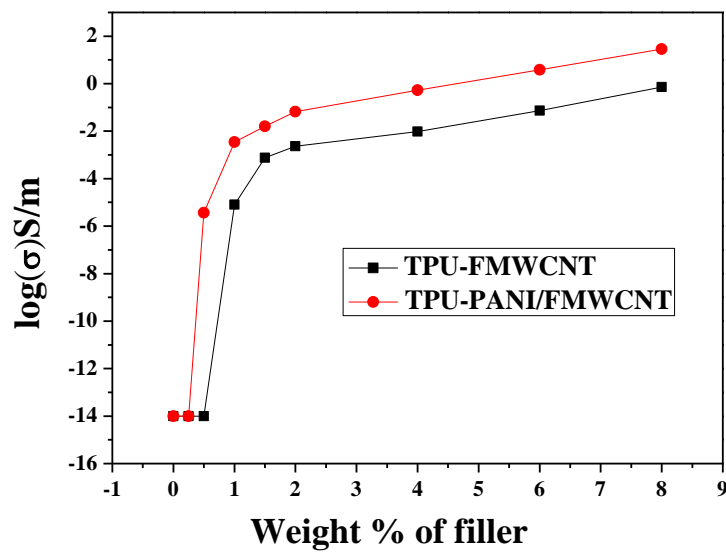
6.3.2 Electrical properties

Fig. 6.2: **Electrical conductivity of composite films as a function of the weight % of the conductive filler**

Fig. 6.2 shows the electrical conductivity versus CNT content in weight% for all composite films. Pure TPU is an insulating material and has an electrical conductivity of 10^{-14} S/m (9). It is seen that the electrical conductivity increases with the increase of CNT content for both composites. Depending on the type of fillers, the composites behave differently. The insulator-to-semiconductor transition of the NC_1 composites shifts to lower CNT content compared to that of the FMWCNT/TPU composites. As the concentration of PANI is too low, the major contribution to conducting path is provided by the CNTs in these composites. The PANI coated FMWCNT/TPU film with 0.5% CNT exhibited an increase in conductivity to 9.7×10^{-5} S/m, indicating the formation of a conductive network. The conductivity of the composite raises greatly to 28.6 S/m with 8% CNT content. In contrast NC_2 composites have a higher percolation threshold. The conductivity reaches to 1.6×10^{-5} S/m only at 1% CNT content. It is noticed that the percolation threshold of NC_1 composites is 0.58 while that of NC_2 is 0.984. At 8 wt% filler content, while the PANI coated FMWCNT/TPU composite reaches a conductivity of 28.6 S/m, the FMWCNT/TPU composites shows only 1.52 S/m. This reveals the advantage of PANI coated FMWCNT as effective conducting filler for improving the electrical conductivity of TPU. This can be attributed to the difference in morphology and level of dispersion of the CNT in TPU, as explained before. Generally polymer systems with non-entangled and well-dispersed CNT fillers show lower percolation threshold and high conductivity (10).

6.3.3 Dynamic Mechanical Analysis

The effect of the PANI coated CNTs on the viscoelastic property of TPU/CNT nanocomposites was analyzed by DMA. The storage modulus of

the composites as a function of temperature are shown in figures 6.3a and b. Below the glass transition region, all the composites show modulus values close 1000 MPa. The modulus drops by an order of 10 across the glass transition temperature. The Tg of the composites show a gradual improvement with increasing filler content (Table 6.1). The effect of fillers is very pronounced at post- Tg temperatures. As the segmental mobility is increased at temperatures above glass the transition temperature, the restraining effect of fillers is specifically effective at these temperatures. A cross plot at $25^{o}C$ shows a linear relationship between the storage modulus and filler loading for both composites (Fig. 6.3c). The steeper slope of the NC_1 samples is due to better bonding of the CNT with the matrix. At a CNT loading of 8 %, the storage modulus is improved by 673 % in the case of NC_{28} and 802% in the case of NC_{18} composites.
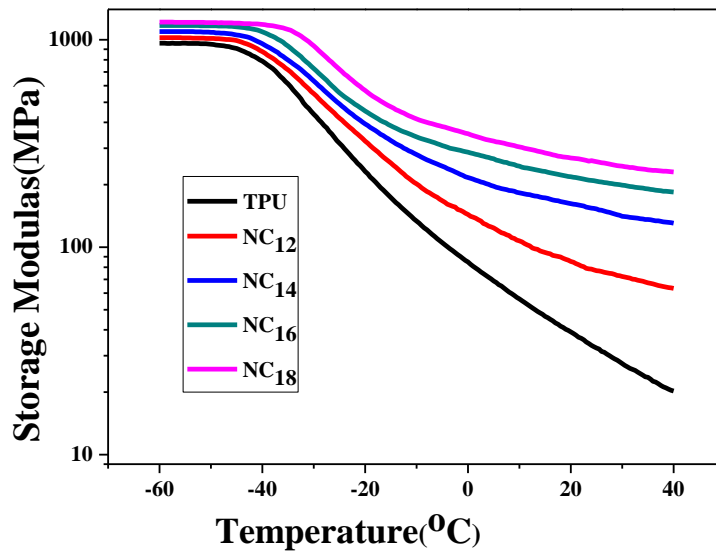
Fig. 6.3a: Storage Modulus of   PANI coated FMWNT/ TPU nanocomposites as a function of temperature
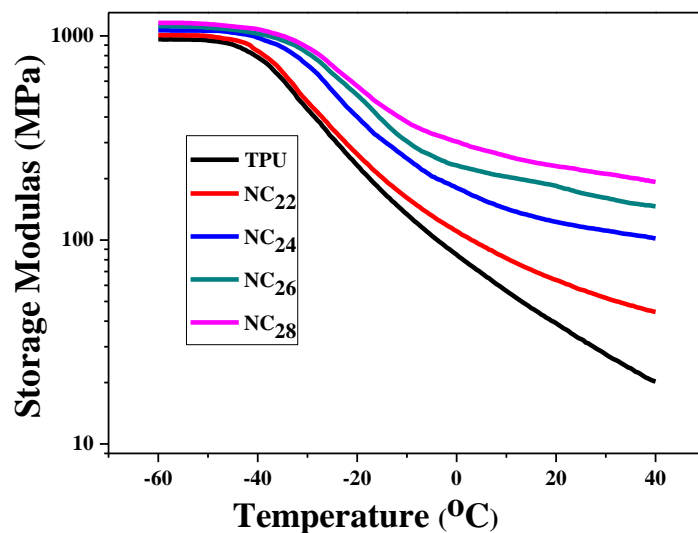
Fig. 6.3b: Storage Modulus of TPU–FMWNT nanocomposites as a function of temperature
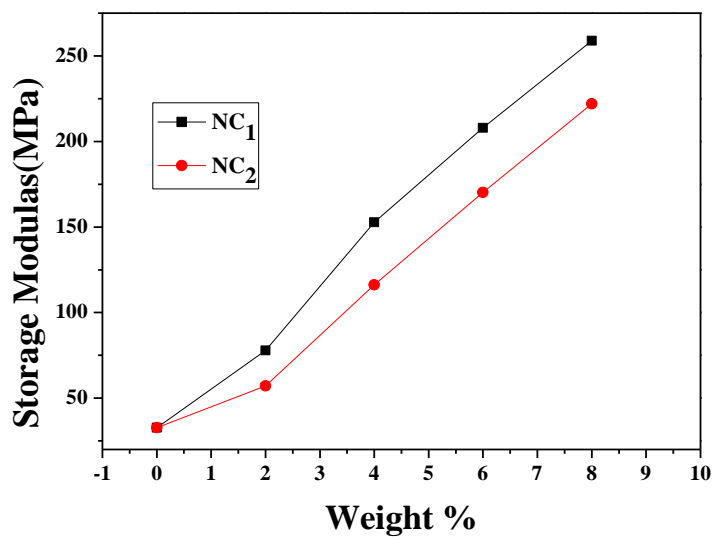
Fig. 6.3c: Storage Modulas of composites at 25°C

Table 6.1: Storage Modulas and Tg of TPU, NC$_1$ and NC$_2$ composite films.

Sample Name	Storage Modulas at -60°C (MPa)	T$_g$ (^{o}C)
TPU	962	-31
NC$_{12}$	1024	-29
NC$_{14}$	1096	-26.5
NC$_{16}$	1171	-25
NC$_{18}$	1215	-22.5
NC$_{22}$	1008	-29.5
NC$_{24}$	1064	-28
NC$_{26}$	1116	-27.5
NC$_{28}$	1159	-26

The variation of loss tangent with temperature is shown in figure 6.3d and e. The tan d peak corresponding to Tg shifts toward higher temperature. For NC$_1$ composites, the Tg increases from -31°C to – 22.5^{o}C on increasing the filler content while for NC$_2$ composites, the increment is to -26 ^{o}C.
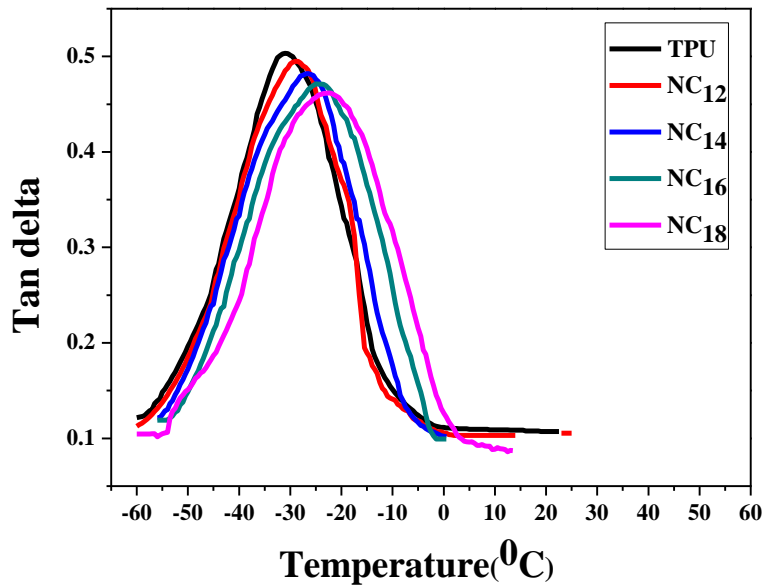
Fig. 6.3d: Tan delta of NC$_1$ composite film as a function of temperature
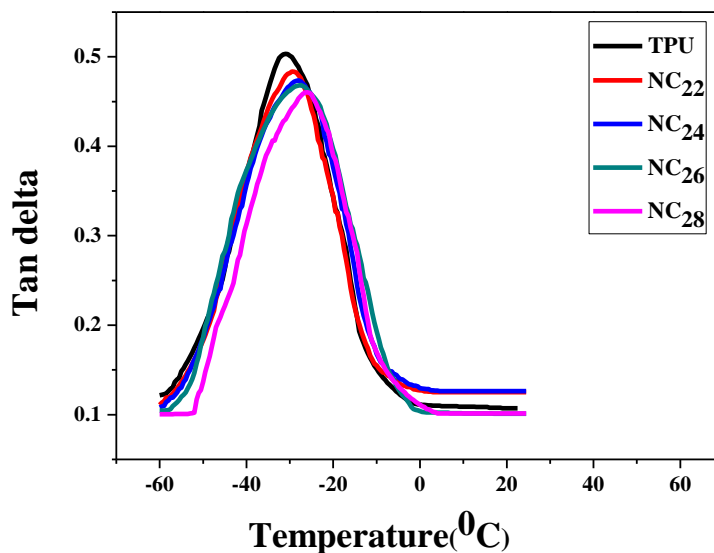
Fig 6. 3e: Tan delta NC_2 composite film as a function of temperature

6.3.4 Tensile properties

The tensile behaviour of the investigated composites is given in figure 6.4a, 4b and in Table 6.2. The tensile strengths of the nanocomposite films are enhanced with CNT content for both the composites. For example, NC_{12} and NC_{22} displayed 1.2 and 1.14 times increased tensile strength, respectively. At the same time the elongation at break is still above 500% for all these composites. For pure TPU, elongation at break is 620%. This shows that the composite films retained excellent stretchability, a key characteristic of elastomeric materials. NC_1 composites exhibit improved tensile strength with minimum reduction in elongation at break. Modulus at 50% strain is increased with increasing CNT content, indicating the reinforcing capability of PANI coated CNT in TPU matrix. The overall improvement in mechanical properties of the composites is due to the

efficient reinforcement effect of the well dispersed PANI coated CNTs in the TPU matrix. The relatively lower elongation in the case of NC_2 may be due to the uneven dispersion of the CNTs.
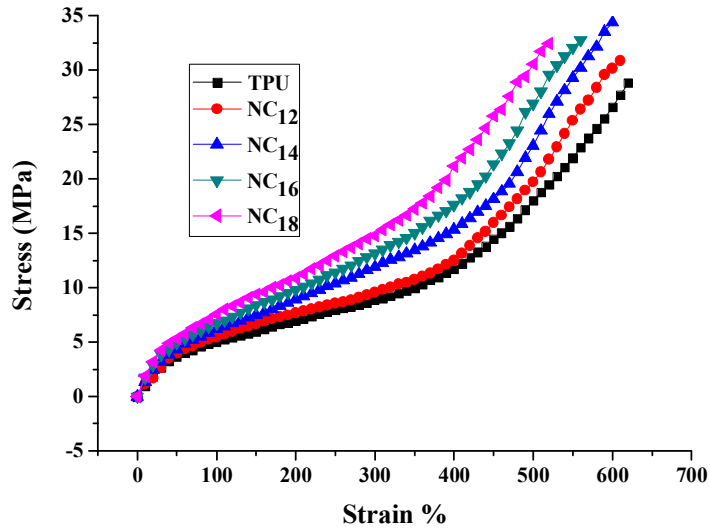
Fig. 6.4a: Stress strain curves of NC$_1$ composites
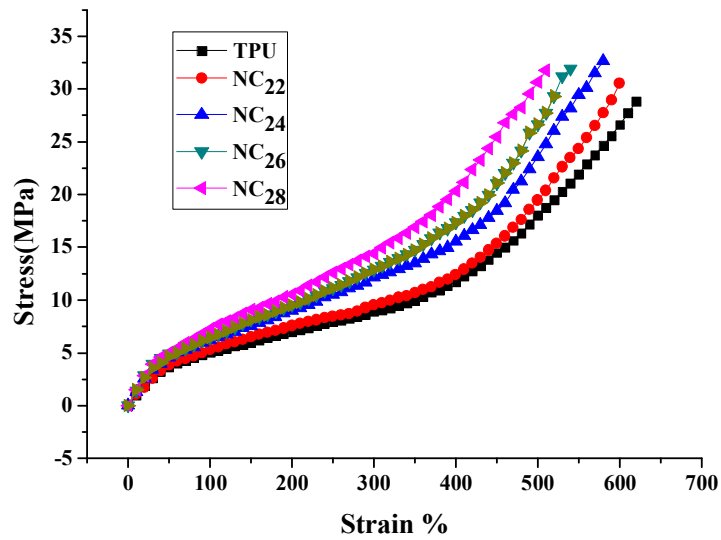
Fig. 6.4b: Stress strain curves of NC$_2$ composites

Table 6.2: **Tensile strength and Elongation at break of TPU, NC$_1$ and NC$_2$ composite films**

Sample Name	Tensile Strength(MPa)	Elongation at break (%)	Tensile Modulas at 50% (MPa)
TPU	28.84	620	7.3
NC$_{12}$	30.86	610	7.9
NC$_{14}$	34.38	600	8.7
NC$_{16}$	32.78	560	9.88
NC$_{18}$	32.45	520	10.64
NC$_{22}$	30.55	600	7.57
NC$_{24}$	32.64	580	8.35
NC$_{26}$	31.93	530	9.09
NC$_{28}$	31.75	500	9.68

6.3.5 Thermo Gravimetric Analysis

Figure 6.6 shows the TGA curves of TPU and composites in nitrogen atmosphere. The data from TGA analysis is shown in Table 6.3. As TPU degraded completely in the nitrogen atmosphere, the residue left is the amount of CNTs in the composite. TPU and composites show two main stages of decomposition. The onset of the initial decomposition (stage I) occurs around 250°C. The temperature corresponding to the maximum rate of degradation for TPU is at 362°C. The composites show only a small increase in the decomposition (stage I) temperature. However, the second decomposition (stage II) temperature increased with the composites showing enhancement in thermal stability.
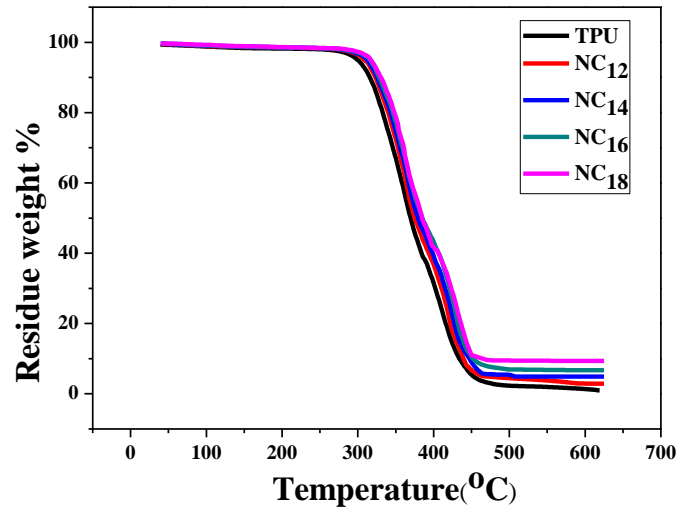
Fig. 6.6a: TGA of NC$_1$ Composites
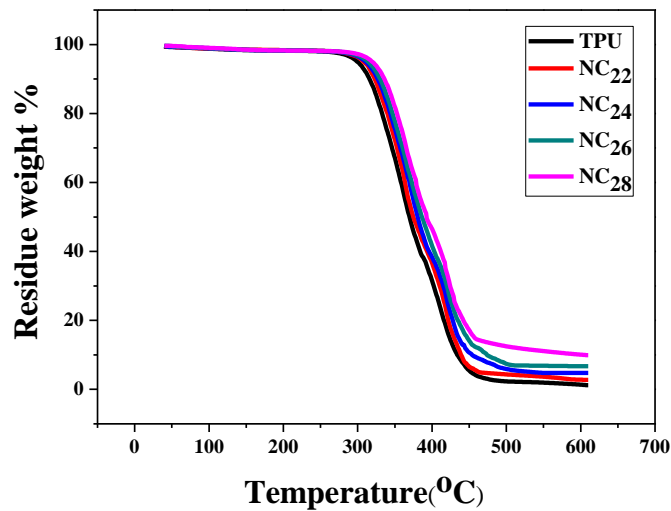
Fig. 6.6b: TGA of NC$_2$ Composites

For NC$_1$ composites, the increment is from 411 to 432°C and for NC$_{28}$ composites to 425°C. This improved thermal stability can be attributed to a favorable interaction between the CNTs and the polyurethane chains in NC$_1$ composites.

Table 6.3: TGA data of TPU, NC$_1$ and NC$_2$ composites.

Sample Name	T$_{degrad.}$(I Stage) (^{o}C)	T$_{degrad.}$(II Stage) (^{o}C)	Wt% (Residue)
TPU	362	411	0.9
NC$_{12}$	364	419	2.76
NC$_{14}$	367	426	4.92
NC$_{16}$	367	429	6.97
NC$_{18}$	368	433	9.25
NC$_{22}$	362	416	2.88
NC$_{24}$	365	420	4.65
NC$_{26}$	366	422	7.03
NC$_{28}$	366	425	8.95

EMI Shielding Efficiency

The EMI SE of the NC$_1$ and NC$_2$ composite films in the microwave frequency was determined in the range of 8-12 GHz. The EMI SE of a material is defined as the ratio between the power (electric field) of the incident (P$_I$ or E$_I$) and transmitted electromagnetic wave (P$_T$ or E$_T$) [11,12]. Total SE in decibels (dB) is given by

$$\text{EMI SE}_{Total} = 10 \log_{10} P_T/P_I = 20 \log_{10} E_T / E_I \quad \text{.............(6.1)}$$

When electromagnetic radiation is incident on a shielding material, phenomena such as reflection, absorption, and transmission take place. The total shielding can be expressed as the sum of three terms ie,

$$\text{SE}_{total} = \text{SE}_A + \text{SE}_R + \text{SE}_M \quad \text{...(6.2)}$$

Where SE$_R$, SE$_A$, and SE$_M$ are shielding due to reflection, absorption, and multiple reflections, respectively. When SE$_{total}$ > 10 dB, SE$_M$ can be neglected (12), and it is usually assumed that

$$SE_{total} = SE_A + SE_R \quad \text{..} (6.3)$$

Scattering (S) parameters i.e., S_{11} (or S_{22}), S_{21} (or S_{12}) are used to investigate the contribution of the absorption and reflection to the total EMI SE of the samples, (14). The transmittance (T), reflectance (R) and absorbance (A) coefficients are obtained using the S parameters as follows (15)

$$1 = A + R + T \quad \text{..} (6.4)$$

$$T = E_r/E_I = |S_{12}|^2 = |S_{21}|^2 \text{.....................................} (6.5)$$

$$R = E_R/E_I = |S_{11}|^2 = |S_{22}|^2 \text{.....................................} (6.6)$$

The shielding efficiency by reflection (SE_R) and absorption (SE_A) are calculated by the following equations (6.16)

$$SE_R = 10 \log 1/1\text{-}R \quad \text{...} (6.7)$$

$$SE_A = 10 \log I - R/T \quad \text{...} (6.8)$$

$$\text{Total } SE = SE_R + SE_A = 10 \log 1/T \text{.............................} (6.9)$$

The S parameters (S_{11} and S_{12}) of the composite films were measured by vector network analyzer.

The EMI SE of NC_1 and NC_2 with various weight % of FMWCNTs as a function of frequency are presented in figure 6.5a and b. It is seen that the SE of each composite is almost constant in the frequency range studied. Neat TPU film doesn't exhibit any EMI shielding efficiency. Therefore, the EMI shielding properties of the films is entirely contributed by the CNTs. The increment of SE in both the composites followed the same pattern. It is observed that the average SE increases with increase in

FMWCNT content. Generally for all samples, there is an increase in SE with increase in conductivity. As the CNT content increases in the TPU matrix, the number of conducting filler interconnections increases. Interaction between the nano fillers and incoming radiation improves the shielding effectively. In the case of NC_2 composite films, up to a weight % of 1, there is no noticeable SE. At 8% filler loading, the SE is 19.65 dB. In the case of the NC_1 films, at 1wt % of FMWCNT, the SE is 4.23dB and the highest SE of 31.35 dB is obtained with 8% FMWCNT. This value much greater than the ones reported in literature for many CNT based composites (17-20). This variation in SE of these composites can be due to the differences in the electrical conductivity and nature of conductive network within the matrix.

There are conflicting views on the relation between conductivity and EMI SE. While conductivity requires connectivity, EMI shielding requires only conductive particles to interact and impede the radiations (21, 22). Figure 6.5a and b show that the increase in the SE is not directly proportional to the increase in conductivity. In the case of electrical conductivity (Fig. 6.2) the increment is slow after the percolation threshold, whereas SE shows a consistent improvement. Al-Saleh et al. (13, 23) have observed that for CNT/Polymer systems, EMI shielding by absorption depends on the spacing between MWCNT particles and/or the composite electrical resistivity in addition to the MWCNT content. Similar mechanism has been suggested by other researchers also (24-26). In order to explore the mechanism of shielding, the contribution of reflection (SE_R) and absorption (SE_A) to the total EMI SE (SE_T) is considered. Figure 6.5c shows the SE_T, SE_A and SE_R values of NC_1 and NC_2 composites at a frequency of 10 GHz. The SE_A

increase greatly with increasing of filler content while the SE_R shows only a nominal increase. It indicates that the major mode of EMI shielding is absorption. The enhancement of SE_T and SE_A of NC_1 composites is more pronounced than that of NC_2 composites. Though both the films contain the same wt % of CNTs the higher SE of NC_1 samples may be attributed to more homogeneous dispersion and effective connectivity of CNTs in the polymer matrix. Shielding occurs by the interaction of electromagnetic radiation with electrical and magnetic dipoles of conductive fillers. In this experiment, NC_1 composites perform better than NC_2 composites. This is because the well dispersed conductive filler interact and absorb the incoming electromagnetic radiation. This confirms the contribution of absorption to the Shielding property. The interfacial interaction between CNT_S and TPU, homogeneous dispersion of CNTs and the conductive network formed in the TPU play a crucial role in the improvement in the SE by absorption of NC_1 composites.
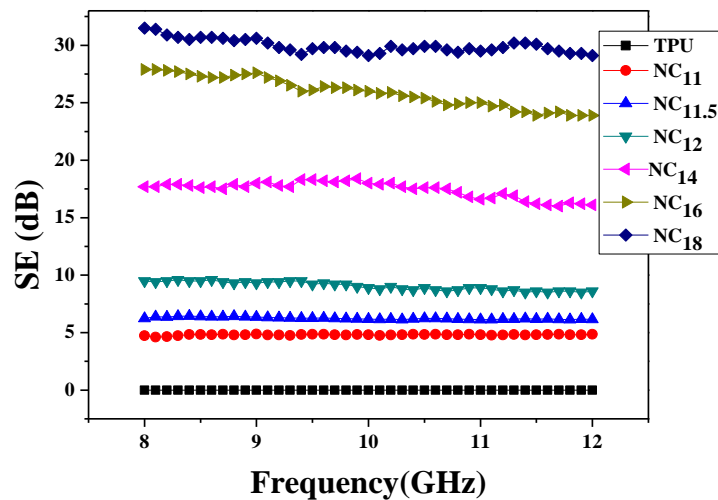
Fig. 6.7a: SE of NC_1 Composite films
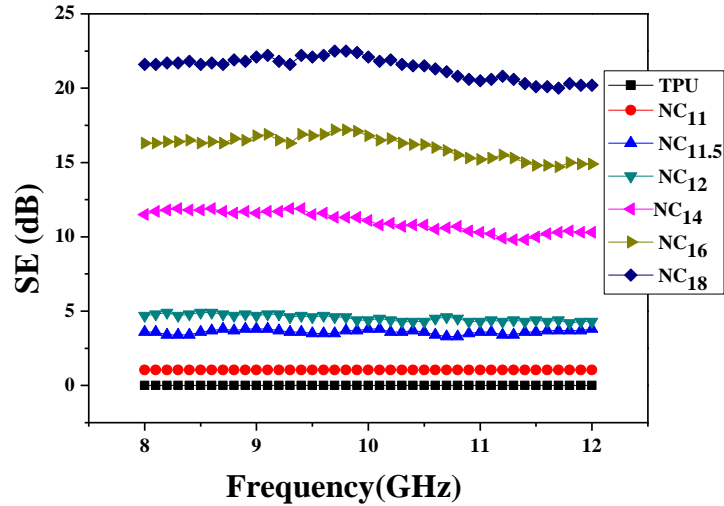
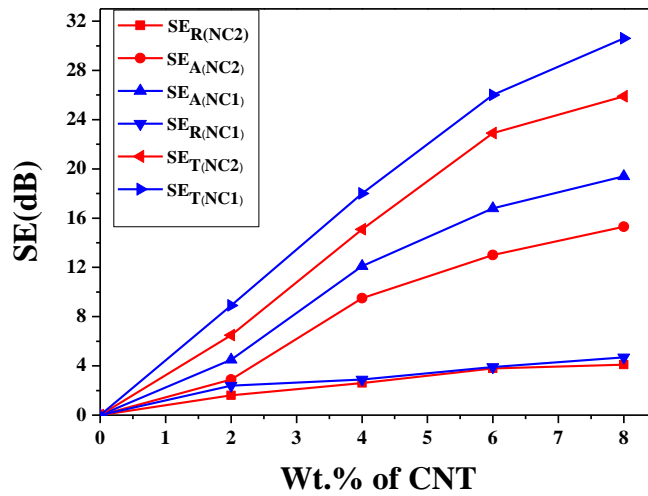**Fig. 6.7b: SE of NC2 Composite films.**

Fig. 5c: SE_T, SE_A and SE_R values of NC_1 and NC_2 Composite films

6.4 Conclusion

High shielding effectiveness as well as good mechanical and thermal properties are produced by PANI/FMWCNT/TPU composites prepared by in-situ polymerization of aniline in TPU solution in presence of FMWCNTs.

In-situ polymerisation assisted by sonication significantly reduces the agglomeration among CNTs and the CNTs formed an efficient conductive network. As a result, low percolation threshold (0.58 wt%), high electrical conductivity and high EMI shielding efficiency are achieved in these composites. EMI SE of 31.35 dB in X band has been obtained by the addition of 8 wt% filler concentration. This is attributed to the good dispersion and the strong interfacial adhesion of PANI coated FMWCNTs in TPU leading to efficient conductive network formation. The homogeneous dispersion of CNTs is confirmed by morphology studies. The experimental results also show that absorption is the primary mechanism of EMI SE. TGA, DMA and tensile analysis reveal the improved thermal and mechanical properties of the composites.

References

[1]   Z. Chen, C. Xu , C. Ma, W. Ren, H.M. Cheng, *Adv. Mater.*, 25, 2013, p. 1296.

[2]   D.D.L. Chung, *Carbon*, 39, 2001, p. 279.

[3]   Z. Fan, G. Luo, Z. Zhang, L. Zhou, Fei, *Materials Science and Engineering: B*, 132, 2006, p. 85.

[4]   A.P. Singh, M. Mishra, D.P. Hashim, T.N. Narayanan, B.K. Gupta, *Carbon,* 85, 2015, p.79.

[5]   Y. Huang, N. Li, Y. Ma, F. Du, F. Li, X. He, L. Xiao, G. Hongjun, C. Yongsheng, *Carbon,* 45, 2007, p. 1614.

[6]   P. Saini, V. Choudhary, B.P. Singh, R.B. Mathur, S.K. Dhawan, *Synth. Met*., 161, 2011, p. 1522.

[7]   S.P. Pawar, K. Pattabhi, S. Bose, *RSC Adv*. 4, 2014, p. 18842.

[8] M. Arjmand, M. Mahmoodi, G.A. Gelves, S. Park, U. Sundararaj, *Carbon*, 49, 2011, p. 3430.

[9] J. Masanoto, T. Iwamot, Polymer data handbook. London: Oxford University, 1999.

[10] Z.M. Dang, M.J. Jiang, D. Xie, S.H. Yao, L.Q. Zhang, J. Bai, *JAppl Phys*, 104, 2008, p. 024114.

[11] T.A. Skotheim, R.L. Elsenbaumer, J.R. Reynolds, Handbook of Conducting Polymers, 2nd edn. (CRC Press, New York, 1997)

[12] K. Singh, A. Ohlan, P. Saini, S.K. Dhawan, *Polym Adv. Technol.*, 19, 2008, p. 229.

[13] M.H. Al-Saleh, W.H. Saadeh, U. Sundararaj, *Carbon*, 60, 2013, p. 146.

[14] American Society for Testing and Materials, Standard Test Method for Measuring the Electromagnetic Shielding Effectiveness of Planar Materials, ASTM, Philadelphia, PA, 1999, p. D-4935.

[15] D.K. Ghodgaonkar, V.V. Varadan, V.K. Varadan, *Trans. Instrum. Meas.*, 39, 1990, p. 387.

[16] P. Saini, V. Choudhary, B.P. Singh, R.B. Mathur, S.K. Dhawan*, Mater. Chem. Phys.*, 113, 2009, p. 919.

[17] S.H. Park, P.T. Theilmann*,* P.M. Asbeck*,* P.R. Bandaru, *IEEE Transactions on nanotechnology*, 9, 2010, p. 464.

[18] P. Bhattacharya, S. Dhibar, G. Hatui, A. Mandal, T. Das, C.K. Das, *RSC Adv.*, 4, 2014, P, 17039.

[19] R.Mathur, S.Pande, B.Singh, T.Dhami, *Polym. Compos.*, 29, 2008, p. 717.

[20] Y. Yang, M.C. Gupta, K.L. Dudley, R.W. Lawrence, *Nano Lett.*, 5, 2005, p. 2131.

[21] DDL. Chung, *Carbon*, 39, 2001, p. 279.

[22] S.Y. Yang, K. Lozano, A. Lomeli, H.D. Foltz, R.Jones, *Compos Part A.*, 36, 2005, p. 691.

[23] M.H. Al-Saleh, U.Sundararaj, *Carbon*, 47, 2009, p. 1738.

[24] Z. Fan, G. Luo, Z. Zhang, L. Zhou, F. Wei, *Materials Science and Engineering B*, 132, 2006, p. 85.

[25] J.S. Im, J.G. Kim, S.H. Lee, Y.S. Lee, Colloids and Surfaces A: Physicochem. Eng. Aspects 364 (2010) 151–157

[26] S.T. Hsiao, C.M. Ma, H.W. Tien, W.H. Liao, Y.S. Wang, S.M. Li, Y.C. Huang, *Carbon*, 60 2013, p. 57.

.....ॐ.....

Chapter 7

CONCLUSIONS

Successful development of novel devices based on conducting polymeric composites requires low percolation threshold, high conductivity and stability in conductivity. The main objectives of the study were to synthesise core-shell nanoparticles of CNT and PANI with high conductivity and retention capability. MWCNTs were functionalised and PANI-FMWCNT composites were synthesised through interfacial polymerisation and single phase polymerisation process. Studies on the electrical, thermoelectric, electro mechanical and EMI shielding were conducted to assess the applicability of these conductive fillers.

Nanocomposites consisting of FMWCNT and PANI were prepared through dynamic interfacial polymerisation process, with CNT content ranging from 0 to 1gm. Presence of CNTs influenced polymerisation and induced formation of a tubular composite with thin PANI coating on the surface of nanotubes. At 12.9% CNT content, DC conductivity shows highest improvement. SEM and TEM images show PANI coated uniformly on the surface of the CNTs. FTIR spectra and TGA analysis confirm strong interaction between PANI chains and CNTs. The role of CNTs and dopants

in stabilising the DC conductivity of composites at elevated temperature is studied through cyclic thermal ageing and isothermal ageing studies. The loss in conductivity of pure PANI is much larger compared to composites and sulphonic acid doped samples have notable retention in conductivity. Deprotonation and polymer chain degradation by atmospheric oxygen are the prime reasons for reduction in conductivity at high temperature. The highly ordered PANI chain structure on nanotubes can retain the dopants and resist the diffusion of oxygen into the interior of composite. PANI-CNT interface and strong interaction between these two are responsible for high conductivity and retention up to a temperature of 150°C. Dopants TSA and NSA, due to their efficient delocalisation of PANI chains exhibit best conductivity retension at high temperature. This excellent property of composites may imply their potential application in high temperature ranges.

NSA doped PANI/FMWCNT composites were prepared by traditional single phase (SP) polymerisation and dynamic interfacial polymerisation (IF) methods to study thermal stability of conductivity and thermoelectric properties. Morphological and structural analysis showed that synthesis by interfacial polymerisation resulted in a well-ordered coating of PANI with a uniform core-shell structure, while single phase polymerisation resulted in thick core shell structure with many protrusions. Interfacial polymerisation makes it possible for aniline molecules to polymerise and grow in an ordered manner on the surface of FMWCNT resulting in highly oriented PANI chain alignment. The electrical conductivity of sample synthesized through interfacial polymerisation is more than ten times that of single phase polymerised sample. This composite shows improved stability in conductivity at high temperature during cyclic ageing and isothermal ageing

studies. The morphology, crystallinity and interaction between PANI and CNTs are crucial in deciding the extent of degradation. XRD studies provide strong evidence that there is enhanced structural ordering of PANI chains in this composite. The sharp and intense peak at 6.47^o is characteristic of nanostructured polyaniline. This can be ascribed to the fact that interfacial polymerisation promotes order and alignment in polymer chain confirmation along nanotubes leading to an integrated crystalline structure. TGA analysis reveals the elevated thermal stability as well as the delay in loss of dopant for this sample. Spectroscopic studies also indicated the role of stabilising interaction between PANI and CNTs. This unique structure of PANI on CNT is responsible for high resistance to conductivity damage under elevated temperature. The excellent properties of this composite are very promising for electronic applications. But single phase sample is devoid of such structural ordering and strong PANI-CNT interaction. The thick and loose polymer chains allow the early deprotonation as well as diffusion of oxygen in to the polymer chains and causes oxidation of polymer chains. This disruption in conjugated chain structure is responsible for conductivity ageing. Regarding thermo electric properties, Seebeck coefficient of interfacial sample shows significant improvement. Simultaneous increment in both electrical conductivity and Seebeck coefficient reveals that the enhancement is due to the improvement of charge carrier mobility. The improved carrier mobility is a consequence of improved molecular ordering in polymer chains. No corresponding improvement in thermal conductivity of composite is seen and it remains equal to that of PANI. In this aspect the composite is much superior to that of inorganic thermoelectric materials. Good electrical conductivity, good seebeck coefficient and low thermal conductivity in CNT based PANI

composites with a power factor (ZT) of 457.5 × 10^{-6} is achieved. This ZT value is currently too low to be considered as a good thermoelectric material. But the results show the possibility of tuning the thermoelectric properties of the conductive polymer and for fabricating efficient thermoelectric devices based on CNT based PANI composites.

When CNTs are introduced into insulating polymer matrix, conducting polymer composites (CPC) with high conductivity and low percolation threshold resulted. Due to the change in electrical properties under applied strain, these ICPs have potential for application in strain sensing. Knowledge regarding the effective aspect ratio of CNT in polymer matrix, conductive network formation, piezoresistivity, reversibility of resistivity are essential to develop a strain sensor. Here, PANI coating of FMWCNT was done by in-situ and ex-situ polymerisation of aniline and CPCs of FMWCNT/PANI/TPU were synthesised. A comparative study with respect to percolation threshold, strain sensitivity, gauge factor and cyclic stability in resistivity of the composite films are carried out. The morphology studies reveal that in-situ polymerised PANI-FMWCNT filler particles are homogeneously dispersed in TPU matrix. The PANI coating on CNT keeps the conductive fillers as individual tubes, avoiding aggregation and increasing its interfaces with the matrix. Consequently low percolation threshold and improved strain sensitivity is achieved. These composites with 2 weight% filler content, showed a gauge factor (GF) of 1075 at 100% strain and exhibited high reversibility in resistivity upon elongating to 20%. The origin of high GF of this composite film is investigated. It has been reported that parameters such as geometry of the percolative network, the CNT nano-structure and the relative contribution of the tunneling resistance to the total electrical

resistance decide the strain sensitivity of such composites. In order to investigate this, a modeling study based on the tunneling theory by Simmons is carried out. The experimental data for strain sensing agrees with the theoretical equations derived from a model based on the tunneling theory by Simmons. Incorporation of PANI coated CNT brings new insight into conductive network formation and strain sensing mechanism in TPU where the effective aspect ratio of nanofillers is a major component.

Another strategy for achieving homogeneous dispersion, low percolation threshold and high conductivity is in situ polymerisation in the polymer matrix. In order to obtain TPU films of high EMI SE, in-situ polymerisation of aniline in presence of CNT assisted by sonication is carried out in TPU matrix. PANI coated CNTs demonstrated better dispersion in TPU and provided lower electrical percolation threshold. The homogeneous dispersion of CNTs is evident from morphology studies. Low percolation threshold, high electrical conductivity and high EMI shielding efficiency are achieved in these composites. EMI SE of 31.35 dB in X band has been obtained by the addition of 8 wt% filler concentration. This is attributed to the good dispersion and the strong interfacial adhesion of PANI coated FMWCNTs in TPU leading to efficient conductive network formation. The primary mechanism of EMI shielding is absorption. TGA, DMA and tensile analysis reveal the improved thermal and mechanical properties of the composites. Thus employing in-situ polymerisation is helpful for successful incorporation of CNTs into TPU, resulting in a composite with increased electrical, thermal and mechanical properties. Here CNTs served as nucleating agents for polymerisation of aniline, thus increasing the dispersibility of CNTs. This provided an ideal environment for good interaction at the CNT-TPU

interface. This reveals a simple guideline for the synthesis of FMWCNT/TPU composite with a modest CNT content, but resulting in mechanically strong and thermally stable EMI shielding films.

.....ഇൗ.....

Abbreviations and Symbols

APS	Ammonium persulfate
ASTM	American society for testing and material
CPC	Conducting polymer composite
dB	Decibel
DBSA	Dodecylbenzene sulphonic acid
DC	Direct current
DMA	Dynamic mechanical analyser
EAP	Electroactive polymer
EB	Emeraldine base
EMI	Electromagnetic interference
CNT	Carbon nanotube
CVD	Chemical vapor deposition
FESEM	Field emission scanning electron microscopy
FIT	Fluctuation Induced Tunnelling
FMWCNT	Functionalised Multi-Walled Carbon Nanotube
FTIR	Fourier transform infrared
GF	Gauge factor
h	Hourour
I	Current
ICP	Intrinsically conducting polymer
k	Thermal conductivity
keV	kilo electron Volt
kN	Kilo Newton
L	length
Min	Minutes
MPa	Mega Pascal

MWCNT	Multi-Walled Carbon Nanotube
MUT	Material under test
NC	Nanocomposite
NMP	N-Methyl-2-pyrrolidone
NSA	Naphthalene sulphonic acid
PANI	Polyaniline
R	Resistance
S	Seebeck coefficient
SE	Shielding efficiency
SEM	Scanning electron microscopy
SWCNT	Single-Walled Carbon Nanotube
TSA	p-Toluenesulfonic acid
TE	Thermoelectric
TEM	Transmission electron microscopy
T_g	Glass transition temperature
XRD	X-ray powder diffraction
TGA	Thermogravimetric analysis
TPU	Thermoplastic polyurethane
UV-Vis	Ultra-Violet Visible
VNA	vector network analyzer
VRH	Variable Range Hopping
ZT	Thermoelectric figure of merit
ρ	Resistivity
ϭ	Conductivity

.....ৡঙ.....

List of Publications

International Journal

[1] **A.P. Sobha** and Sunil K. Narayanankutty, "Electrical and Thermoelectric Properties of Functionalized Multiwalled Carbon Nanotube/Polyaniline Composites Prepared by Different Methods", *IEEE Transactions on Nanotechnology,* DOI: 10.1109/TNANO.2014.2323419, (Volume:13, Issue 4) 835– 841, July 2014.

[2] **A.P. Sobha** and Sunil K. Narayanankutty, "Effect of Dopants on DC Conductivity of Functionalized Multi-Walled Carbon Nanotubes and Polyaniline Composites", *Advanced Science, Engineering and Medicine* DOI: 10.1166/asem.2014.1570 (Volume 6 Issue7) 756-764 , July 2014.

[3] **A.P. Sobha** and Sunil K. Narayanankutty, "A promising approach to enhanced thermal stability of DC conductivity of polyaniline – functionalised multi-walled carbon nanotube composites", *International Journal of Nanoparticles*,DOI: 10.1504/IJNP.2014.064868, (Volume 7, No. 2)112-132, 2014.

[4] **A.P. Sobha** and Sunil K. Narayanankutty, "Improved strain sensing property of functionalised multiwalled carbon nanotube/polyaniline composites in TPU matrix", *Sensors & Actuators: A. Physical* DOI:10.1016/j.sna.2015.06.012, (Volume 233) 98–107, September 2015.

[5] **A.P. Sobha** and Sunil K. Narayanankutty, "DC Conductivity Retention of Functionalised Multiwalled Carbon Nanotube/Polyaniline Composites", *Materials Science in Semiconductor Processing,* DOI:10.1016/j.mssp.2015.06.018,Volume 39, November 2015, Pages 764–770

[6] **A.P. Sobha,** Shreekala. P.S and Sunil K. Narayanankutty, "Electrical, Thermal, Mechanical and Electromagnetic shielding properties of polyaniline coated FMWCNT/TPU composites", Communicated

International Conference

[1]   **A.P. Sobha** and Sunil K. Narayanankutty, "A study on the DC conductivity and thermoelectric Properties of Carbon Nanotube based Polyaniline Composites, IEEE - International Conference on Power, Signals, Controls and Computation (EPSCICON) 2012, VAST, Thrissur, Kerala, India.

[2]   **A.P. Sobha** and Sunil K. Narayanankutty, "An elegant way of improving the electrical conductivity and thermoelectric property of MWCNT/PANI nanocomposites, 4th International Conference on Advanced Nano Materials(ANM) 2012,IIT Madras, Tamilnadu, India.

[3]   **A.P. Sobha** and Sunil K. Narayanankutty, "Improved EMI shielding of FMWCNT/Polyaniline composites in TPU matrix", International Conference on Advanced Functional Materials (ICAFM) 2014, . NIIST, Thiruvananthapuram, Kerala, India.

National Conference

[1]   **A.P. Sobha**, Shreekala P.S and Sunil K. Narayanankutty, "FMWCNT-PANI/TPU Composite as efficient EMI shielding material, 6th National Conference on Advances in Polymeric Materials (polycon-2014), SJCE, Mysore, Karnataka, India.

.....ை�‍ൽ.....

▌▌▌ Curriculum Vitae ▌▌▌

Sobha A. P
Associate Professor
Department of Applied Science,
Vidya Academy of Science and Technology
Thalakkottukara P.O
Thrissur – 680 033.   Ph: +919495740461
Kerala, India.   Email: sobha@vidyaacademy.ac.in

Academic Profile

Doing Ph.D in Department of Polymer Science and Rubber Technology CUSAT from 2010 onwards.

Received M.Sc (Chemistry) from Calicut University in 1990.

Professional Experience

- Working as Associate Professor in the Department of Applied Science, Vidya Academy of Science and Technology, Thrissur from July 2013 - Till date.

- Worked as Assistant Professor in the Department of Applied Science, Vidya Academy of Science and Technology, Thrissur July 2003 to June 2013.

Research Experience

- Doing Ph. D (Part time) from October 2010 in the Department of Polymer Science and Rubber Technology, CUSAT under the supervision of Dr. Sunil. K. Narayanankutty.

Awards and Honours

Received University Merit Scholarship during the academic year 1988-1990.

Publications

International Journal	**5**
International Conference	**4**
National Conference	**1**

.....ഊ.....